USDOT Tier 1
University Transportation Center
on Improving Rail Transportation
Infrastructure Sustainability and Durability

Final Report VT-3

DISCRETE ELEMENT MODELING OF RAILWAY BALLAST FOR STUDYING RAILROAD TAMPING OPERATION

By

Dr. Mehdi Ahmadian, J. Bernard Jones Chair Professor
Director & Founder of CVeSS and RTL
Department of Mechanical Engineering
Virginia Polytechnic Institute and State University
ahmadian@vt.edu

and

Nilesh Dama, Graduate Research Assistant
Department of Mechanical Engineering
Virginia Polytechnic Institute and State University

August 10, 2020

Grant Number: 69A3551747132

DISCLAIMER

CONTENTS

LIST OF FIGURES

LIST OF TABLES

EXECUTIVE SUMMARY

Railway Technologies Laboratory (RTL) studied the behavior of the ballast particles during their interaction with tamping tines in tamping operation by developing a simulation model using the Discrete Element Model (DEM). Through a parametric study, it is found that squeeze and release velocity of the tines should be lesser for better compaction of the particles and linear tamping is better compared to elliptical tamping.

A comprehensive literature review is presented showcasing the applicability of DEM techniques in modeling ballast behavior and its feasibility in studying the fundamental mechanisms that influence the outcome of railroad tamping process is analyzed. The analysis shows that DEM is an excellent tool to study tamping operation as its important and unprecedented insights into the process, help not only to optimize the current tamping practices but also in the development of novel methods for achieving sustainable improvements in the track stability after tamping. The simulation model is developed using a commercially available DEM software called PFC3D (Particle Flow Code 3D).

A detailed explanation is provided about how to set up the DEM model of railway ballast considering important parameters like selection and calibration of particle shapes, ballast mechanical properties, contact model, and parameters governing the contact force models. Tamping operation is incorporated into the simulation model using a half-track layout with a highly modular code that enables a high degree of adjustability to allow control of all process parameters for achieving optimized output.

INTRODUCTION

Motivation

Railroads all over the world spend around several billion dollars on the maintenance of their existing infrastructure and assets (roughly 20% of their budget). Almost 58% of this amount is spent on maintaining tracks and substructure [1]. In 1945, mechanized railway track maintenance was implemented so that the track stability can be enhanced, and the precision of the track geometry can be improved. The running speeds of trains have increased over the years and for them, the precision of transitions and curves has also increased. Thus, the track should be accurately maintained to its designed geometry with the help of equipment and processes. Wear of the rolling stock is reduced because of the smoother, reliable and accurate track geometry thereby being an important economical factor and hence is a major aim for the railway industry [2]. Tamping is a track maintenance activity that is used for the elimination of defects in the track geometry and to correct the spatial alignment of the rail tracks. This is one of the very important track maintenance activities that influence the overall track maintenance costs for the railroads and can potentially help in saving about $9,500 per mile annually.

The optimal tamping procedure is often a point of debate among the leading rail engineers and railroad companies [3]. Many researchers have worked and tried to study the effects of various parameters of the tamping process like vibration frequency, amplitude, depth of insertion, etc. on the resulting ballast compaction, but there is still a lack of agreement on the ideal tamping cycle routine and the value of the tine motion parameters for the ideal tamping cycle. One of the reasons for this is the development of the tamping process being predominantly based on physical experimentation with less theoretical formulation. American railroad companies rely on the tamping equipment manufacturers for aggrandizing tamping technology and these manufacturers often claim their own values and practices as favorable. This makes it difficult to follow one standard practice while performing a tamping cycle. For example, three different manufacturers claim three different vibrating frequencies as an optimum value - 35 Hz, 42 Hz and 50 Hz. Of course, the tamping machines are not the same and differ in terms of the design of tamping tools (tines) and the nature of vibration used while inserting these tines into the ballast. Since tamping is such an important railway activity, the advancement of tamping techniques is an area of active research for the railway (railroad) companies.

Railway ballast is a complex system that is difficult to model as a dynamic problem using theoretical models to estimate their response behavior to any kind of disturbance. Mostly, empirical and semi-empirical methods of scientific development have paved the way for the advancement of tamping technology. Several experimentalists such as Audley, Andrews [4], Koc et al. [5], Soleimanmeigouni et al. [6], etc. have set up experiments using full- scale model and have collected track alignment data over long periods of time to develop mathematical models for prediction of the track settlement. No matter how good a full-scale model experiment may sound, such research methods have long incubation periods, need high capital investments, and take lots and lots of time (possibly years in some cases). Another issue with such tests is the measurement of ballast compaction that cannot be practically measured in realistic conditions.

The advent of computers and an increase in computational prowess have paved the way for techniques like Distinct Element Modeling (also called Discrete Element Modeling) to be used as a powerful technique to solve and understand complex granular systems. DEM allows

mathematical modeling of the dynamic behavior of ballast for different tamping parameters by resolving each inter-particle contact individually. Forces at each contact point amongst ballast particles are calculated based on pre-determined force-laws and the resulting kinematics of all ballast particles are determined. Consequently, the collective behavior of railroad ballast can not only be studied for different physical and forcing conditions but accurately predicted as well. The entire tamping process can be simulated in a virtual environment and its effect on track stability can be studied, obviating the requirement of extensive physical testing. Therefore, numerical simulation of the tamping process is an invaluable tool for railroad engineers for validating their current tamping practices and radically accelerating the development of the process and the equipment in the future.

The work presented in this thesis highlights the efforts taken by Virginia Tech Railway Technologies Laboratory (VT RTL) in developing a simulation model to study the complex dynamics of railway ballast. The simulation model has been extended further to study the tamping process and can be modified for performing several other advanced studies involving the railroad ballast.

Objectives

The goal of this project is to develop a simulation model to understand the tamping process and eventually study track alignment, track stability, ballast gradations and ballast degradation. The following steps were taken to achieve this goal:

1. Find the best way to model tamping dynamics trying to include all the necessary relevant parameters as practiced by the railway industry professionals.
2. Evaluate the modeling means that would accurately and adequately represent tamping dynamics.
3. Determine the limitations of the simulation model, e.g. simulation runtime, errors, complexity, etc.
4. Run test cases and parametric studies to understand the tamping operation.
5. Evaluate results from parametric studies to suggest better practices to be adopted to increase the tamping efficiency.

Adopted Approach

The approach adopted to achieve the required objective involved a series of smaller steps as explained below:

1. Determine the applicability of DEM techniques in studying the railway ballast dynamics.
2. Perform a literature survey to identify the most recent and practical DEM practices, suited for the railway ballast simulation.
3. Compare DEM software packages and select a suitable package and hardware as per the software requirements.
4. Calibrate the model parameters for the accuracy of the model and to reduce the simulation runtime.
5. Establish a simulation model to generate and study ballast motion.
6. Extend this ballast model to a fully-developed model capable of studying the tamping operation.

DEM helps in the determination of certain physical properties of granular systems that cannot be measured directly experimentally or is very difficult to do it experimentally in practice. DEM also

helps in the study of the effects of unquantifiable variables like particle shape and angularity. A literature survey conducted helped VT RTL researchers understand the different types of modeling methodologies available to simulate railway ballast. These methods were different in terms of the parameters being studied, e.g. particle velocities, frequency of inter-particle collisions, solid fraction and compaction of particles inside the assembly, etc. The modeling methodologies not useful for the general objective of this research are out of the scope of this document and thus have not been discussed here. The important information required to study and perform this research, that was obtained from various other sources (journal papers, books, discussions, conference proceedings, etc.) have been cited and referenced in this document with thorough careful consideration.

The software selection for this project was done after comparing various available soft- ware packages and analyzing their costs, functionality, features, usability, versatility, user-friendliness, customer support, etc. *PFC3D* by the ITASCA Consulting Group was chosen for the project after trying some open source codes (YADE, ESyS-Particle and LIGGGHTS) available online. Careful selection of parameters like material properties, contact physics, particle shapes, etc. was done to represent the real-world conditions and a model to generate ballast was created. The properties were then calibrated by changing the parameter values (increase and decrease) by a power of ten to see if there occurs a significant change in the output results and simulation runtime. The precision and accuracy of the model are also other important factors carefully given consideration while setting up the model. By adding tines and a railway sleeper (railroad tie), the tamping model is completed and parametric studies are performed by changing the values of essential tine motion parameters.

Contributions

The focus of this project is to advance the previous work done by Mr. Ashish and study the effect of the tamping process on the ballast. For this, a tamping model is set up using clumps where a single clump is made by a combination of 2 spheres. The simulation model is modified enough so that the results obtained can be trusted completely. This research also considers different tine motions during tamping, such as linear and elliptical tamping. Parametric studies were performed to identify the best values of tine motion parameters to get the best tamping performance. Thus, the results obtained from this work advance our knowledge in the field of tamping by helping us understand the effect of particle shape, tine motion, etc. and various other factors involved in the tamping process.

The work done in this research focus more on studying the tamping process, the effect of tine motion on the ballast and identifying the best set of values of tine motion parameters required to obtain the best tamping performance.

Following are some of the contributions from this research:

1. Provide a better understanding of DEM application techniques to model the railway ballast.
2. Determining important elements of DEM methodology like contact force laws, material properties selection, particle gradations, etc. for modeling the ballast behavior.
3. Selection of particle shape to accurately depict the ballast dynamic behavior.
4. Developing a routine to replicate a complex arbitrarily shaped ballast particle using 3D scanning techniques.

5. Establishment of a complete simulation model to study the tamping operation and the interaction of sleeper and tamping tines with the ballast.
6. Parametric studies to identify the best set of values of tine motion parameters for linear tamping.
7. Finding out that linear tamping is better than elliptical tamping.

Such virtual environment simulations reduce the capital investment and time required to study such processes. Thus, DEM has a lot of potential in accelerating the progress of designing of track designs and maintenance activities. An improvement in the tamping efficiency would save rail companies a lot of money due to longer maintenance cycles.

Organization of the Report

Section 2 (Background) of this document talks about an extensive literature review on track stability, tamping and DEM. The resultant track stability after tamping is a function of the ballast state. Thus, due to this reason, the applicability and feasibility of DEM techniques in simulating ballast behavior to study tamping have been discussed.

Section 3 (Model Development) gives a general introduction of the *PFC* software followed by important features related to the *PFC* software and the model generated inside the *PFC* environment. Modeling methodology, general solution procedure and general commands and terminologies related to the *PFC* model have been discussed.

Section 4 (Model Components) reveals in detail about the working of the *PFC* software as discussed in Section 4.1. This chapter basically helps the reader understand what happens behind the code. Important available particle shapes like balls, clumps and walls are dis- cussed along with their features, specialties, etc. The most important part of this chapter is about the modeling of contact physics which forms the very basis of how the ballast particles would behave when they come in contact with each other. The most relevant contact models along with the mathematical formulas used by them to establish and represent accurate contact physics between the particles have been discussed. Configuration of the physical parameters involved in the mathematical formulation of these discussed contact models has also been explained.

Section 5 (Simulation Model) discusses the effect of ballast particle shape and size distribution called gradation on track stability. The results of DEM simulation have been provided to support the stated claims. Spherical and irregularly shaped ballast particles performance is compared and their results have been analyzed. The initial and boundary conditions, as well as input and output parameters have been encapsulated. The final simulation model created in *PFC*, consisting of 5 stages has been explained in-depth with the underlying assumptions as per the information flow of the model. At last, the parametric studies and the type of studies that have been performed have been presented.

Section 6 (Results and Discussion) analyzes and summarizes the results obtained after performing parametric studies. Section 7 (Conclusions) discusses the potential applications of the developed *PFC* simulation model beyond the tamping operation.

BACKGROUND

Railway Tracks and Tamping

Railway Tracks

A representation of a cross-section of railway track structure with its various components is shown below in Figure 1. This top component comprises of the rails, fasteners and sleepers. Fasteners and sleepers are used to maintain rail position and alignment. Train wheels only come in contact with the two rails. This bottom component comprises of the ballast, sub-ballast and subsoil. This component transfers traffic loads from the superstructure (via sleepers) to the ground (via ballast). This component is also responsible for maintaining the alignment of the superstructure and to provide drainage for water. Ballast and sub-ballast are granular aggregates of randomly crushed stones and are usually made of materials like basalt, granite, limestone, gravel, etc.

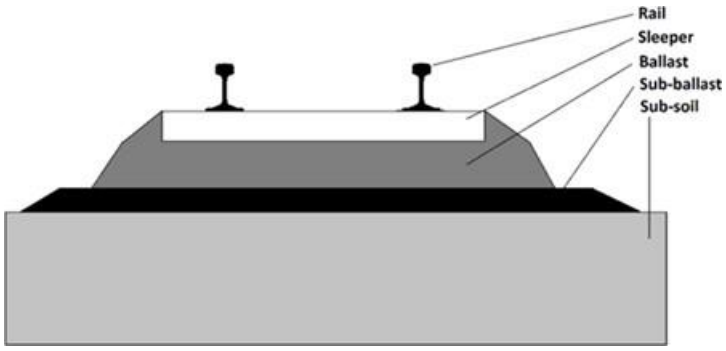

Figure 1 Structure of a ballasted railway track

Track Settlement and Stability

Due to repeated loading imposed by the traffic, the ballast is non-uniformly consolidated below the sleepers. As a result, a number of long-wavelength defects are introduced in the track geometry [7] and the vertical alignment of the track is disturbed. This is called track settlement. Figure 2 shows defects in the track geometry cased due to settlement of the ballast.

Track stability can be defined as the resistance offered by the tracks to misalignment in the vertical and lateral directions.

Figure 2 Defects in railway track geometry (Suiker 2002)

Thermal stresses, drainage, etc. are some of the factors affecting track stability. It is primarily influenced by sleeper displacement resistance. Track stability in the vertical direction is directly dependent on the ballast compaction directly below the sleeper (Lichtberger 2011). The higher is the compaction, the lower the settlement of track below its initial level. The ballast compaction below the sleepers cannot be found out directly by experiments. So, vertical track settlement is measured as an amount of settlement over time or cumulative loading or by manipulating compaction levels in the lab. Traffic speed, axle loads and traffic density are other factors influencing the ballast resistance and thus the vertical track settlement.

Buckling could occur due to high thermal stresses or due to the presence of the uneven forces in the lateral direction. Figure 3shows the buckling of tracks in the lateral direction due to thermal stresses. Lateral track stability as the name suggests is the resistance of the railway track to displacement in the lateral direction. Friction between the ballast particles and sleepers, and normal resistance to the lateral displacement of the sleepers by the ballast influence the lateral track stability (Lichtberger 2011). The friction generated between the ballast and sleepers is influenced by the value of the normal load on the track, compaction of ballast around sleepers, and the number of ballast particles directly in contact with the sleepers.

Figure 3 Buckling of tracks in lateral direction (Knapton 2015)

Defects in track geometry, both in vertical and in lateral directions, arising due to insufficient support from railway ballast are undesirable because they lead to low traffic speeds, fluctuating wheel-rail contact forces, deterioration of ride quality for passengers, and in extreme cases,

derailment. Hence, it is utmost important to correct such defects as a part of track maintenance activity, as soon as possible or prevent them from happening altogether.

Tamping

Tamping is the track maintenance process used to restore the track settlement by lifting the track and sleeper at a location where they settled. This is done by mechanically lifting the track and sleeper and then squeezing the surrounding ballast below the raised sleepers. The goal of the tamping process is to achieve the maximum possible ballast compaction below the sleepers while also taking care of the damage caused or particle breakage of the ballast particles that may occur due to the high squeezing forces that may be generated during the squeezing phase of the tamping process. Tamping machines, or tampers, traverse on rails and perform tamping of ballast below every sleeper in a repetitive manner. Figure 4shows a tamper in operation.

Figure 4 Tamping machine in operation (Plasser and Theurer 2010)

A single tamping cycle consists of the following five steps.

Lifting of track Tamper lifts the track and sleeper by a certain height which is decided based on the track settlement. A small amount of compensation must always be included in the calculation to account for the initial track settlement after the sleeper and then rail is dropped back onto the ballast after the tamping cycle. The usual gain achieved in track height ranges from 20-70 mm. A minimum lift of 20 mm is often recommended to ensure that enough space is created below lifted sleepers to squeeze ballast particles below them (Lichtberger 2011). While lifting the tracks, the tamper can also correct the lateral track position.

Insertion of tamping tines Tines are the tamping tools that get inserted into the ballast. Usually, for each sleeper there are eight tines, four on each rail (two on each side of each rail). So, a single rail would have two tines inserted to the left of it and two to the right of it. However, tines with a higher or lesser number are also developed by some manufacturers. The tines follow a vibratory motion throughout the tamping cycle since this helps to reduce the resistance to their motion by the ballast.

Perhaps the most striking characteristic of a granular material is its dual nature of behaving as a solid or fluid. Even though the individual particles are solid, the tendency of the ballast aggregate to flow readily is a fluidic property. This is actually in contrast with the fixed geometric form property that solids possess as explained by Deresiewicz (1958).

It is said that ballast liquefies locally when subjected to vibrating tines and with a higher vibrating frequency of tines, higher liquefaction of the ballast occurs. At lower vibrating frequencies, tines cannot effectively mobilize the ballast particles and power required for the operation increases thereby increasing the total cost of the operation. Also, a stable consolidation of particles cannot happen at higher frequencies due to the high mobility of ballast particles. Tine motion parameters like frequency, amplitude, nature of oscillation vary from manufacturer to manufacturer. While the effect of different vibration behaviors of tines on ballast is well researched, an appropriate set of values of vibration parameters required for minimizing track settlement after tamping is considered ambiguous.

The depth of the insertion of tines is another important parameter widely discussed about. This depth depends on the shape of tines as well, but usually the tines are inserted until their top edge or face is 10-20 mm below the bottom face of the sleepers (Lichtberger 2011).

Squeezing of the ballast Figure 5 shows the squeezing of the ballast below the sleeper. Tines squeeze ballast with constant pressure, irrespective of the amount of travel required to attain that particular pressure.

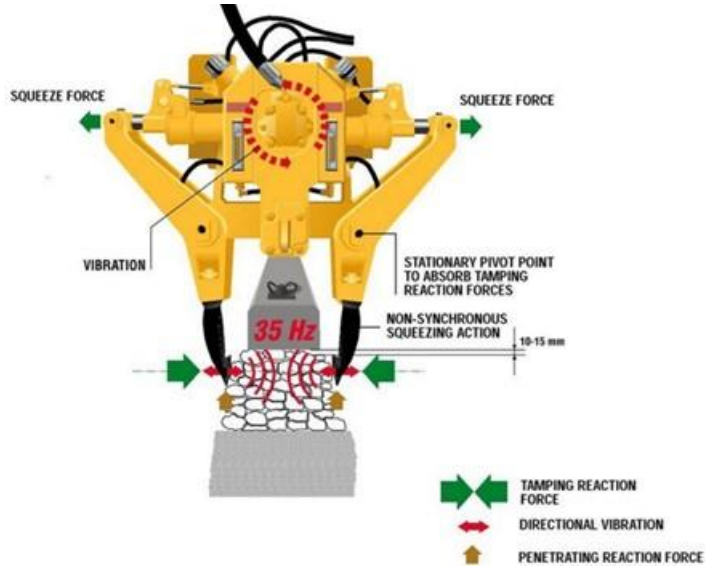

Figure 5 Squeezing of ballast below the sleeper (Jain 2017)**.**

There are two types of squeezing possible. The first is asynchronous (non-synchronous) where the tines don't travel the same amount. This has two major advantages. First, voids below the sleepers may be of varying sizes and using constant pressure to squeeze the ballast ensures a certain level of ballast compaction irrespective of the void size. The value of pressure used by various manufacturers, normally lies between 100 to 150 bar. Since the tamper moves along the rail in one direction, this means that at any given instant, the one side of the new sleeper is tamped due to the tamping done on the adjacent sleeper in the previous cycle. Thus, the condition of ballast below sleeper is not symmetric and the non- synchronous action of tines helps mitigate the difference by adjusting the required travel to squeeze the ballast to the same pressure on either side. The second type is synchronous where both the tines, i.e., tines on the left and right travel the same amount. The problem here may arise if the ballast is not equal or one side is fouled and the other is not. This means one side of the sleeper would offer more resistance to the tine motion while other would

not and thus equal pressure even though it would be applied to the tines, it won't reflect the same way on the ballast.

The ballast particles take a finite amount of time to rearrange themselves while being squeezed and after the squeezing phase. Thus, the squeezing velocity (related to squeezing pressure) and the amount of time for which the tines hold their position after desired squeeze pressure is applied, influences the compaction level of the ballast after tamping.

Release of tines After the squeezing phase, tines are moved horizontally outwards to a point where they can be lifted up. They are moved out horizontally till the same point where the tines were positioned after the insertion stage.

Withdrawal of tines This is the last step following the Release stage where the tines are lifted vertically upwards and then these tines move on to tamp the next sleeper. The velocity of release and withdrawal of tines affect the loss of compaction that occur after the withdrawal. There is a compromise here as well. If the withdrawal velocity is less, it minimizes the disturbance to the squeezed ballast and results in better compaction, however, it increases the overall time required to tamp a single sleeper and thus it considerably adds up to the total time required to tamp a particular section of a track.

Tamping is also done to improve the quality of the rail track to reduce its rate of settlement in the future. However, the improvement achieved after tamping majorly depends on the initial quality before tamping [1]. No doubt that tamping is an excellent way of improving track settlement rates, but it is also responsible for reducing the lateral track stability by up to 60% [13]. So tamping operation is usually followed by other track stabilizing operations such as stone blowing, dynamic track stabilization, etc.

Distinct Element Method

Granular systems are disordered aggregates of a large number of particles, characterized by abrupt changes in mass density, anisotropy, non-conservative internal forces and irreversible deformations of constituent bodies. Traditionally, granular assembly behavior has been modeled using the assumptions of continuous mass density and homogeneity. But such approaches are only suitable for predicting specifically targeted macroscopic parameters of the subject granular assembly for a small range of input conditions. Parameters and constants used in such models don't correspond to any actual physical properties in most cases. DEM, on the other hand, considers the discontinuous nature of granular systems and allows accurate modeling of both microscopic and macroscopic properties.

PFC (Particle Flow Code) uses the Distinct Element Method (DEM) (also called Discrete Element Method) to model the movement and study the interaction between rigid particles in a stressed assembly. Cundall (1971) introduced the concept of DEM for the analysis of rock-mechanics problems and then this concept was applied to soils by Cundall and Strack (1979). Cundall (1988)] and Hart et al. (1988) explain in detail about this method in the two-part paper. The basis for categorizing *PFC* as a discrete element code is given in the review by Cundall and Hart (1992). *PFC* allows finite displacements and rotations of discrete bodies to an extent where complete detachment is also possible. New contacts are recognized automatically as the calculation progresses and an explicit dynamic solution for solving Newton's laws of motion is used, thereby helping in the time evolution of the discrete system. *PFC* software is a simplified implementation

of the DEM as it assumes the particles to be rigid (circular in 2D; spherical in 3D) only. However, in general, DEM is capable of handling deformable polygonal-shaped particles (Itasca Consulting Group 2015).

The interaction between particles is a dynamic process in the DEM, wherein the system achieves equilibrium state if the internal forces are balanced out. Tracking the individual particles helps finding the forces, displacements and movements associated with the particle assembly. The propagation through the particle system of disturbances caused because of specified wall and particle motion and/or body forces result in the movements. The speed of propagation depends on the physical properties of the discrete system.

A timestepping algorithm is used to numerically represent the dynamic behavior of the system. Within each timestep, velocities and accelerations are assumed to be constant. The explicit finite-difference method for continuum analysis is quite identical to this method. The main idea of using DEM is that during a single timestep which is extremely small, disturbances are not allowed to propagate further from any particle than its immediate neighbors. Thus, at any given instance, the interaction of a particle with the particles it is in contact with helps determine the forces acting on that particle. Nonlinear interaction of a large number of particles can also be simulated without excessive memory requirements or the need for an iterative procedure because of the use of an explicit numerical scheme instead of an implicit one.

The application of Newton's second law to the particles and a force-displacement law at the contacts are used to perform calculations in the DEM. Newton's second law is used to determine the motion of each particle arising from the contact and body forces acting upon it, whereas the force-displacement law is used to update the contact forces arising from the relative motion at each contact. For walls, only force-displacement law is used whenever there is a contact of a particle with wall-facet.

Contact Resolution

Balls and clumps both have spherical surface profiles (except walls). Thus, only one point of contact is possible between particle-particle (spheres-spheres). This contact is detected by comparing center to center distance of spheres with their radii as shown in Figure 6.

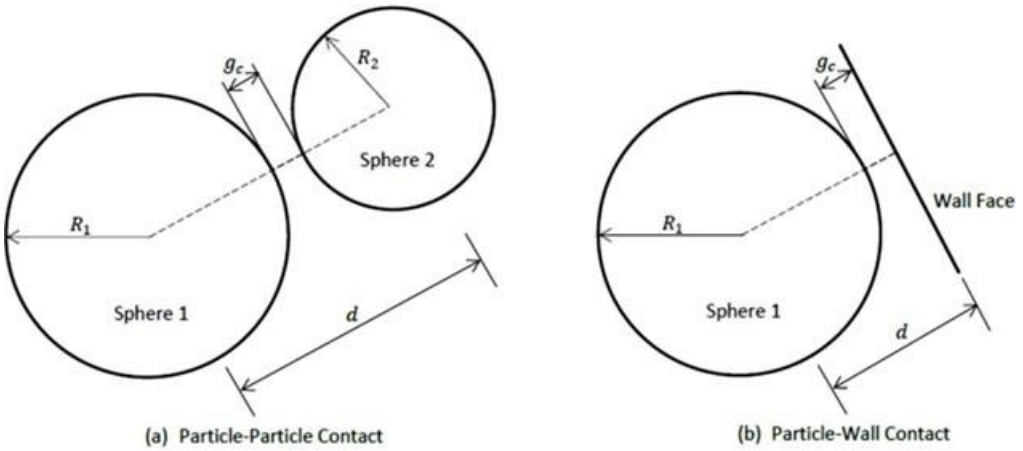

Figure 6 Contact detection between (a)particle-particle, (b) particle-wall

For particle-particle interaction, the contact gap is given by

$$g_c = d - (R_1 + R_2) \tag{2.1}$$

For particle-wall interaction, the contact gap is given by

$$g_c = d - R_1 \tag{2.2}$$

where

g_c = contact gap between 2 bodies
R_1 and R_2 = radii of two spheres
d = distance between two bodies
If $g_c > 0$, there is no contact between two bodies.
If $g_c < 0$, then the bodies are in contact, contact is called 'active' and there is an overlap.

For a detailed explanation of this concept, please refer Section 4.5.

Calculation of contact force and moments

Contact force between two bodies is defined as follows:

$$F_c = f(k, \beta, g_c) \tag{2.3}$$

where

k: stiffness of contact, β: damping of contact, F_c: net contact force
F_c is the resultant of normal (F_n) and shear (F_s) components of force.

Figure 7 represents the hypothetical arrangement of springs and dashpots used to derive the equations for the calculation of normal and shear contact forces. In Figure 7, term g_s is used instead of g_c, wherein g_s refers to the surface gap and is defined as the difference between the contact gap g_c and the reference gap g_r. So, when the reference gap g_r is zero, the notional surfaces coincide with the piece surfaces (see Figure 8). The contact is active if and only if the surface gap is less than or equal to zero and the force-displacement law is skipped for inactive contacts. For general considerations, $g_s = g_c$ since $g_r = 0$.

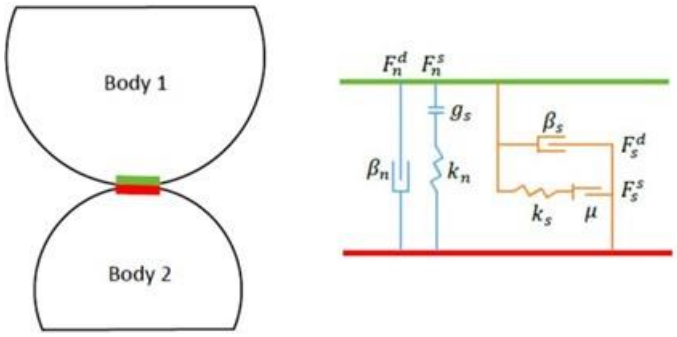

Figure 7 General arrangement of forcing and damping components at the contact point
(Itasca Consulting Group 2015)

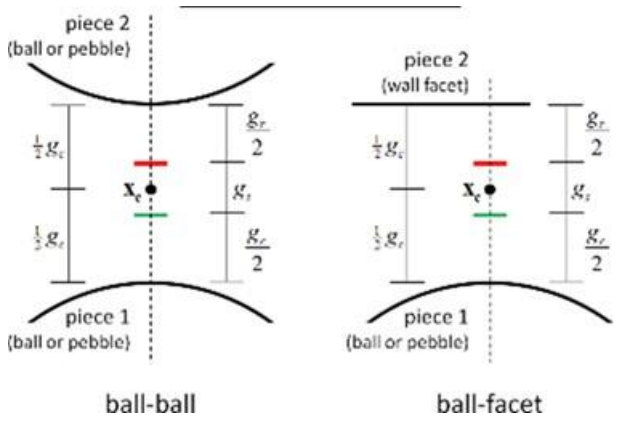

Figure 8 Surface Gap for linear based models (Itasca Consulting Group 2015)

The general normal component is thus calculated as:

$$F_n = F_n^s + F_n^d \tag{2.4}$$

Normal spring force F_n^s depends on the normal contact stiffness k_n and can be linearly or non-linearly dependent on contact gap g_c. Normal damping force F_n^d is dependent on the damping coefficient β_n. Element g_s ensures that the normal contact force is applied in compression only. Similarly, for the shear component,

$$F_s = F_s^s + F_s^d \tag{2.5}$$

Shear spring force F_s^s depends on the shear contact stiffness k_s and shear damping force F_s^d is dependent on the damping coefficient β_s. The total magnitude of contact force in shear F_s is limited by the maximum available frictional force as defined by the Coulomb's law of friction.

$$max(F_s) = F_s^{\mu} = -\mu F_n \tag{2.6}$$

Since, for spheres, the contact force passes through the contact point and hence the contact moment $M_c = 0$. So, spheres do not resist relative rotation about the point of mutual contact.

Springs and dashpots can be rearranged to model more complex granular behaviors such as particle fracture, inter-particle adhesive forces, etc. This introduces bonding forces at the points of contact between particles, and the spring forces to act in tension until they reach a specified maximum value. After this maximum value is attained, the bond breaks and particles separate. In such conditions, contact moment M_c may not always be zero. The exact equations for contact forces are discussed in Section 4.6.

DEM applicability for studying railway ballast

Multiple researchers have used DEM to study railway ballast to understand mechanical behavior, mesoscopic and macroscopic dynamics, particle kinematics, loading behavior and particle breakage. Discrete Element Models of railway ballast have been presented in the literature by

Tutumluer et al. (2007, 2011), Lu (2008), Irazábal González (2015), Cholet et al. (2001), Stahl, Konietzky (2011), Hossain et al. (2007) among many others.

Researchers like Saussine et al. (2006), Indraratna et al. (2012) and Lu and McDowell (2010, 2008) studied the ballast response to standard loading conditions like monotonic loading, cyclic triaxial loading and direct shear loading. Mechanical behavior of railway ballast due to cyclic loading from rail traffic has also been studied using DEM. A famous ballast box experiment to record track settlement data due to traffic loading was performed by Lim and McDowell (2007) and McDowell et al. (2005), which they then compared with their DEM simulation results. Indraratna et al. (2009) studied cyclic loading on ballast using simulation and tried validating it with the experimental data. Lobo-Guerrero, Vallejo (2006) also studied the response of the railway ballast to cyclic traffic loading.

Change in the properties of ballast due to variations in shape and size distribution (gradation) of its constituent particles is one of the interesting areas of research. The papers by Tutumluer et al. (2006, 2009) and Boler et al. (2014) presented spearheading analysis about the effects of ballast gradation on the track stability, tamping, aggregate packing and overall ballast performance. The difference in ballast response for the same identical loading conditions caused because of the different particle shapes has been explained by Lu and McDowell (2006).

Quite a good amount of literature is also available on the modeling of ballast using DEM for tamping operation. Zhou et al. (2012, 2012, 2015) have shown how the ballast mechanical properties and inter-particle contact forces are affected during the tamping process by changing the tamping tine frequencies and amplitudes. Parametric studies to understand the effects of tamping have also been performed by Saussine et al. (2008, 2009) and Perales et al. (2009, 2011). Another notable research in the tamping area has been done by Wang et al. (2012).

DEM has also been employed occasionally to model fouling and degradation of ballast particles during the service (Hossain et al. 2007, Thakur et al. 2012, Huang et al. 2009), comparison of ballast compaction by different maintenance methods (Ferellec et al. 2017), comparison of sleeper designs (Laryea et al. 2014).

Thus, DEM is a versatile tool for simulating the granular system. Its application for furthering scientific understanding of the properties and behavior of railway ballast is incontestable and it provides a huge advantage over conventional experimental methods that are very costly and take a lot of time. Modeling railway ballast is not that easy and some of the challenges are highlighted in the next section 2.4.

Challenges in Modeling Railway Ballast Using DEM

Accuracy and correctness of the DEM simulations are dependent on the following considerations regarding calibration of modeling parameters, validation of simulation results and numeric execution of the model (Jain 2017)

Computationally intensive

Computational requirements of a DEM simulation are contingent upon-

a) Number of bodies in the simulation model,

b) Complexity of particle shape,
c) Number of pair-wise contacts that need to be detected and resolved.
d) Magnitude of kinematic acceleration of the moving bodies.

Railway ballast consists of a large number of randomly shaped particles with varying sizes and a large number of contacts among each other. Also, since ballast particles are stiff and rigid, large accelerations occur due to steep changes in the contact forces. Smaller timestep values need to be used if the accelerations are large, to capture all the particle dynamics and important physics of the system. The simulation time may further increase because of hardware availability.

Contact Physics Calibration

Contact stiffness, damping coefficients, local damping, friction coefficient, etc. are required to define a contact model. Most of these coefficients have no physical significance and can't be measured directly via experimentation (e.g. damping). The values of these parameters are calibrated à posteriori by comparing simulation results with experimental results, often based on the overall collision time between two bodies and their coefficient of restitution (Stevens and Hrenya 2005, Pöschel and Schwager 2005, Navarro and Braun 2013 and Shäfer et al. 1996). Even though there may be anomalies in contact model application, overall macroscopic behavior of the granular assemblies can be still captured reliably and modeling and development of new contact laws to accurately represent the behavior of the granular system is an area of active research.

Experimental validation of simulation results

Accurate calibration of the contact model in the simulation requires extensive experimentation to study contact forces between bodies as a function of microscopic deformations of the contacting bodies during the collision. As discussed earlier, it is not practical to physically measure many of the simulation output variables such as compaction, inter-particle contact forces, distribution of contacts, etc. Additional experimentation may be needed to study and compare the practically observable effects of such fundamental simulation output variables. At last, granular systems are random, disordered and chaotic. For example, it has been shown by Esveld et al. (1988) that two identical rail tracks with identical ballast gradations and subsoil do not settle at the same rate when subjected to identical loading conditions. A DEM simulation thus gives one of many possible solutions for a particular granular assembly. The results obtained from a simulation or experiment may be different each time and thus the perfect behavior cannot be assured but only estimated (Pöschel and Schwager 2005).

MODELING DEVELOPMENT

Particle Flow Code (*PFC*) Introduction

PFC software developed by Itasca Consulting Group has been used to run the simulations and understand the tamping process (Itasca Consulting Group, Inc. 1994-2019). The information provided in this entire chapter is sourced from the *PFC* software documentation (Itasca Consulting Group 2015). *PFC3D* has both a graphical user interface and a computational engine of its own that provides a distinct-element modeling framework. *PFC* 's functionality is extended by the use of *FISH* language which is an embedded programming language using which new variables and functions can be defined.

Special particle generators may be implemented, servo controls may be applied, unusual distributions of properties may be specified and parametric studies may be automated using *FISH*. Error-checking that happens in *FISH* is less compared to most other compilers, so before using functions on real applications they should be tested on simple data sets. A detailed description about the use of *FISH* commands, rules, built-in functions, etc. can be found in Section *FISH Scripting* (Itasca Consulting Group 2015). *PFC* also allows users to write their code in Python programming language. It has the advantage of being faster, easy to use and has added functionality and the *FISH* environment is still available. An important difference between the Python and *FISH* programming environments is that the Python state is not saved in save files and is not affected by new or restore commands.

The particles used in *PFC* software have a finite mass and are rigid bodies that can move independent of each other undergoing a translational as well as a rotational motion. Internal forces and moments at each contact between two pieces are updated using contact mechanics with the help of particle-interaction laws. *PFC* due to its easily customizable design has been used for problems ranging from fundamental research on soil and rock behavior at the laboratory scale to many large scale applications such as slope stability and rockfall hazard mitigation, hydraulic fracturing, rock-tool interactions, bulk flow, mixing, conveying and compaction of aggregates and powders, blast furnace modeling, cave mining, etc. *PFC* has also been used to simulate a wide range of other applications in the fields of carbon nanotubes, molecular dynamics, magnetic materials, and medicine. Thus, the market for *PFC* software mainly is the research conducted in the area of Geo-sciences and Geotechnical Engineering. So, common particle size used for studies in *PFC* software ranges from few millimeters to study sand, ballast, etc. to an order of meters to study breaking of rocks, etc.

PFC Model

PFC model simulates the mechanical behavior of a system made up of arbitrarily shaped particles. Particle as per *PFC* is any object that occupies a finite amount of space. Newton's laws of motion are the fundamental relationship provider between particle motion and the forces that cause the motion. There may be a static equilibrium condition in the system in which case there is no motion or the particles may be moving in the system. A soft contact approach is used to model the behavior of contacts in which a finite normal stiffness is taken to represent the measurable stiffness that exists at a contact and the rigid particles are allowed to overlap in the vicinity of the contact point. Much more complex behavior can be simulated in *PFC* by allowing the particles to be bonded at contact points in a way that the bond gets broken if the inter-particle forces acting at that bond exceed the

bond strength and this in turn results in the development of tensile forces between particles. This can be used to model the formation of cracks in the rocks wherein a bigger rock is broken into smaller rock fragments.

The assumption of particle rigidity is good when most of the deformation in a physical system is accounted for movements along interfaces. This assumption helps to portray the deformation in a particle assembly tightly packed or in a granular assembly such as sand, since the sliding and rotation of the rigid particles causes deformation. Deformation is also caused here because of the opening and interlocking at interfaces, not from the individual particle deformation. *PFC* can also be used to study solids with defined boundary conditions and subjected to initial conditions. Such solids are treated as a compacted assembly of many small particles and thus their continuum behavior can be studied. So interior stresses for soils, solids like rock or plastics formed by powder compaction can be studied.

Multi-threading

PFC uses the optimal number of threads available on a laptop or workstation with multi- core processors by splitting the computational load during cycling among multiple threads. Nature of the simulation (static or dynamic), the number of model components (ball, clumps, walls, etc.), type of contact model used, amount of *FISH* used during cycling affects the run time of the simulation. Also, it is important to note that *FISH* processing is not multi- threaded. Since *PFC* does numerical simulations, it is obvious that there will be round-off errors that would occur due to the order in which computations are performed. For example, the order of contacts in two copies of the same *PFC* model would be different at the same time instance of simulation. So, contact forces would be summed to the balls in different orders, resulting in slightly different total forces at each ball. Repeatability of the simulation is thus affected. To overcome this issue, *PFC* by default uses a deterministic mode that ensures repeatability by enforcing ordering conventions but at the cost of efficiency. So this is a compromise between repeatability and fully functional multi-thread performance. The simulation runs for this project were done using deterministic mode only to ensure repeatability. The reason for doing this was to reproduce the exact model state again in order to debug the problems encountered while running the simulation model.

By default, *PFC* inserts a null contact model. The friction created at contacts, dissipation at contacts (viscous damping, inelastic contact laws, etc.) or dissipation introduced in the equations of motion of balls and/or clumps are three different ways in which energy dissipation may occur. The last one is called local damping which is usually set to a large value to accelerate convergence toward a stable configuration for quasi-static simulations. For dynamic analysis, this value should be lowered or even set to zero in some cases.

Bodies and Pieces

Balls, walls and clumps are called bodies whereas pebbles and facets are called pieces that make up these bodies (pebbles make clumps and facets make walls). Pieces are used for contact detection and resolution, whereas data collected using equations for the body are used to integrate the time evolution of the system. Hence, all contacts exist between pieces (e.g., ball-ball, ball-pebble, ball-facet and pebble-facet). It is important to note that in *PFC*, wall facets cannot be in contact with other wall facets and walls do not obey the equations of motion. Also, it is interesting to note that a ball is both a body and a piece.

Wall is a manifold, orientable and edge-connected surface made up of linear facets in 2D and triangular facets in 3D, wherein manifold means that the wall facets belonging to the same wall are not allowed to interpenetrate. These walls can be caused to deform by providing them velocity in the form of vertex velocity. Another way is to assign conveyor velocity to each facet, simulating nonzero velocities without making the walls move. This feature of applying velocity boundary conditions to walls allows them to be used for the purpose of compaction and confinement of balls or clumps. The equations of motion are not satisfied for each wall, unlike balls and clumps. The user has to specify the wall's motion and it remains constant irrespective of the contact forces acting on it.

Attributes and Properties

Intrinsic characteristics of model components (bodies, pieces, contacts) are called attributes. Examples of attributes are position, velocity, size, etc. which can be given to bodies, pieces and contacts. It is very important to note that properties are only exclusively applicable to pieces. Timestep determination is done automatically by *PFC* software. However, for a dynamic or highly agitated system timestep calculated automatically may not be apt. Also, since the automatic calculation of timestep is computationally intensive, *PFC* allows the user to input his own value. This can become tricky as the user has to be sure of the changes in the system configuration that may demand for a different value of the timestep for stability.

Properties are the characteristics held only by the pieces to define their surface conditions. Properties help the *PFC* software to understand how pieces interact with each other. Contact models used in *PFC* use piece properties to determine the resulting interaction of particles at the contacts.

Modeling Methodology

General Approach

It is impossible to obtain complete field data at a rock or soil site such as information about stresses, properties and discontinuities since they may vary considerably. This issue occurs for processes involving the interaction of many discrete objects. Also, an unknown contact behavior occurs at high packing densities in powder technology. The effect of the flow of the distribution of irregularities in the flow material cannot easily be quantified during the bulk flow of material. Since the input data available for such processes is limited, a numerical model should be employed to understand the dominant mechanisms affecting the behavior of the assembly of particles. If sufficient data and understanding of material behavior are available, *PFC* can directly be used in the design.

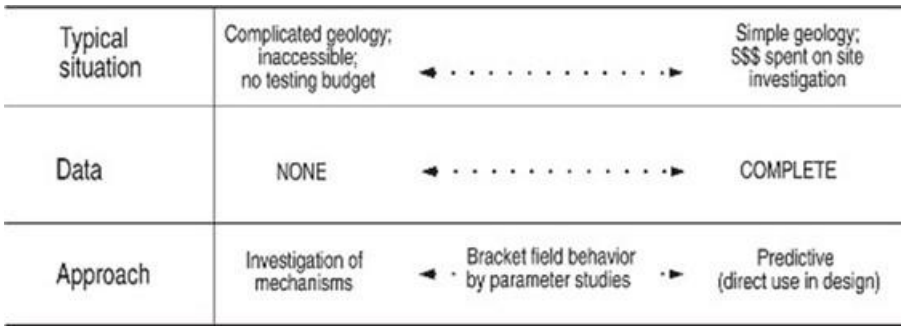

Figure 9 Spectrum of modeling situations (Itasca Consulting Group 2015)

PFC can be used either in a fully predictive mode (as shown in the right-hand side of Figure 9or as a numerical laboratory to test ideas as shown on the left-hand side. *PFC* provides a guideline to be followed if it is used as a numerical laboratory, to solve problems efficiently.

Step 1: Define the objective for the model analysis. It is often tempting to include complexity in a model just because it exists in reality. However, if the response of the model is influenced only slightly or if the complicating features are irrelevant to the model, they should be omitted.

Step 2: Create a conceptual picture of the physical system. A user must have an initial estimate of the response/behavior of the system under the given set of conditions. Several questions should be asked in this particular step. Example: Can the system become unstable at any point? Will the movements be large or small compared to the particle sizes? Is the system physically bounded or has limitless boundaries? Can the response be categorized as linear or non-linear? Are there any discontinuities in the system or will the material behave as a continuum? Does any geometric symmetry exist in the system? All such questions would define the characteristics of the numerical model, such as the design of the particle assembly, the type of contact model, the boundary conditions and the initial equilibrium state for the analysis.

Step 3: Construct and run simple idealized models. It is more efficient to construct and run simple test models before building the bigger complicated and detailed model. The user should breakdown the problems into smaller problems and solve the smallest problems individually. A simple model also helps understand the conceptual behavior of the system. It is important to note that in *PFC*, unlike continuum codes, the particle generation, boundary conditions and initial conditions are interrelated. Several model runs may be required to attain the final required initial state for analysis. The simple model results will further help us gain an insight into making the plan for the collection of data actually relevant to the analysis.

Step 4: Assemble problem-specific data. A model analysis requires a variety of data. For geomechanics, these include (Itasca Consulting Group 2019):

- geometry details (e.g., profile of underground openings, surface topography, dam profile, rock/soil structure);
- material behavior (e.g., post-failure behavior, elastic/plastic properties); geologic structure locations (e.g., joint sets, faults, bedding planes);
- initial conditions (e.g., pore pressures, in-situ state of stress, saturation); and
- external loading (e.g., pressurized cavern, explosive loading).

A reasonable range of parameters must be thus selected for the investigation of parameters involving large uncertainties.

Step 5: Prepare a series of detailed model runs. While preparing a set of model runs for calculation, several aspects should be considered. How much time would be required for each model calculation? Model runtimes shouldn't be excessive. Parameters should be varied on multiple computers to shorten the total computational time. The state of the model should be saved at several intermediate stages so that no information is lost in case of any accidental shutdown or if you need to re-run the simulation from a particular point with a new varied parameter this time. Also, this saves time since you don't have to run everything from the start again. The unbalanced force in the

system should always be monitored to check the equilibrium or granular-flow state at each stage of the analysis.

Step 6: Perform the model calculations. It is always a good idea to run the smaller blocks of code and ensure every line of code is working correctly. Then, one should do one or two detailed model runs before launching a series of runs. Once it has been ensured that response is as expected, several model data files can be linked together to run a number of simulations in sequence.

Step 7: Present results for interpretation. A graphical output of obtained results should be created for efficient analysis. Plots should clearly reflect the regions of interest from the analysis such as locations of calculated load concentrations or areas of stable movement versus unstable movement in the model. Also, the user should set up the model in a way that he has the numeric values of the parameters he is monitoring at any point for detailed understanding and interpretation.

Keeping all the above seven steps in mind, the *PFC* model for the tamping process is created and is explained in greater detail in Section 5.

Important Considerations

2D versus 3D Models Runtimes for 2D models are less compared to their 3D counterparts since they have lesser degrees of freedom (i.e., only two force components and one moment component exist in a *PFC2D* model, as opposed to the three force components and three moment components that exist in a three-dimensional particle assembly). So in earlier stages, to conceptualize the problem and understand the system response, it is advisable to run 2D simulations.

Porosity is defined in general as a ratio of void dimension to total dimension. In *PFC2D*, it is defined as the ratio of total void area to the total area and in *PFC3D*, it is defined as the ratio of total void volume to the total volume. There is no direct relation between 2D porosity and 3D porosity value for arbitrary assemblies of spherical particles. It is shown by Deresiewicz [11] that the closest of all regular packing of uniform spheres in 3D has a porosity of 0.2595, while the closest of all regular packing of uniform circles in 2D has a porosity of 0.0931. These presented values are the theoretical lowest values of porosity possible in the absence of any external compressive forces acting on the system and with no particle interpenetration. This shows that in general, the void space in a 3D assembly would be more than that in a 2D. The particles usually 'lock-up' before reaching this ideal optimal packing condition and thus in the real material, porosities are higher.

The Coordination number defined as the average number of contacts per particle is another important characteristic related to packing. In the paper presented by Agnolin and Roux (2007), the authors show that the coordination number, rather than the porosity, dictates the small- strain mechanical response of dense, isotropic, frictional assemblies in the rigid grain limit. An upper bound limit on the coordination number of dense assemblies of rigid frictional particles (in the absence of hyperstaticity) is shown by Roux (2000) in the form of equation $C_n \leq d(d + 1)$ for the general case, and $C_n \leq 2d$ for spherical particles where d denotes dimensionality. For frictionless particles, these inequalities in the equation become equalities.

Another big difference is of percolation. Small particles can easily seep through an assembly consisting of larger 3D particles, but this isn't possible in a packed 2D model irrespective of relative particle sizes.

Particle shape The fundamental element used by *PFC* software is a disk that has a unit thickness in 2D and for 3D, a sphere. If complex shapes have to be included in the simulation model, the following are the options available: cluster and clumps. Cluster involves bonding of two or more spherical particles together. Since the particles are rigid, but the contacts are soft, the response of the assembly is studied by adjusting the parameters at the particle and contact levels. This technique is employed by Cheng et al. (2003) to simulate the mechanical response of assemblies of such clusters or crushable agglomerates under isotropic compression and triaxial compression. Silica sand specimen's experimental data was compared to the numerical results obtained from the simulation and it verified that the model was capable of replicating the complex behavior of sands in relation to their strength, dilatancy and critical states. The resulting assembly that arises by considering a limiting case where every particle may be bonded to its neighbor, can be considered to be a solid that has elastic properties and is capable of fracturing when bonds break in a progressive manner. This is the main concept of the Bonded-Particle Model (BPM) methodology described by Potyondy and Cundall (2004) and Potyondy (2015) provides a comprehensive overview of the BPM methodology and its applications.

Clumps comprise of rigidly attached pebbles and clump itself is also a rigid body. The inertia parameters of the clump can be automatically computed from the shape geometry or from the outer surface delineated by the pebble distribution or by an input from the user.

Modeling of data limited systems A paper written by Starfield and Cundall (1988) should be consulted before any serious modeling with PFC software is attempted. In the field of geomechanics, field data such as in-situ stresses, material properties, and geological features will never be known completely. If there is massive uncertainty in the input data itself, it is not feasible to expect a perfect output response. However, the model may still help the designer or engineer to understand the behavior of the system or at least provide an intuition about the mechanisms that may occur in the process. It is worthless to develop a very large and complicated model considering all the uncertainties and input parameters making it as difficult to understand as the real case.

Modeling of chaotic systems In some models involving discontinuous materials, the results can be extremely sensitive to very small changes in initial conditions. This can be explained by two reasons. First, a certain geometric pattern may exist in the system which forces the system to choose randomly between two different outcomes and the further progress of simulation would de- pend on this particular outcome. Suppose there are two triangle-shaped blocks in contact with each other where one triangle is placed inversely on the top of another triangle such that they form an hour-glass kind of structure. Now if the upper triangle is forced downwards by providing it with a force, it can slide to the left or right of the lower triangle block and this would be governed by microscopic irregularities in geometry, properties or kinetic energy. Second, "softening" processes or in general cases of positive feedback may be another reason. A cycle of positive feedback can be illustrated by an example of a fairly uniform stress field, wherein a particular region that has more strain softens more and thereby attracts more strain and thus these small perturbations are magnified in the subsequent model evaluation.

The observed sensitivity of the computer simulation model to small changes in initial conditions or numerical factors is a reflection of a similar sensitivity in the real world to small irregularities. The best we can expect from such a model is a finite spectrum of expected behavior. One way would be to construct models with distributions of initial irregularities and each model should be run several times with different distributions of particle assemblies and this method is the same as taking averages to eliminate the uncertainties. Thus, if fluctuations still persist, it would be because of the imposed irregularities and not because of the numerical solution scheme employed by the software.

Localization, Physical Instability, and Path-Dependence. Bifurcation is a phenomenon in which a system's solution can take several paths depending on small changes in the initial conditions. For example, a shear test on an elastic/plastic material may either deform uniformly, or it may exhibit shear bands, in which the shear strain is localized rather than being uniformly distributed. Some programs are incapable of reproducing the band formation phenomenon but PFC can do it partly because it models the dynamic equations of motion (i.e., the kinetic energy that accompanies band formation is released and dissipated in a physically realistic way).

Chaos, physical instability and bifurcation are controlled by path-dependence. There is no one perfect or correct solution to a physical problem in most of the nonlinear inelastic systems that would satisfy equilibrium, compatibility, etc. unless a path is specified. If a path is not specified, all of the infinite possible solutions are correct. This becomes a matter of debate if a seemingly irrelevant parameter like damping is seen to affect the final result. For example, a simulation of a mining excavation with low damping may show a large overshoot and, hence, large final displacements, while high damping will eliminate the overshoot and give lower final displacements. If the excavation is done by an explosion (i.e., suddenly), then the solution with overshoot may be the appropriate one; if the excavation is done by pick and shovel (i.e., gradually), then the second case may be more appropriate. For cases in which path-dependence is an important factor, modeling should be done considering a sequential set of operations that mimics the system evolution in the real world.

Solution Procedure *PFC* asks for a logical flow to model the problem or process wherein four fundamental components of the problem as mentioned below should be specified: the model domain, an assembly of particles, contact behavior and material properties, and boundary and initial conditions.

The particle assembly consists of the locations and size distribution of particles. The type of response to be displayed by the model is controlled by the contact behavior and associated material properties. Boundary and initial conditions help describe the in-situ state. *PFC* uses an explicit time-marching method to solve the algebraic equations. A schematic procedure for the solution is shown in Figure 10.

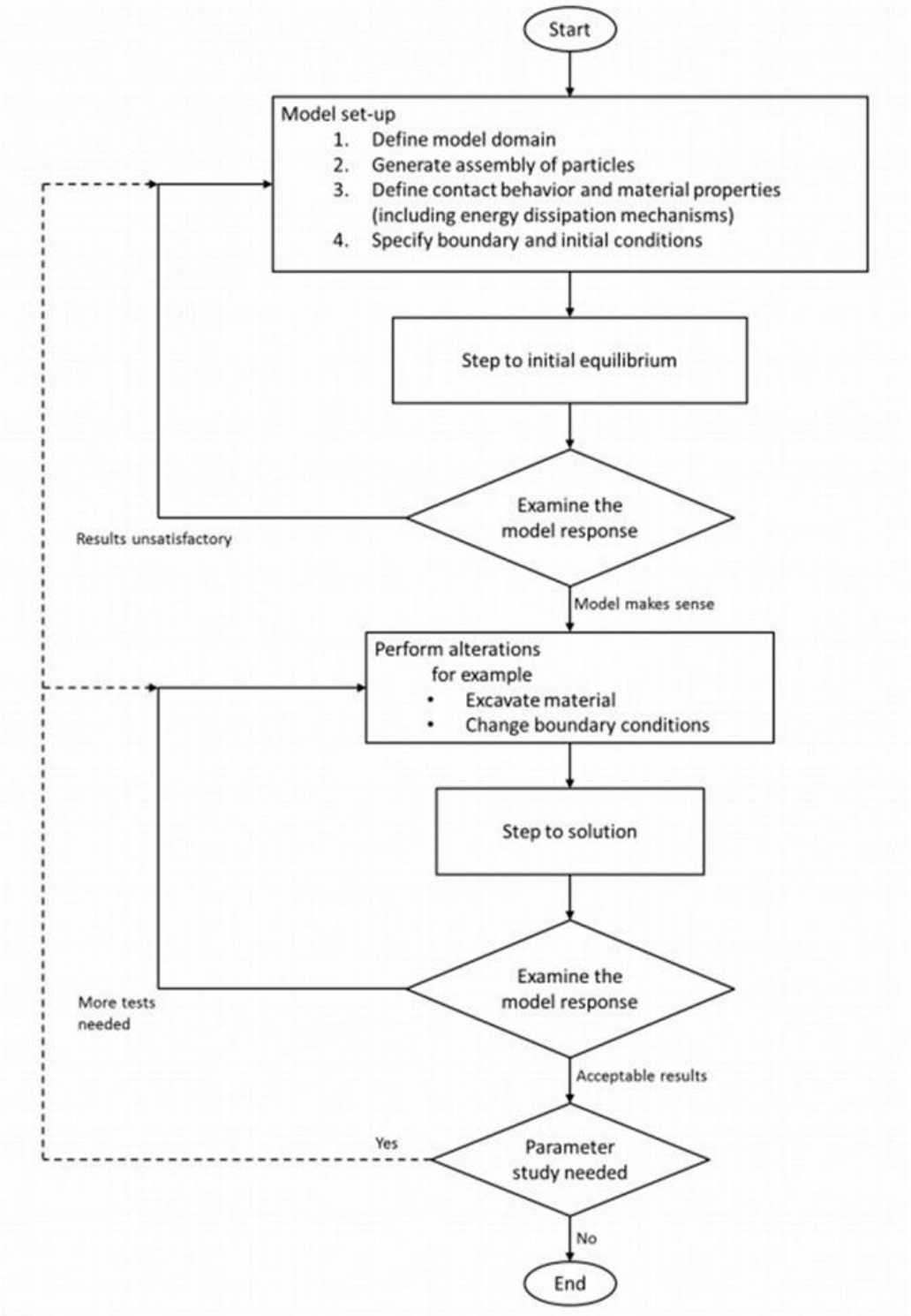

Figure 10 General solution procedure (Itasca Consulting Group 2015)

General Components

A particular instance of the DEM model, i.e., PFC model consists of bodies and mechanical contacts. A body is made out of one or more constituent pieces that make up the body surface. Bodies, pieces and contacts essentially make up the PFC Model Components which are discussed

in the following Section 4. Before discussing the Model components further, let us understand the general components used in PFC.

The domain is an axis-aligned bounding box that does not change its size except if it is distorted during cycling by setting non-zero strainrate conditions. It is a must to define the domain before proceeding to any other step in setting up the model. All the *PFC* model components can be created only after defining the domain and they all ought to lie within this domain. The domain boundary conditions are different from the model's boundary conditions. Following are the four domain boundary conditions:

Stop

This condition implies that if the body centroid falls outside the model domain, spin and the velocity of the respective body are zeroed.

Reflect

An opposite sign of velocity is applied to the body if its centroid falls out of the model domain meanwhile the spin is unchanged. This condition may lead to instabilities. It is important to note that this condition is not compatible with walls intersecting the domain.

Destroy

Here, balls, clumps and wall facets are deleted.

Periodic

Periodic condition causes the ball or clump whose centroid falls outside of the model domain to return inside the model from the other (opposite) side of the domain. This condition, to provide contact creation in a way as if the model is continuous, creates 'ghost' balls and clumps. This condition like reflect condition is not compatible with walls intersecting the domain.

Geometry

This allows the user to create, import and export geometric data. This helps in the creation of complex shapes that are not directly possible by using the PFC body generation commands like wall generate or ball generate. Geometry objects are not model components, but templates for model components can be created using the geometry imported shapes, which in turn can be used to create the model components.

History

Variables defined in the *PFC* simulation model can be sampled and stored for the entire model run using the *history* command. This allows the user to plot the values of important parameters with respect to time or other values recorded using the *history* command and identify trends or patterns in the results. It is important to note that the *history* command should be written before the *solve* or *cycle* commands to record that history throughout the solve runtime. The sampling rate of all the histories (default is 10 steps) for recording the values can be changed.

Measure

Measure command helps to record some important output parameters in a user-specified region of interest (area in 2D, volume in 3D) called the measurement region. Thus, a circular disk in 2D and sphere in 3D are the measurement regions that return average values of parameters computed for objects that lie fully within the measurement region or intersect with it. Quantities measured using the measure logic include Coordination number, porosity, stress and strain rate. A detailed explanation about the calculation of these quantities within the measurement region is explained in Section 5.4.

Application commands

These are some of the useful *PFC* commands that help start a simulation or present in- formation to the user. Some of the widely commands used from this category include call, calm, clean, cycle, fish, gui, new, quit, restore, save, set, solve, etc.

MODEL COMPONENTS

Particle Flow Code (*PFC*) Model Formulation

Cycle Sequence

The information presented in this chapter is taken from Itasca Consulting Group (2019). Balls, clumps, walls and contacts are referred to as the *PFC* model components because they constitute the physical components of a *PFC* model. The *PFC* model state refers to the current spatial configuration and state (e.g., velocities, forces, moments, etc.) of the model components at a specific time during a simulation. The final state is achieved by advancing the model state in time by a series of calculation cycles using *solve* or *cycle* commands. While cycling toward a terminal model state, it is possible to observe, study and query behavior of the system. The cycle sequence denotes a series of operations that are executed during a single *PFC* cycle. Figure 11depicts a simple version of the cycle sequence implemented in *PFC*. The operations in a single *PFC* cycle include:

Timestep Determination A valid, finite timestep is required to ensure the numerical stability of the model and that all contacts are created between pieces prior to the point that forces/moments develop between interacting bodies.

Law of Motion The position and velocity of each body/piece are updated using Newton's laws of motion using the current timestep and the forces/moments calculated during the previous cycle.

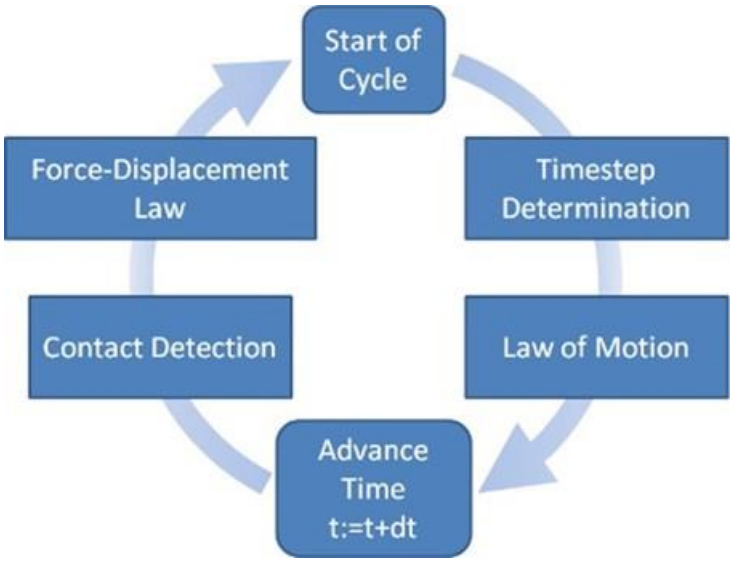

Figure 11 Cycle Sequence (Itasca Consulting Group 2019)

Advance Time The model time is advanced by adding the current timestep to the previous model time.

Contact Detection Contacts are dynamically created/deleted based on the current position of the pieces.

Force-Displacement Law The forces/moments developing at each contact are updated by the appropriate contact model using the current state of the pieces.

Conventions

The following sign conventions are used in PFC.

Direct Stress Positive stresses indicate tension and negative indicate compression.

Shear Stress **In Figure 12, a positive shear stress points in the positive direction of the coordinate axis of the second subscript if it acts on a surface with an outward normal in the positive direction. Conversely, the positive shear stress points in the negative direction of the coordinate axis of the second subscript if the outward normal of the surface is in the negative direction (not shown in the figure). The convention for the strain rate is analogous to that for stress. The distortion that arises due to positive and negative shear strain is shown in** Figure 13.

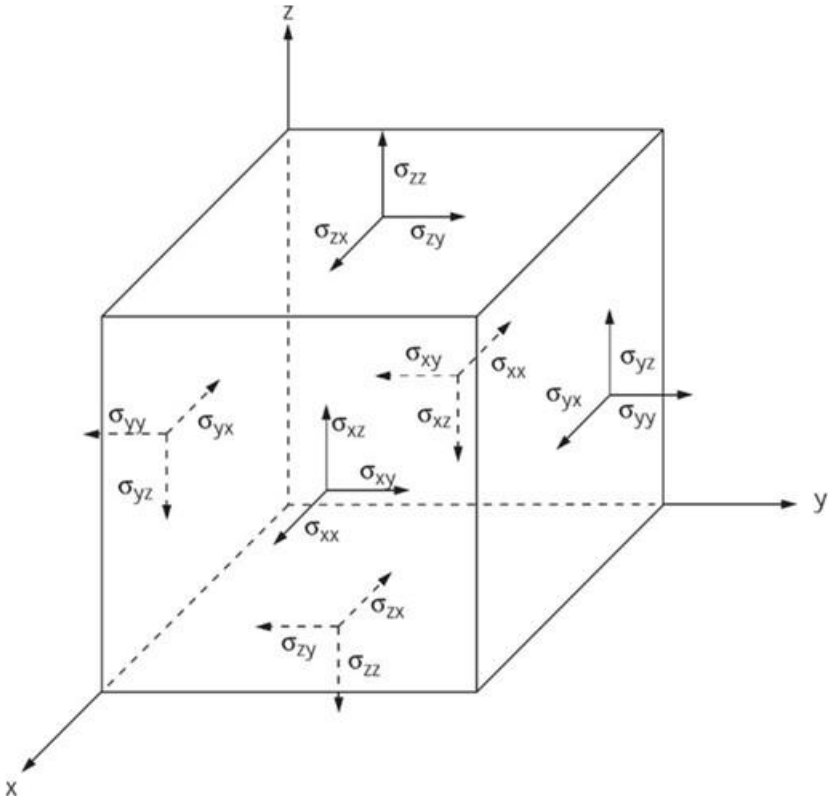

Figure 12 Sign convention for positive stress component (Itasca Consulting Group 2019)

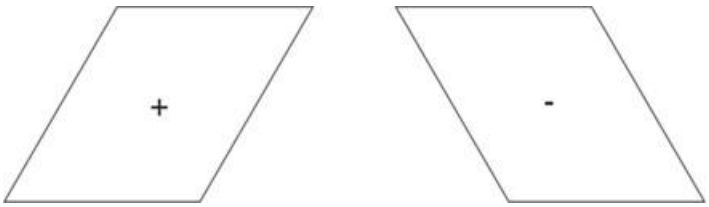

Figure 13 Positive and negative strain distortion (Itasca Consulting Group 2019)

Contact Force Contact forces can be resolved into two components, shear and normal with respect to the contact plane. Normal contact forces act normal (perpendicular) to the contact plane and shear contact forces act in the contact plane. Positive normal contact forces indicate compression.

Vector quantity The x-, y-, z- components of all vector quantities (e.g. forces, moments, displacements, velocities, etc.) are regarded as positive if they point in the directions of positive global x-, y-, z- coordinate system.

PFC doesn't have any particular unit system which it uses, i.e., it can accept any consistent set of engineering units. *PFC* does not allow the automatic conversion of a parameter value from one unit to another (e.g. from SI units to Imperial units).

PFC uses double-precision floating-point values for its calculations thereby providing 14 digits of precision. If you choose a system of units in which the coordinates are offset by a very large value, this may remove the effective digits of precision available to the user. So, it is a good practice to have the origin located near or inside the model extent and if possible at the centroid of the domain.

Contact Plane and Contact

Pebbles forming a clump can overlap each other, however, *PFC* does not create contact between these two pebbles of the same clump, instead, contacts are created if these pebbles interact with pieces of other bodies. Balls and clumps have mass properties (mass, centroid position, and inertia tensor) and loading conditions (the force/moment applied from contacts, a body force arising from gravity, and an externally applied force/moment) and thus obey Newton's laws of motion.

Contacts are created and deleted during the contact detection step of the cycle sequence based on piece proximity. A contact consists of a contact plane with location x_c, a normal direction n_c, and a coordinate system *nst*. The contact plane is centered within the interaction volume (either gap or overlap) of the two pieces, oriented tangential to the two pieces and rotated to ensure that relative motion of the piece surfaces remains symmetric with respect to the contact plane. A force F_c and a moment M_c is stored by every contact, in an equal and opposite sense of two bodies. However, contact models that simulate interaction at a distance, may not create forces and moments that are equal and opposite always. The internal forces/moments are updated by the particle-interaction law (contact model).

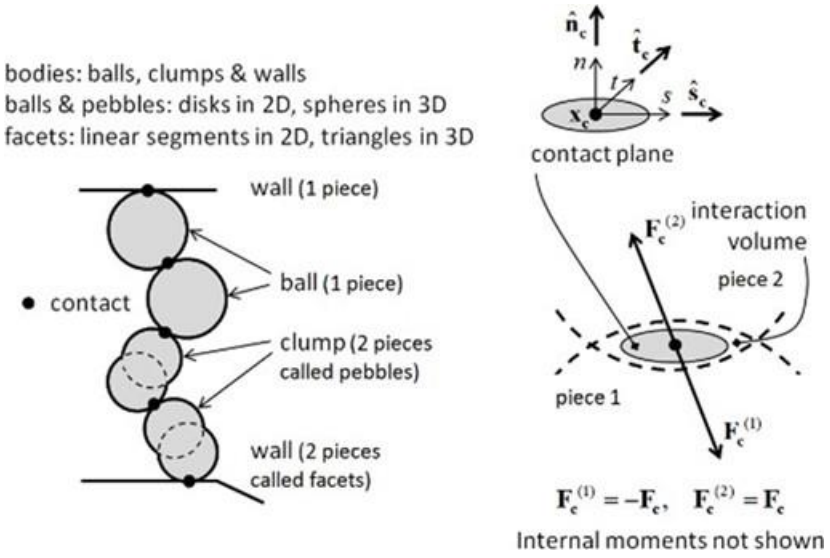

Figure 14 Contacts (left) and the contact plane (right) (Itasca Consulting Group 2019)

Cycling

PFC solves the model problem by running a series of cycles using the *solve* or *cycle* command. Cycling continues until one or more solve limits are reached. Cycle command is one- dimensional meaning it can only ensure the completion of one solve limit. Solve command however, has multiple solve limits (including the *FISH* functions) and cycling is finished when at least one solve limit is met. Figure 15 shows a schematic of executing a series of cycles. During the initialization phase, contacts are formed and broken, variables used during cycling are reset and the model state is checked for possible errors (like massless clumps or balls) that may prevent cycling. Before giving the user power to proceed with the next steps, in the finalization phase, contacts are created/deleted and data structures requiring validation are updated to ensure that the model is consistent and stable.

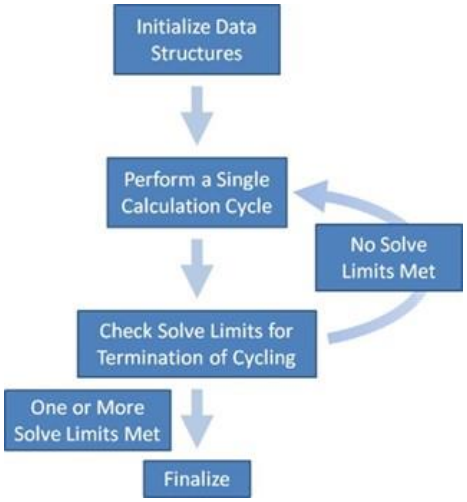

Figure 15 Schematic of a series of cycles (Itasca Consulting Group 2019)

Each calculation cycle goes through a sequence of operations termed cycle sequence which consists of an ordered set of operations where each operation has a floating-point number assigned to it as the cycle point.

Refer
for cycle operation and their associated cycle point.

Table 1 Cycle operations and associated cycle points

Cycle Point	Cycle Operation
-10.0	Validate data structures
0.0	Timestep determination
10.0	Law of motion (or update thermal bodies)
15.0	Body coupling between processes
20.0	Advance time
30.0	Update spatial searching data structures
35.0	Create/delete contacts
40.0	Force-displacement law (or thermal contact update)
42.0	Accumulate deterministic quantities
45.0	Contact coupling between processes

This system was introduced so that additional operations using *FISH* functions and *FISH* callbacks can be easily added into the cycle sequence. *FISH* callbacks can be explained as functions that are called during the execution of every cycle at a specific point in the cycle sequence. Callbacks cannot be installed with cycle points exactly equal to any predefined cycle points as mentioned in Table 1. It is important to note that callbacks cannot be installed between cycle points 40.0 and 42.0 since it may cause *PFC* to crash because of undefined behaviors, instability and interference with software's internal method of calculations. Also, the creation and deletion of model components (balls, clumps or pebbles and walls or facets) is only permitted before cycle point 0.0 (timestep evaluation). For a more detailed explanation of Cycle Operation as mentioned in Table 1, refer "Cycling" from *PFC* documentation (Itasca Consulting Group 2019).

Energy and Dissipation Mechanisms

Energies are accumulated every cycle for the model components. Mechanical energies in PFC fall into two categories: body energies and contact energies. Body motion creates mechanical body energies. For balls and clumps, these energies arise due to body forces (gravity loading and applied forces and moments), locally dissipated energy and kinetic energy. The boundary work is accumulated for walls and at each timestep, it is defined as the sum of the dot product of the force on a wall and the incremental displacement, and the dot product of the moment on the wall with the incremental angular displacement. Mechanical contact energies are directly defined in the contact models as explained in Section 4.5.

The energy in the particle system is dissipated via the contact models, through frictional sliding or viscous damping. But, these mechanisms may not be sufficient enough to reach a steady-state solution in a reasonable number of cycles. Thus, to remove additional kinetic energy a body-based damping scheme called local damping is used. Local damping acts on each ball or clump, applying a damping force with a magnitude proportional to the unbalanced force. For quasi-static simulations, non-zero local damping is

preferred whereas, for dynamic simulations, the local damping coefficient should be set to 0 or a very low value. For problems involving a free flight of particles, like particles falling under the action of gravity, and/or impact between particles, local damping is inappropriate and contact model based damping strategies should be used.

Balls A ball is the only body that also acts as a piece. A ball is a rigid disk with unit thickness in 2D and a sphere in 3D. A ball has a single set of surface properties. Balls can translate and rotate and they obey Newton's laws of motion. Thus, for this to be obeyed balls must have velocity conditions, mass properties and loading conditions defined. Properties that define mass are: mass, centroid position, inertia tensor (m, x, I). Density and radius (volume) define them. Externally applied force or moment, gravity and force and moment resulting from interaction with other pieces define the loading conditions.

Balls are introduced in the system in three different ways:
1. Creating one ball at a time (*ball create*)
2. Generating non-overlapping sets of balls (*ball generate*)
3. Distributing overlapping balls to match a specified size distribution (*ball distribute*)

Clumps

As discussed earlier in the previous sections, clump (a body) is a rigid collection of spherical pebbles (a piece). The surface of this clump which can help represent arbitrary shapes is defined by the positions of the pebbles and their respective radii. Each pebble can be assigned surface properties independently. Clumps are allowed to translate and rotate and like balls obey the equations of motion. Similar to balls, this requires the mass properties, loading conditions and velocity conditions exist and properties specifications are similar to the ball properties.
Mass properties are defined by:

1. The reference configuration and clump density. The mass properties, in this case, are found out using the positions and sizes of the pebbles in the reference configuration accounting for sphere overlap.
2. The reference configuration and (*m, x, I*) for the reference configuration. The mass properties are determined for this case by direct specification thereby separating the mass and pebble distributions in a way that pebbles are only used for surface representation.
3. A closed surface and associated mass properties given by the clump density. Here, automatic computation is used (Blow and Binstock 2004) assuming that the reference configuration is consistent with the closed surface.

As seen in the above three points, the reference configuration is a must as it defines the clump surface used for contact detection and resolution. Firstly, a set of clump templates that reflect the desired particles are described. A surface description in the form of a closed geometry of line segments in 2D, triangular facets in 3D, that is orientable is used to create the pebble distribution and calculate the mass properties. The clump template create bubble pack command is used to automatically create the pebbles to represent the surface to the desired fidelity. The surface descriptions being discussed in this section can be convex or concave. Once the user defines the clump templates, clumps can be inserted into the domain in three ways:

1. Replicating the clumps one at a time (*clump replicate*)

2. Generating non-overlapping sets of clumps (*clump generate*)
3. Distributing overlapping clumps to match a specified size distribution (*clump distribute*)

It is also possible to create clumps without the use of a clump template using clump create command. The command clump creates calculate calculates the actual mass properties based on the sphere distribution using a voxelization approach that accounts for the sphere overlaps or the user can specify the mass properties directly.

Walls

Line segments in 2D, triangular facets in 3D make up a manifold surface called 'wall'. Walls are bodies while facets are pieces. The surface of this model component named wall is defined by a mesh. The user can independently specify the surface properties for each facet. Walls can translate and rotate but they don't obey the equations of motion as it has been discussed several times before. If the wall specified is allowed to deform, then independent translational velocities can be applied to each vertex.

Walls can be created using wall create command and facets may be added one at a time using wall addfacet command. The facets must connect to a vertex in 2D, edge in 3D of previously existing facets. Simple wall configurations like box, plane, sphere, cylinder, cone, etc. can be generated using wall generate command. For complex shapes, one may import a wall using the geometry generated in some other modeling software using .stl or .dxf format of the geometry file.

A faceted wall is a body made of a triangular mesh of 'n' facets. Faceted walls are used to depict open or closed bounded surfaces, with or without missing facets. A large overlap is allowed between balls/clumps and wall facets. By default, all the wall sides are active. It is in the user's control if he wants to set a facet as inactive on either or both facet sides. PFC doesn't stop a ball or pebble from experiencing large forces when migrating from the inactive to the active side of a wall facet. These large forces may lead to unrealistic velocities.

Wall motion can be either rigid or deformable, but not both simultaneously. Inter-wall and intra-wall interactions are not allowed in PFC which in simple terms means that walls can't interact with other walls. Only one mechanical interaction (or one active mechanical contact) exists between two different bodies, but multiple mechanical contacts may exist between the constituent pieces of those bodies. Thus, it can be said that a mechanical interaction acts as a container unit, which stores a list of contacts between the constituent pieces along with the resultant force and moment acting at each of the contacts.

Faceted Wall Contact Resolution

As discussed, it is undesirable to have multiple contacts active during a ball-wall or clump- wall interaction. This is because the effective normal and shear contact stiffness would become multiplied by the contact stiffness for the case of a ball or a clump overlapping a single facet. The contact activity state in case of multiple contacts is found out using an associative logic as explained in the section Faceted Wall Contact Resolution of the topic Faceted Walls in *PFC* documentation (Itasca Consulting Group. Minneapolis, 2015). It is advised that one must go through this section to understand how only one of the multiple contacts created is deemed active.

Continuity of Contact-State Information

Also, in a case when multiple contacts between a ball/clump and a wall are created and as the ball/clump translates a particular distance over numerous timesteps along a single facet, the shear force incrementally accumulates. As the active contact is only one and it keeps on transitioning from one facet to another in the case of a multi-facet example, there is a problem of enforcing continuity in contact-state information in order for the two examples to yield identical results. If there is no continuity in the contact state information, it will lead to the loss of shear force when the ball starts moving. Each contact model defines the process by which contact state information is propagated, and this propagation is only possible for contacts having the same contact model. Also, if there is no link between the previously active contact in the previous timestep and a new active contact in the new subsequent timestep, contact state information is not propagated but the associative logic is used as a proxy for path construction in such cases. For detailed explanation and understanding, the user should read the material presented in the Section Continuity of Contact-State Information of the topic Faceted Walls in *PFC* documentation (Itasca Consulting Group 2015).

Contact Model

A generalized internal force is generated at the contacts when there is an interaction of par- ticles in the *PFC* model. This generalized internal force consists of a force and moment that act at the contact location in an equal and opposite sense on the two pieces. An additional moment due to the application of the force at the contact location is added to each piece.

These force and moment contributions are updated by the contact models that simulate surface-surface interactions. However, contact models simulating interaction at a distance update the force and two internal moments that need not be equal and opposite. Contacts are created and deleted automatically while the cycling of the *PFC* model happens, during the cycle point '35.0 - Create/delete contacts' as shown in Table 4.1. The Subsection Contact Resolution 4.5.1 specifies the kinematic variables used to define the motion of bodies and contacts. Contact models may be assigned manually or via the Contact Model Assignment Table (CMAT) as explained in Section 4.5.2.

Contact Resolution

When the contacts are created at Cycle point 35.0 as shown in

, contact resolution occurs. The contact state variables are updated as discussed in this section. The procedure using which these variables are calculated is described below.

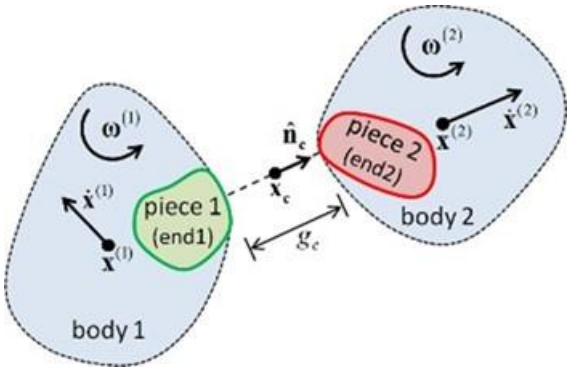

Figure 16 Contact between the pieces of two bodies (Itasca Consulting Group 2015)

The contact shown in Figure 16shows a contact formed between pieces of two bodies. Each contact has two ends, end1 and end2 with the associated pieces and bodies labeled 1 and 2. Rigid bodies motion is defined by its rotational velocity ($\omega^{(b)}$) and the translational velocity ($\dot{x}^{(b)}$) of its centroid ($x^{(b)}$).

The first contact state variables to be updated are: the effective inertial mass of the contact(m_c), the location (x_c), normal direction ($\hat{n}_t$) and coordinate system (*nst*) of the contact plane and the contact gap (g_c) which is the minimal signed distance separating the piece surfaces. The contact mass is given by

$$m_c = \begin{matrix} \dfrac{m^{(1)}m^{(2)}}{m^{(1)}+m^{(2)}} & ball-ball\ (particle-particle) \\ m^{(1)} & ball-ball\ (particle-facet) \end{matrix} \tag{4.1}$$

where $m^{(b)}$ is the mass of body (b) forming a contact with another body. The surface geometry of the two contacting pieces in the contact vicinity decides the location, normal direction and gap. This is defined in the section Contact Plane of the topic Contact Resolution [19]. Contact activity state is updated next using the updated contact gap. If the contact is not active, an additional check is performed to check if it could become active in the near future. Both the active and could-be-active contacts participate in the timestep estimation procedure. For an active contact, the variables defining the relative motion of the piece surfaces are computed as described in the Section Relative Motion at a Contact of the topic Contact Resolution (Itasca Consulting Group. Minneapolis, 2015).

Contact Model Assignment Table (CMAT)

The Contact Model Assignment Table (CMAT) controls the assignment of contact models and the properties associated with the contact models to the newly created contacts. CMAT also provides the detection distances used by the contact-creation procedure. CMAT specifies an ordered set of slots as well as a default slot for each contact type, wherein a single slot contains a contact model and its specifications like properties and methods. When a new contact is created, it is mapped into one of the slots in the CMAT and then information from this slot is used by the *PFC* to assign contact model and properties to the system. The slot mapping happens as described below:

1. Non-default slot is visited first in order and if a contact is within its range, then that slot is selected.
2. If no slot has been selected, then the default slot corresponding to a contact type is selected.

The CMAT can also be applied to specific contacts that are a part of a specific range (range in terms of position, group names, etc.).

Contact Model Framework
Before studying the contact models, it is necessary to understand the concepts and the terminology involved. The contact model discussion revolves around the force-displacement behavior at the contact but it excludes the macroscopic behavior of the granular assembly. The concepts associated with contact models are discussed below:

1. <u>Activity-Deletion Criteria</u>

A contact model contains a particle-interaction law which is entered if the contact is active and otherwise the internal force and moment for the created contact are set to zero. A contact model can control the activity state using the activity criterion, wherein if a contact is deemed inactive then it won't have any particle-interaction law assigned and thereby its computational speed would increase. Also, a contact model can prevent a contact from getting deleted by the contact detection logic at Cycle point 35.0 in

.

2. Force-Displacement Law

The formulae related to force, moments and displacements are expressed in terms of internal parameters using rheological components which are shown in Figure 17.

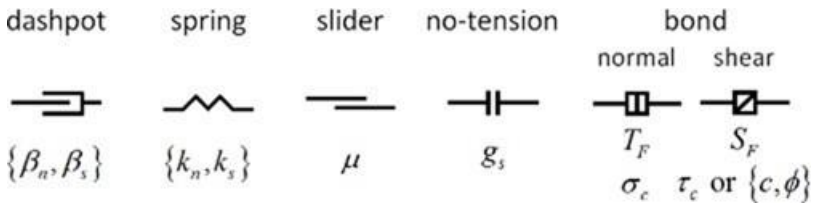

Figure 17 Icons and parameters associated with rheological components

3. Energy Partitions

Energy partitions keep a track of the energy that is stored or dissipated by the contact model. For example, the linear model stores energy as strain energy and dissipates energy via slip and dashpots.

4. Contact Properties

Properties are name-value pairs. Inheritable properties are the properties whose values can be derived from the surface properties of the two pieces and thus they get updated if the surface property of either piece in contact is modified. The only condition for this to happen is that the inheritance flag should be set to true and both the surface properties should have the same name as the inheritable property. For each contact mode, a properties table provides a concise property reference. The property table gives details about the following:

1. The keyword
2. The mathematical symbol
3. Property description
4. Value type specifying if its a boolean(BOOL), integer(INT), floating-point number (FLT) or a vector(VEC)
5. The range over which the property may vary
6. The default value of the property
7. If the property is modifiable (Only modifiable properties are writable)
8. If the property is inheritable

5. Methods

Method defines contact properties for a contact model in a special way. The difference be- tween methods and contact model properties is that the methods do not correspond directly with any property and they may modify multiple contact properties.

Built-in Contact Models

PFC allows users to create their own custom contact models using the C++ plug-in option. Built-in contact models in the *PFC* software are as described in **Table 2**

Table 2 Built-in Contact Models (Itasca Consulting Group 2015)

Keyword	Name	Behavior Summary
null	null	No mechanical interaction
linear	linear	Linear elastic law with viscous dashpots
linearcbond	linear contact bond	Linear model with contact bonding for BPM
linearpbond	linear parallel bond	Linear model with parallel bonding for BPM
hertz	hertz	Non-linear elastic law with viscous dashpots for impact problems
hysteretic	hysteretic	Non-linear elastic law with viscous dashpots for impact problems—directly specify the normal restitution coefficient
smoothjoint	smooth joint	Frictional/bonded interface for BPM
flatjoint	flat joint	Faceted/bonded interface with partial damage for BPM
rrlinear	rolling resistance linear	Linear elastic law with viscous dashpots and rolling resistance mechanism for granular applications
burger	Burger's	Creep mechanisms using a Kelvin model and a Maxwell model connected in series in both normal and shear directions

Linear based models

The linear, rolling resistance linear, linear contact bond, and linear parallel bond contact models share many characteristics and are called linear-based models. The linear-based models provide two standard bonding behaviors embodied in the contact bonds and parallel bonds. These bonds can be installed at both ball-ball and ball-facet contacts. One can think of these bonds as some glue joining the contact pieces. This contact-bond glue is so small that it acts only at the contact point, while the parallel-bond glue (comparatively bigger size) acts over a (rectangular in 2D; circular in 3D) cross-section lying between the contacting pieces. Only force is transmitted by the contact bond but the parallel bond can transmit both a force and a moment. By default, none of the pieces are bonded. Bonds are created by invoking the bond method and removed when their strength is exceeded or by invoking the unbond method.

Comparison of Contact Models

Contact models express the contact force as a function of the overlap at the contact point, g_c. Each of the nine Built-in contact models as highlighted in Subsection 4.5.4 is suitable for a particular type of application and focuses on different aspects of the granular behavior. Linear contact model, linear contact bond model, rolling resistance linear model and the Hertz contact model are suited for the analysis of granular systems. The above-mentioned contact models are the ones most frequently used to model the railway ballast.

Null

This is the basic contact model applied to the newly created contacts unless a specific contact model is applied. The null model has a generalized internal force of zero ($F_c = M_c = 0$).

Linear

Linear model's linear and dashpot components act in parallel with each other. The linear component provides linear elastic (no-tension) frictional behavior while the dashpot compo- nent provides viscous behavior. The specialty of this model is that both of these components act over a very small area and thus they transmit only a force. The linear model with inactive dashpots and a reference gap of zero is explained by Cundall and Strack (1979). The important equations pertaining to the linear model are defined below: Normal linear spring force, F_n^l

$$F_n^1 = \begin{matrix} k_n g_c & g_c < 0 \\ 0 & otherwise \end{matrix} \tag{4.2}$$

where k_n is the normal contact spring stiffness.

Shear linear spring force, F_n^l

F_s^l is computed in an incremental manner by a multistep procedure. First, a trial shear force, F_s^* is calculated as

$$F_s^* = F_s^l|_0 - k_s \Delta\delta_s \tag{4.3}$$

where

$F_s^l|_0$ is the shear force at the beginning of the timestep,
k_s is the shear contact spring stiffness,
$\Delta\delta_s$ is the incremental shear displacement during the timestep.

The shear strength of the contact F_s^μ is determined by the limit of Coulomb's friction.

$$F_s^\mu = \mu F_n^l \tag{4.4}$$

Finally, the shear contact force F_s^l is calculated as

$$F_s^l = \begin{matrix} F_s^* & \|F_s^*\| \le F_s^u\| \\ F_s^u - \dfrac{F_s^*}{\|F_s^*\|} & otherwise \end{matrix} \tag{4.5}$$

The slip rate s is updated to set the sliding status of the contact

$$s = \begin{matrix} true\ (sliding) & \|F_s^l\| = F_s^u \\ false\ (not\ sliding) & otherwise \end{matrix} \tag{4.6}$$

Normal damping force, F_n^d

$$F_n^d = \left(2\beta\sqrt{m_c k_n}\right)\dot{\delta}_n \tag{4.7}$$

where β_n: normal damping coefficient,

$\dot{\delta}_n$: relative normal translational velocity and

m_c: equivalent mass of the contact as defined in Equation 4.1.

Keyword	Symbol	Description	Type	Range	Default	Modifiable	Inheritable
linear		Model name					
Linear Group							
kn	k_n	Normal stiffness [force/length]	FLT	$[0.0, +\infty)$	0.0	YES	YES
ks	k_s	Shear stiffness [force/length]	FLT	$[0.0, +\infty)$	0.0	YES	YES
fric	μ	Friction coefficient [-]	FLT	$[0.0, +\infty)$	0.0	YES	YES
rgap	g_r	Reference gap [length]	FLT	$\mathbb{R}$	0.0	YES	NO
lin_mode	M_l	Normal-force update mode [-] 0: update is absolute 1: update is incremental	INT	{0,1}	0	YES	NO
emod	E^*	Effective modulus [force/area]	FLT	$[0.0, +\infty)$	0.0	NO	N/A
kratio	κ^*	Normal-to-shear stiffness ratio [-] $\kappa^* \equiv \frac{k_n}{k_s}$	FLT	$[0.0, +\infty)^*$	0.0 *	NO	N/A
lin_slip	s	Slip state [-] true: slipping false: not slipping	BOOL	{false,true}	false	NO	N/A
lin_force	$\mathbf{F}^l$	Linear force (contact plane coord. system) $\left(-F_n^l, F_{ss}^l, F_{st}^l\right)$ (2D model: $F_{ss}^l \equiv 0$)	VEC	$\mathbb{R}^3$	**0**	YES	NO
Dashpot Group							
dp_nratio	β_n	Normal critical damping ratio [-]	FLT	[0.0, 1.0]	0.0	YES	NO
dp_sratio	β_s	Shear critical damping ratio [-]	FLT	[0.0, 1.0]	0.0	YES	NO
dp_mode	M_d	Dashpot mode [-] 0: full normal & full shear 1: no-tension normal & full shear 2: full normal & slip-cut shear 3: no-tension normal & slip-cut shear	INT	{0,1,2,3}	0	YES	NO
dp_force	$\mathbf{F}^d$	Dashpot force (contact plane coord. system) $\left(-F_n^d, F_{ss}^d, F_{st}^d\right)$ (2D model: $F_{ss}^d \equiv 0$)	VEC	$\mathbb{R}^3$	**0**	NO	NO

* By convention, $\kappa^* = 0.0$ if either the normal or the shear stiffness is 0.

Figure 18 Properties of a linear model (Itasca Consulting Group 2015)

Shear damping force, F_s^d

$$F_s^d = \begin{matrix} \left(2\beta\sqrt{m_c k_s}\right)\dot{\delta}_n & s = false \\ 0 & s = true \end{matrix} \tag{4.8}$$

The properties related to the linear model are defined in Figure 4.8 below:

Hertz

The Hertz contact model consists of a nonlinear formulation based on an approximation of the theory of Mindlin (1953). This model produces normal as well as shear forces and viscous dashpots may be considered for further energy dissipation in simulations involving impact. Only force is transmitted through the components. The important equations pertaining to the hertz model are defined below:

Normal hertz spring force, $F_n{}^h$

$$F_n^h = \begin{matrix} -h_n|g_c| & g_c < 0 \\ 0 & otherwise \end{matrix} \tag{4.9}$$

$$h_n = \frac{2\bar{G}\sqrt{2\bar{G}}}{3(1-\bar{v})} \tag{4.10}$$

$$\bar{G} = \frac{G_1 G_2}{2} \tag{4.11}$$

$$\bar{v} = \frac{v_1 + v_2}{2} \tag{4.12}$$

$$\frac{1}{\bar{R}} = \frac{1}{2}\left(\frac{1}{R_1} + \frac{1}{R_2}\right) \tag{4.13}$$

where

α: model exponent, h_n: normal Hertzian contact stiffness,
G_1 and G_2: shear moduli of the two bodies in contact,
v_1 and v_2: Poisson's ratios of the two bodies in contact, and
R_1 and R_2: Radii of the two particles in contact. For a wall, R_2=0.

Shear hertz spring force, F_s^h

F_s^h is computed in an incremental manner by a multistep procedure. First, a trial shear force F_s^* is calculated as

$$F_s^* = F_s^h|_0 + h_s \Delta\delta_s \tag{4.14}$$

$$h_s = \frac{2(1-v)}{2-\bar{v}} a h_n (F_n^h)^{\frac{a-1}{a}} \tag{4.15}$$

where $F_s^h|_0$: shear force at the beginning of the timestep,
h_s: shear contact stiffness, and
$\Delta\delta_s$: incremental shear displacement during the timestep.
The shear strength of the contact F_s^μ is determined by the limit of coulomb's friction.
'

$$F_s^\mu = -\mu F_n^h \tag{4.16}$$

At last, the shear contact force F_s^l is calculated as

$$F_s^h = \begin{matrix} F_s^* & \|F_s^*\| \le F_s^u\| \\ F_s^u - \frac{F_s^*}{\|F_s^*\|} & otherwise \end{matrix} \tag{4.17}$$

The slip rate s is updated to set the sliding status of the contact

$$s = \begin{matrix} true\ (sliding) & \|F_s^u\| = F_s^u \\ false\ (not\ sliding) & otherwise \end{matrix} \tag{4.18}$$

Normal damping force, F_n^d

$$F_n^d = \left(2\beta\sqrt{m_c k_n}\right)\dot{\delta}_n \tag{4.19}$$

$$k_n = \alpha h_n \delta^{\alpha-1} \tag{4.20}$$

where k_n: normal tangent stiffness,
$\dot{\delta}_n$: relative normal translational velocity and
m_c: equivalent mass of the contact as defined in Equation 4.1.

Shear linear spring force, F_n^d

$$F_n^d = \left(2\beta\sqrt{m_c k_n}\right)\dot{\delta}_n \tag{4.21}$$

where β_s: shear damping coefficient and
$\dot{\delta}_s$: relative shear translational velocity.

The properties related to the hertz model are defined in the figure below:

Keyword	Symbol	Description	Type	Range	Default	Modifiable	Inheritable
hertz		Model name					
Hertz Group							
rgap	g_r	Reference gap [length]	FLT	$\mathbb{R}$	0.0	YES	NO
hz_shear	G	Shear modulus [stress]	FLT	$[0.0, +\infty)$	0.0	YES	YES
hz_poiss	ν	Poisson's ratio [-]	FLT	$(-1.0, 0.5]$	0.0	YES	YES
fric	μ	Friction coefficient [-]	FLT	$[0.0, +\infty)$	0.0	YES	YES
hz_mode	M_s	Shear-force scaling mode [-] 0: no scaling 1: scaling is active	INT	{0; 1}	0	YES	NO
hz_alpha	α_h	Exponent [-]	FLT	$[0.0, +\infty)$	1.5	YES	NO
hz_slip	s	Slip state [-]	BOOL	{false,true}	false	NO	N/A
hz_force	$\mathbf{F^h}$	Hertz force (contact plane coord. system) $(-F_n^h, F_{ss}^h, F_{st}^h)$ (2D model: $F_{ss}^h \equiv 0$)	VEC	$\mathbb{R}^3$	**0**	YES	NO
Dashpot Group							
dp_nratio	β_n	Normal critical damping ratio [-]	FLT	$[0.0, 1.0]$	0.0	YES	NO
dp_sratio	β_s	Shear critical damping ratio [-]	FLT	$[0.0, 1.0]$	0.0	YES	NO
dp_alpha	α_d	Exponent [-]	FLT	$[0.0, +\infty)$	0.0	YES	NO
dp_mode	M_d	Dashpot mode [-] 0: always active 1: no tension 2: no shear damping if s=1 3: combine modes 1 & 2	INT	{0;1;2;3}	0	YES	NO
dp_force	$\mathbf{F^d}$	Dashpot force (contact plane coord. system) $(-F_n^d, F_{ss}^d, F_{st}^d)$ (2D model: $F_{ss}^d \equiv 0$)	VEC	$\mathbb{R}^3$	**0**	NO	NO

Figure 19 Properties of a hertz model (Itasca Consulting Group 2015)

Selection of Appropriate Contact Model

The performance and accuracy of a contact model are often judged by the validation of the coefficient of restitution and for how much time is the pair of bodies in contact during the collision. The coefficient of restitution is defined as the ratio of the relative velocity of the particle after a collision to their relative velocity before the collision. It is a measure of elasticity of the collision and comparing the simulated value of the coefficient of restitution to the experimental results is a pretty common way of accepting a contact model for a given use. The duration of the collision isn't used much to determine the accuracy of a contact model. This information is also presented by Stevens, Hrenya (2005) wherein they created a setup to experimentally validate various contact models by studying their coefficient of restitution and collision duration for a pair of colliding spheres. They were able to show that the Hertzian contact model is closer to experimentally observed behavior than the Linear model. The graph of contact force plotted against overlap was much better in case of the Hertzian model. Also, the Hertz model was able to predict the collision time within 10% of experimental values, however, the coefficient of restitution didn't follow the expected realistic experimental trend for any of the contact models studied by the researchers.

Railway ballast is highly stiff and the impact velocities generated are small and thus, Goldsmith, Frasier (1961) established that the Hertz model is well suited for modeling railway ballast. Another research conducted by Lim, McDowell (2005) also suggests the use of the Hertz contact model for railway ballast. They used three different experimental methods and were better able to predict the variability in contact stiffness of ballast particles due to changing contact forces using the Hertz contact model. Another important factor to be considered is that the stiffness constants used in the linear model, k_n and k_s, do not represent any real physical quantity and can only be heuristically

established by performing some sort of experimental or calibration tests and comparing it with simulation results. These parameters can thus only be assessed à posteriori, after analyzing the results from the simulations. Pöschel, Schwager (2005) also showed that the choice of contact model does not have any visible significant effect on the overall computational time of the simulation. The stiffness constants defined in the Hertz model, h_n and h_s relate to the material properties and can be defined by the Equations 4.10 and 4.15. Thus, since these parameters are easier to determine and since the Hertz model depicts better recreation of the physical contact behavior, the Hertz model is chosen for this project.

SIMULATION MODEL

While developing the actual model, all the factors described in Section 3.2 were considered and the final model developed takes care of not violating the specifics mentioned. The simulation model created for this project used the *FISH* environment and *PFC* commands and didn't involve the use of Python. The values for the parameters used have been defined in the upcoming sections along with their source of reference.

Comparison of Particle Shapes

Modeling ballast using spheres

If the ballast is modeled using spherical particles, shape information is discarded and only size information needs to be provided. The size of a particle is the minimum sized mesh or sieve through which it can pass. The simplest case is the one where all spheres have the same size (radius) and size distribution information is not required, otherwise, the size distribution of the ballast must be similar to the size distribution of sample ballast being modeled. *PFC* allows the use of predefined distributions like Gaussian and allows the user to create his own size distribution.

Modeling ballast using clumps

Here, along with size and size distribution, shape information needs to be provided as well. *PFC3D* accepts the 3D scanned surface profiles of stones to be modeled. This 3D scanned profile imported as a '.stl' file is used to create a clump template which is a reduced version of clump itself and holds the surface description for the calculation of inertial parameters and clump visualization. Then clump is generated using this pre-defined clump template shape and size specifications. A clump though is a collection of many spheres (called pebbles), acts as a single rigid body. Figure 20 Clump generation from a 3D scan shows how a clump is generated using a 3D scan of an actual ballast stone particle.

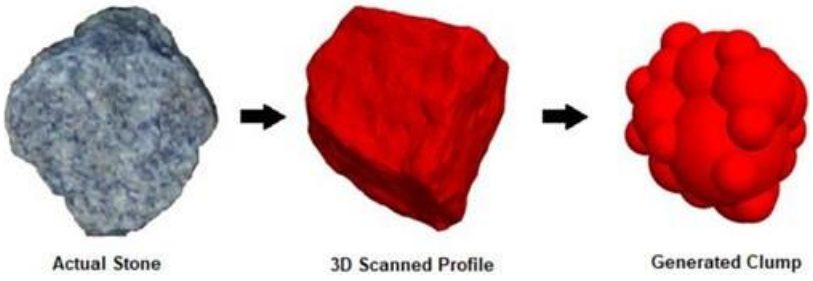

Figure 20 Clump generation from a 3D scan

The arrangement and size of the spheres used in a clump are governed by Bubble Pack algorithm (Taghavi 2011) in this research, although there are other ways within *PFC* to generate the clumps and specify their inertial parameters. Clump template's inertial attributes can be defined directly (volume, inertia, position, etc.) or by specifying their calculation from their pebble distribution (*pebcalculate* command) or by surface description (*surfcalculate* command). Bubble pack command is a part of the *clump template* command. Two important keywords required to be specified to make bubble pack algorithm work are the *distance* and *ratio*. *distance* links to an angular measure of smoothness in degrees $0 <$ value < 180 as defined in (Taghavi 2011). ratio which ranges from $0 <$ value < 1, indicates the ratio of the smallest to the largest sphere used in filling up

the clump shape. The algorithm starts by including the largest sphere first and then the smaller spheres would be included as pebbles if the ratio of their radii to the largest sphere radii is above the value of ratio. 0 value of distance means that spheres just touch at one point externally (do not overlap) whereas 180 means spheres just touch at one point internally in a way that one sphere is inside the another (complete overlap). The greater the distance value, smoother is the pebble distribution and more detailed the clump would eventually become. More detail about this can be found out in the description of clump template command in the PFC documentation (Itasca Consulting Group. Minneapolis, 2015). In short, this algorithm helps the user to manipulate the number of spheres to be used as pebbles inside the clumps, plus control their radii and locations, thus allowing full control of the level of detail of surface profile of the clumps.

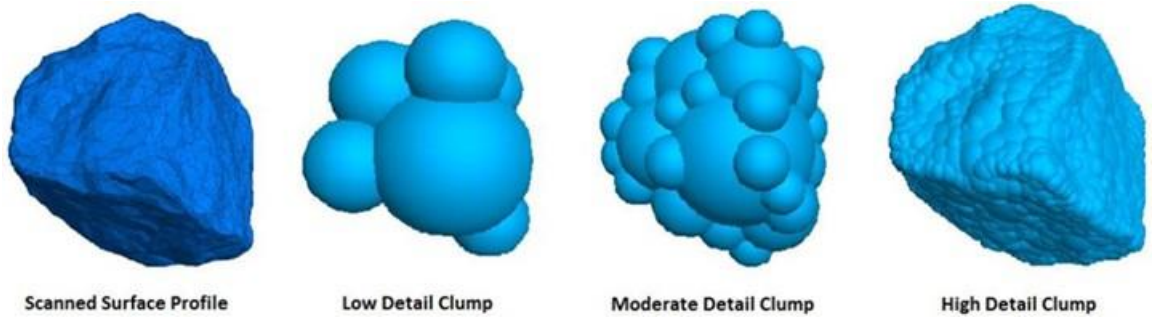

Figure 21 Surface detail variation of a generated clump

Figure 21taken from Jain (2017) shows the difference in surface detail description by changing the two values *ratio* and *distance*. A highly detailed clump would increase the computational requirements of the simulation. Frictional properties and collision behavior of clumps are affected by the size and the density of their constituent spheres (pebbles) (Abbaspour-Fard 2000).

Modeling ballast using convexblocks

An alternate way to model ballast particles is by the use of convex blocks, i.e., convex rigid polygons in 2D and polyhedra in 3D. A polyhedral closed surface made of small planar elements is shown in Figure 22.

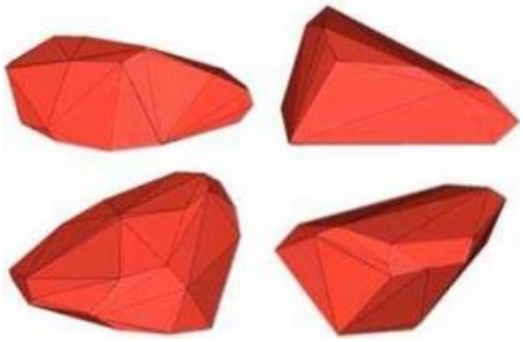

Figure 22 Polyhedrons as ballast particles (Azéma 2009)

***PFC* version 6.0** software which was recently released allows to directly model particles as convex blocks. This allows modeling of non-spherical objects when the shape is of importance (granular or cohesive systems) without requiring clumps. Contact detection and resolution use a variation of the

GJK (Gilbert–Johnson–Keerthi) algorithm with only one contact between two objects (i.e., no sub-contacts) to maximize efficiency. Interactions between rigid blocks and between other *PFC* components, such as balls, clumps, or walls, are possible using regular contact models. These convex blocks in *PFC3D* 6.0 can be worked upon and worked with as easily as other particle shapes like balls or clumps. Convex block utilities apart from general clump-like utilities include cutting blocks into smaller ones (stochastically or deterministically), merging blocks and rounding edges and corners to reduce the number of active contacts.

Clumps offer some advantages over the polyhedrons. Every contact in a clump-clump interaction is a contact between two spheres. Complexities may arise in contact detection for a pair of highly angular polyhedrons due to the possibilities of multi-point contact and through penetration during modeling of overlap at the contact (Matuttis and Chen 2014). As shown in Figure 23, two angular sharp polyhedrons can intersect each other at their sharp edges and vertices, complicating the contact resolution and increasing the solution time. Secondly, since clumps are made of smaller spheres and don't have a unified entity like a polyhedron, particle breakage and crushing can be modeled easily in clumps. Very few studies have been done using convex blocks as ballast particles, so in the next section, we will discuss about whether spheres or clumps would be a better choice to model ballast.

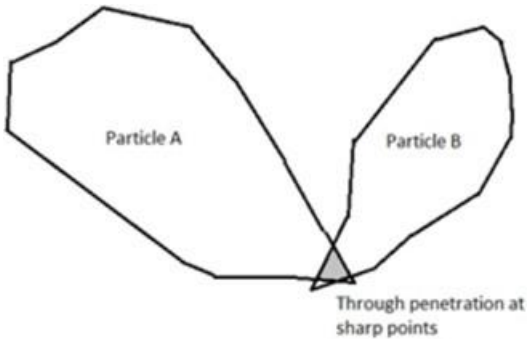

Figure 23 Complicated contact resolution for sharp polyhedrons

Discussion and selection of particle shape

Shape selection (spheres vs clumps) not only determines the quality and credibility of the results but also the time taken to completely solve the simulations. Spherical particles are easy to calibrate and computationally economical. Crushing of ballast particles due to cyclic loading from rail traffic was analyzed by Lobo-Guerrero and Vallejo (2006) using 2D simulation model containing of circular discs as particles. They acknowledged that the approximation of particle shape as discs was a potential source of error in their results. Irazábal González (2015) studied lateral track stability using spherical railway ballast particles. He modeled artificial rolling resistance at the contact points between the spherical particles to compensate for interlocking between angular ballast particles and claimed to obtain experimentally accurate results. By approximating ballast as a lattice of identical spheres, Ricci et al. (2005) studied the dynamic behavior of rail track structure under loading. He used a hybrid continuum model with discontinuities in the railway ballast being accounted for by representing the ballast as a 3D lattice of discrete spheres.

Applied loading, particle breakage, the effect of ballast gradations, fouling, track stability, tamping effect, etc. have been studied and validated on ballast modeled as clumps by Lu (2008), Lu and

McDowell (2006, 2008, 2010), McDowell et al. (2005), Laryea et al. (2014), Hossain et al. (2007), Indraratna et al. (2009, 2012) and Thakur et al. (2012).

Similar kind of studies but using polyhedrons as ballast particles, have been done by Tutumluer et al. (2006, 2007, 2009, 2011), Boler et al. (2014), Saussine et al. (2008, 2009), Perales et al. (2009, 2011) and Azéma et al. (2009).

Clumps and polyhedrons are thus effective in reproducing complex ballast response for a lot of different input conditions. Spherical particles can also sometimes reliably predict gross ballast performance at a fraction of the computational cost of clumps and polyhedrons. Rounded particles have lesser shear strength and lack of capacity for particle-particle inter- locking. Spherical ballast particles would have high track settlement rates and low stability under traffic loading (Tutumluer et al. 2009) Spherical particles' performance was compared to that of clumps under traffic loading and the results were validated using a Ballast Box test by Lim and McDowell (2008). He showed that spherical particles' performance was unrealistic whereas clumps behaved similarly to the ballast in his experimental setup. Lu and McDowell (2006) tried suggesting that such a difference in the behavior of spheres and clumps can be compensated by adding artificial rolling resistance and weak bonding forces at the inter-particle contacts. However, many other researchers claim that such artificial forces make DEM simulations inconsistent with the classical mechanics concept and thereby introduce anomalies in mesoscopic behavior (2014).

Simulation study for spheres v/s clumps

A test was conducted by Jain (2017) at Virginia Tech Railway Technologies Laboratory (VT RTL) to portray the difference between the performance of sphere and clumps. In that respect, a simulation study was designed wherein the following four test cases were considered: (1) Identical Spheres: All spheres of diameter 40 mm, (2) Assorted Spheres: Gaussian distribution for radii of spheres as follows- 20-36 mm (10%), 36-44 mm (80%) and 44-70 mm (10%). (3) Identical Irregular: Clumps roughly of same size as 40 mm diameter sphere, and (4) Assorted Irregular: 17 arbitrarily shaped clumps. This represents the most realistic case since actual stones were 3D scanned and used for simulation.

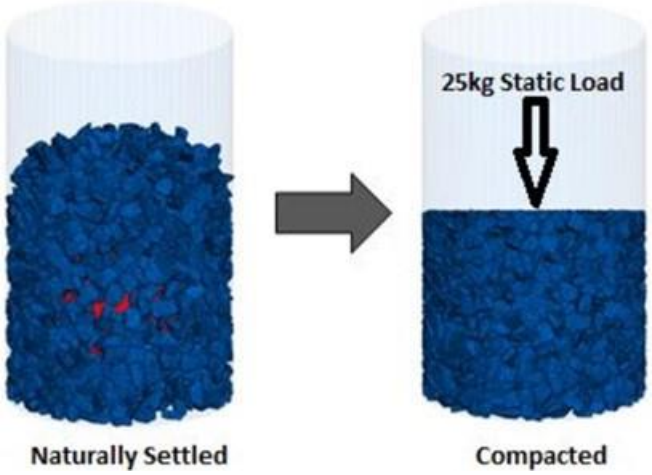

Figure 24 Simulation study for spheres v/s clumps

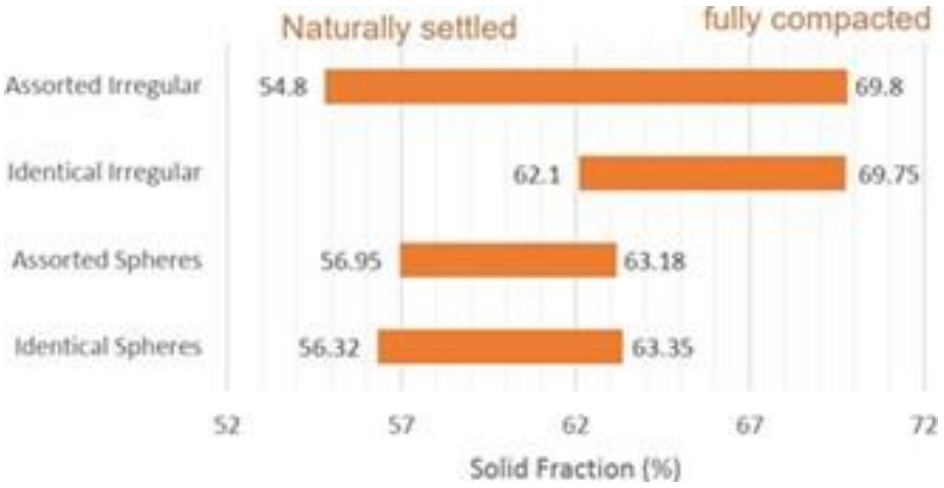

(a) Solid fraction percent for natural v/s fully compacted state

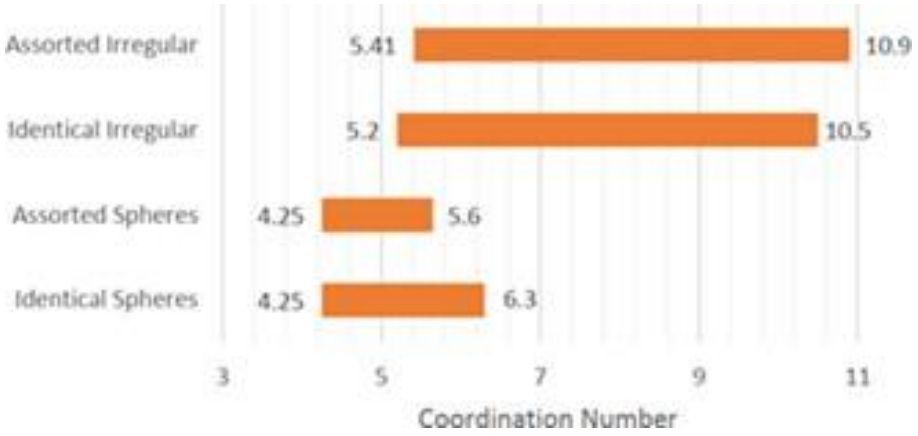

(b) Coordination number for natural v/s fully compacted states

(c) Total contacts for natural v/s fully compacted state

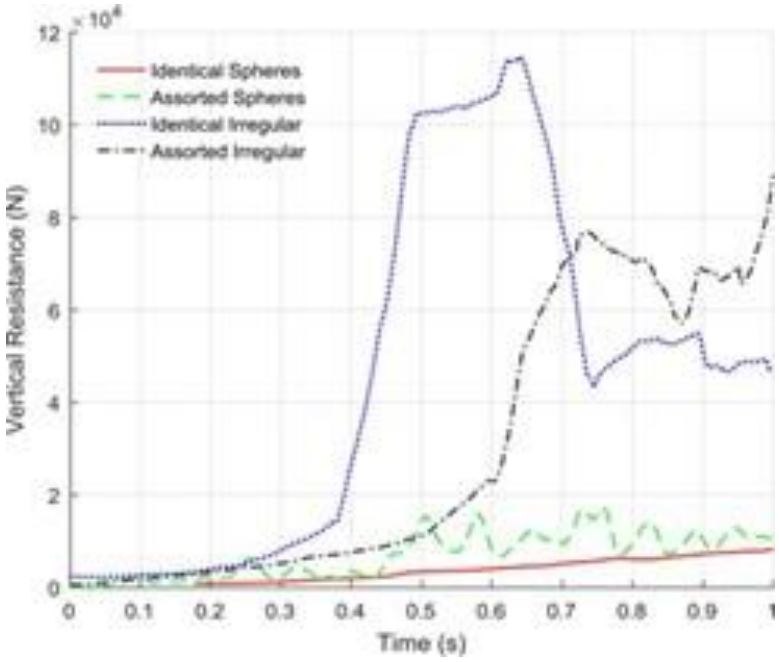

(d) Tine vertical resistance

Figure 25 Output results of simulation study: spheres v/s clumps

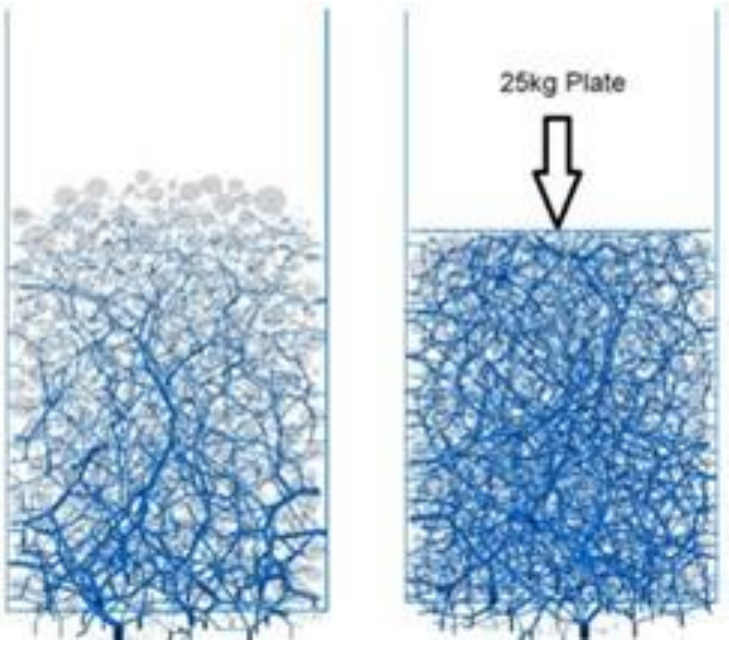

(a) Spheres: natural v/s compacted

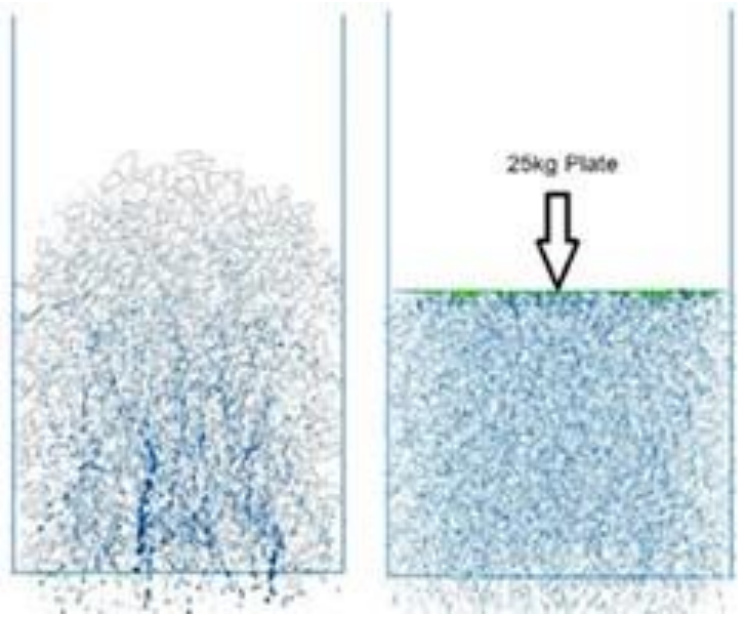

(b) Clumps: natural v/s compacted

Figure 26 Output loadpath results of simulation study: spheres v/s clumps

Compaction, Coordination number (average number of contacts per body), Absolute (total) number of contacts, Loadpaths, Vertical contact force on tines and Simulation Time were the output variables used to record the performance of the four test cases.

4300 particles were generated and allowed to naturally settle under the action of gravity in an identical cylindrical container in all cases. A static load of 25 kg was applied at the top of the settled heap of

particles as shown in Figure 24and output parameters were recorded. The inter-particle friction was set to zero during the compaction phase, to facilitate maximum possible compaction. A tamping tool was inserted into the ballast up to a depth of 0.5 m at a constant velocity of 0.5 m/s and vibrating at 45 Hz. During this downward penetration, vertical contact force on tine was recorded. Material properties were assumed to be isotropic and material for walls and particles was set as basalt and the Hertz contact model was used. Mass density was kept at 2750 kg/m^3, Young's Modulus at 50 GPa, Poisson's ratio as 0.2 and friction and damping coefficient as 0.6.

Many important observations can be made from the results of this study. Some of the very important facts have been explained below. In

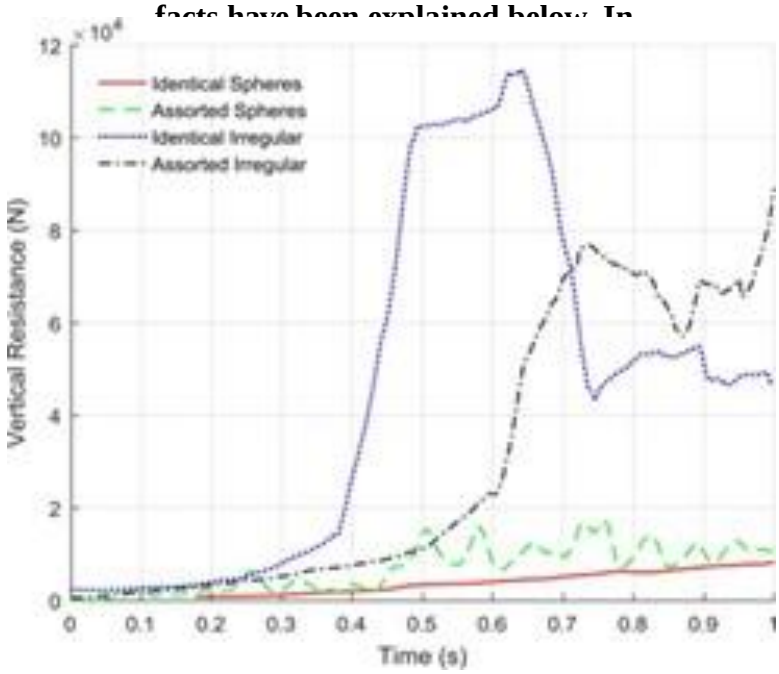

(d) Tine vertical resistance

Figure 255.6a, 5.6b and 5.6c, left end of the bar indicate naturally settled ballast whereas right end denotes the fully compacted state of the ballast. Assorted spheres have lower compaction range than their assorted clump counterparts. An observation can be made here that the absence of random projections and protuberances in spheres make them less effective in occupying interstitial void spaces among particles. Also, spheres under-represent the actual ballast compaction and thus the track settlement rates. This behavior is entirely due to particle shape and not because of the contact model or contact physics. Also, it is theoretically not possible for a disordered arrangement of spheres (assorted spheres) to have a solid fraction higher than 64% (Weaire and Aste 2008).

Coordination number shows a similar trend as compaction. Thus, one can say that when a load is applied, spheres will experience higher load per contact and there will be less diffusion on load. Clumps are therefore more resilient to deformation. Figure 26 shows the total combined number of particle-particle and particle-wall contacts. In the naturally compacted state, both spheres and clumps have almost the same number of total contacts but that is not the case later after applying a load. Particles with larger coordination number will have more number of particle-particle contacts for the same number of particles. This is also indicative of a larger number of contacts between the particles and the walls of the container in the case of irregularly shaped particles. This implies that irregular particles will have more number of contacts with a sleeper, and will apply higher lateral frictional forces, thereby increasing lateral track stability. Measurements of lateral track stability based on simulation results of spherical particles will, therefore, lead to underestimation of it.

A pair of spheres can have only one mutual point of contact, with its normal aligned radially to both spheres. Contact forces form long bifurcated chains and provide branched but concentrated paths of load transmission. Distribution of force is not uniform and larger force is transmitted per contact. In clumps, inter-particle contacts are arbitrary and their normals are randomly aligned. Any applied external force is diffused uniformly throughout the aggregate. So, spherical aggregates yield at lower loads due to poor distribution of external loads and higher particle stresses as seen from Figure 26 and stated by Tutumluer et al. (2006) and Lim and McDowell (2005).

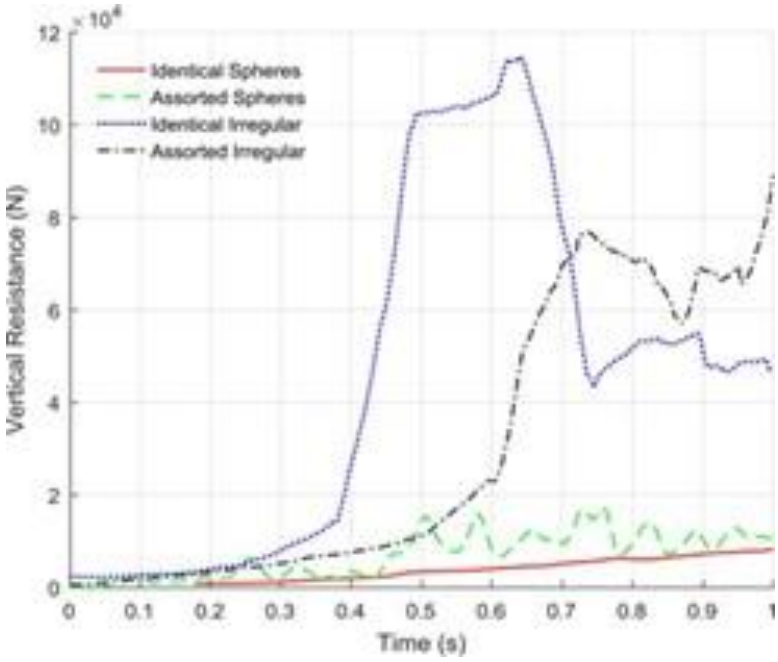

(d) Tine vertical resistance

Figure 25 shows that spheres have much lower resistance to penetration by tines. Also, more the tine penetrates inside the spheres, more is the resistance offered by them but in case of clumps, it is totally arbitrary. Simulation time increases as the complexity of particle shape and its associated detail (low detail vs high detailed clump in Figure 20 increases.

Thus, clumps are the preferred choice for modeling ballast in this research.

Particle Flow Code 3D (PFC3D) Model

PFC3D uses a command line interface and all scripting is done using the *FISH* language. A script constitutes several sections of code corresponding to the definition of the following

1. Simulation domain,
2. Particle and wall geometry,
3. Particle and wall contact properties,
4. Simulation physics and wall motion,
5. Output variables, and,
6. Solution criteria.

PFC3D offers some flexibility in the order of the definition of these components within the script. Additionally, a few components are optional or have preset default values, and therefore, do not require explicit definition. The beginning and the end of a script also contain some auxiliary commands for loading, closing, and saving of data files.

The *PFC3D* model created for tamping operation utilizes the features of symmetry to reduce the size of the simulation model and also the amount of calculation and simulation time required to obtain the solution. Tamping process is performed symmetrically about the common longitudinal axis of the pair of rails, so modeling only one half of the track is enough. Only one sleeper is simulated since every sleeper is subjected to the same kind of identical input. The rail tracks are not included in the model for simplicity. Tamping tines and a sleeper are introduced in the system. Traffic loads are thus directly applied to the sleeper. The other assumptions and approximations involved in the Half-track model are

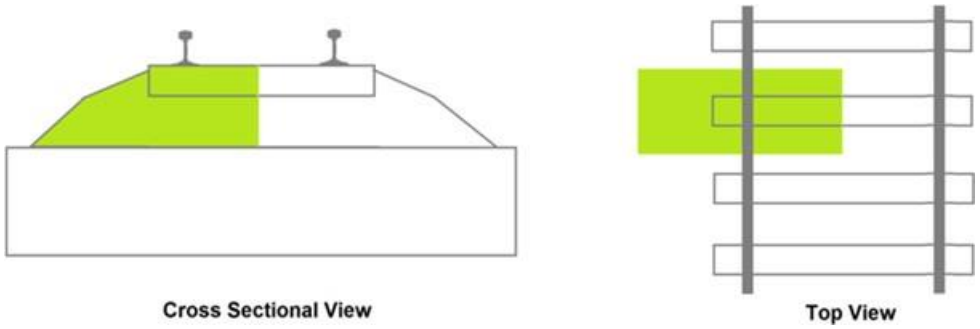

Figure 27 Half-track model

1. Influence of adjacent sleepers on ballast during tamping is ignored
2. No thermal or environmental factors are considered
3. Breakage (crushage) and fracture of ballast particles due to tine squeezing is ignored.
4. As sleepers are tamped in a sequential manner, ballast condition at the front of the sleeper being tamped is different than at its rear. For simplicity, ballast in the model is considered identical at the front and at the rear of the sleeper, since pressure based squeezing action (asynchronous tamping) of tamping tines is designed to compensate for this difference. Due to this identical ballast assumption, left and right tines travel an equal amount as in the case of synchronous tamping.
5. Entire motion of the tamping tines is assumed to be at a constant velocity (slower constant velocity for tine motion in the ballast and faster constant velocity for tines in the air).
6. Ballast particles are modeled using clumps where 1 clump is made of 2 spheres.

In *PFC3D*, it is possible to discretize the code into separate blocks of code and run each one sequentially and independently. Each code can be saved as a separate data file. This functional modularity offered by *PFC3D* for their code scripts offers multiple practical advantages listed below:

1. The solution can be saved at different stages of progress and in case of loss or unexpected crash, one doesn't need to run the simulation model from the beginning.
2. Troubleshooting and bug fixing within the script is streamlined as separate blocks of code can be run and tested and debugged independently.

3. The user does not need to write the entire code at once. Running one block of code (or data file) takes so long, that the user may productively use this time to write the next stage of code and debug it.
4. Some parts of the code may require repetitive solutions within one simulation study itself. For example, the tamping parametric study would require that initial conditions be repetitively changed before the start of the next simulation run. Such cases can thus be handled by saving the initial condition of the ballast in a separate data file and loading it before the tamping data file code is run.

A schematic representation of the Simulation model created in *PFC3D* is shown in Figure 28. Sections 5.2.1 to 5.2.5 represent the five data files used in the *PFC3D* code.

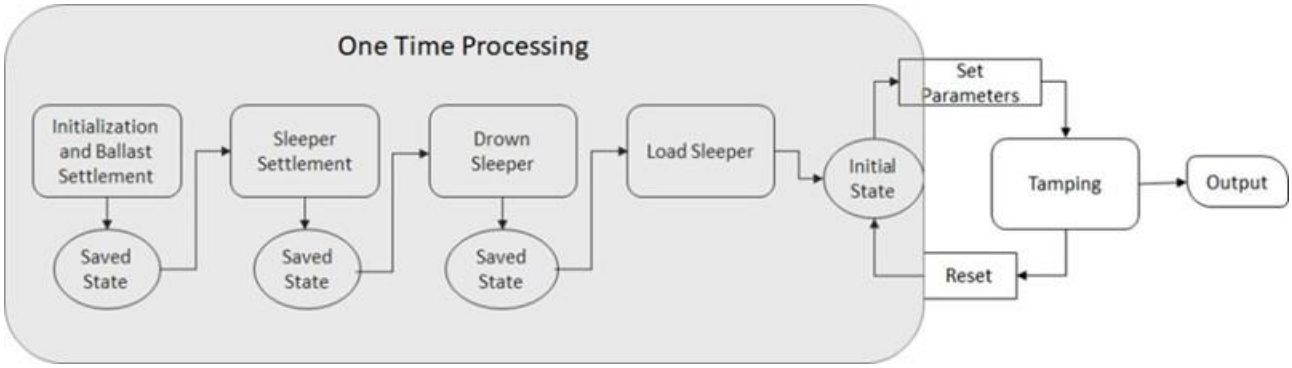

Figure 28 Information flow in the simulation model

Ballast Settlement

This data file creates a new simulation project and deals with initialization of the simulation environment, definition of physics including contact models and material properties for all bodies, definition of ballast gradation and consequential generation of particles, and finally, the settlement of the generated ballast particles under gravity until a specified target criterion, such as compaction, is met. After this file is completely run, the settled ballast gets saved as a standalone model state. Domain of size -0.901 m to 0.901 m in x-direction, -0.501 m to 0.501 m in y-direction and -1.30 m to 4 m in z-direction with a 'periodic' condition is used for the model. In a densely populated granular system like railway ballast, the periodic boundary can be used to replicate the effects of 'infinite' ballast, i.e., the boundary acts as a flexible wall of ballast particles and the granular system has no effective edges. Clumps at the top surface, i.e., above which no other clumps exist can be said to be subjected to an Open boundary. A *wall* is created at the bottom of the domain on which the ballast clumps can fall. This boxholder can be said to act as the ground surface for the ballast, as in real life and sleeper properties are assigned to this boxholder wall. Another reason for the introduction of the wall is to prevent clumps from flying out because of the periodic condition applied to the domain. Specification of ballast gradation includes a description of particle shapes and declaration of the size distribution of particles in the granular assembly. The details about the use of Bubble Pack algorithm and the significance of its parameters have been explained in Section 5.1.2.

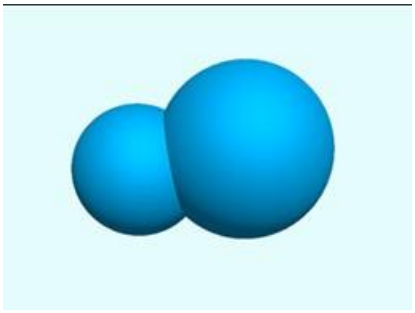

Figure 29 Clump used in the simulation

17 different size real stones were 3D scanned and their '.stl' profiles were imported into *PFC3D* to create ballast. However, using this complex arbitrarily shaped 3D scanned particles consisting of many spherical pebbles inside each clump, drastically increased the simulation runtime for each of the data files. If the number of spherical pebbles inside a clump was reduced, the clump surface wouldn't be properly represented to the corresponding 3D scanned profile. Thus, to avoid higher simulation runtimes, clumps corresponding to 3D scanned profiles were discarded and for this simulation presented in the document, the ballast is made up of clumps, wherein a single clump is made up of only two spherical pebbles. Figure 5.10 shows a single clump used in the simulation. The clump used in the simulation is formed using two spherical pebbles of radii 0.01875 m and 0.025 m with an overlap of 0.013 m and volume of each of the clump produced as $8 * 10^{-5}$ m^3.

Ballast is considered to be made up of granite (or basalt) rock. Initially, two simulations were performed with the following wooden (Pine western white) sleeper properties:

1) Young's modulus = $10.1 * 10^9$ Pa, Poisson's ratio = 0.33 and Shear modulus for the Hertz model calculated using the formula *Shear modulus* = $\frac{Yong's\ Modulus}{2(1+Poisson's\ Ratio)}$. This is assuming isotropic wooden properties.
2) Shear modulus for the Hertz model is directly defined as $0.57772 * 10^9$ Pa, Poisson's ratio= 0.025662. This is assuming that wooden properties are different in different directions. The results for these simulations with different wooden properties were almost exactly similar following the same graphical trend for all of the observed output parameters. Thus, it was decided to use the isotropic wooden properties for simplicity.

Table 3 shows the properties of various parameters used in the simulation and the reference from which the value was taken if available. For the table not showing any reference citation, a value as shown in some of the tutorials or solved examples of Itasca Consulting Group (2015) has been chosen. Granite, basalt properties were found online and from a reference cited in Schultz (1993).

Track ballast thickness should not be less than 6 in and high-speed railway lines may require ballast up to 20 in thick. Insufficient depth of ballast causes overloading of the underlying soil, and in unfavorable conditions overloading the soil causes the track to sink, usually unevenly. Ballast less than 300 mm (12 in) thick can lead to vibrations that damage nearby structures. However, increasing the depth beyond 300 mm (12 in) adds no extra benefit in reducing vibration (https://en.wikipedia.org/wiki/Track_ballast). As per the above conditions and as per AREMA Manual (2010), total ballast thickness (ballast plus sub-ballast) for this simulation is kept as 24 in (0.6096 m).

All the measured output parameters have been converted to Imperial units in this data file and the subsequent data files. Thus, output has been recorded in SI and Imperial units.

Table 3 Property values of ballast and sleeper material

Property	Value	Reference
Gravity	9.81 m/s^2	Default
Number of ballast stones	6000	
Ballast Density (Granite/Basalt)	2700 kg/m^3	[42, 73]
Ballast Young's Modulus	50 * 10^9 Pa	[70, 74]
Ballast Poisson's ratio	0.25	[70]
Ballast Shear modulus	2 * 10^{10} Pa	[70]
Friction coefficient of ballast	0.6	
Normal critical damping ratio between ballast particles	0.8	
Local damping coefficient of ballast	0.6	
Sleeper density (Pine Western White wood)	615 kg/m^3	[75, 76]
Sleeper Young's Modulus	10.1 * 10^9 Pa	[75, 76]
Sleeper Poisson's ratio	0.33	[75, 76]
Sleeper Shear modulus	3.7969 * 10^9 Pa	[75, 76]
Friction coefficient of sleeper, tines and boxholder	0.6	
Normal critical damping ratio between ballast and sleeper, tines, boxholder	0.5	

Sleeper Settlement

The settled ballast state, saved by the previous data file, is loaded and a half-sleeper is generated in the simulation environment. The sleeper is made to settle on the top of settled ballast particles under the influence of gravity until the net unbalanced force on the sleeper reaches below a specified threshold. The settled sleeper is then saved as a new model state.

The wall does not follow Newton's laws of motion. It is difficult to control its motion and hence clumps were used to represent the sleeper (rectangular block). Thus sleeper was subjected to natural gravity forces and body forces. Sleeper of dimensions: 7 in height * 9 in width * 8.5 feet long obtained from AREMA Manual (2010) is introduced in the system at a particular height and naturally allowed to fall under the gravity. To calculate the output parameters, measurement spheres are created. Since the calculation of the output variables measured by measurement spheres is limited to only the extent of the measurement sphere, and not the entire bulk of the ballast in the simulation model, multiple measurement spheres are created to record output at all different points of interest below the sleeper. Contact overlap volume of bodies (clumps and balls) is not accounted for total material volume in the porosity calculation. However, if wall insertion displaces clumps or causes disorientation in the arrangement of bodies, porosity results would change. The problem here is that the sleeper is made of clumps. When a clump is added to the measurement sphere region it affects porosity even if it doesn't disorient the original ballast arrangement. Thus, if the measurement sphere is not properly located false readings would show up.

A grid of 35 small spheres (covering almost entire xy domain) with 7 spheres in the x- direction * 5 spheres in the y-direction is created with each measurement sphere of size 0.125 m. It has been made sure in all of the data files - two to fifth (5.2.2 to 5.2.5) that this grid of measurement spheres

is always below the sleeper in z-direction, such that the bottom-most surface of the sleeper would touch the uppermost surface of the measurement sphere. This is done to avoid any miscalculations caused due to the sleeper intersecting with the measurement sphere region as explained in the paragraph above.

In a verification problem, 'Measure Logic' in Itasca Consulting Group (2015, it is shown that the lowest errors in readings and higher accuracy are observed when larger measurement spheres are used. Thus, in addition to a grid of 35 small spheres, 3 big measurement spheres of radii 0.3 m are also added to record the output variables. For further sections, a row of 7 small spheres in the x-direction is referred to as a 'layer'. So, as shown below in Figure 30, we have total five layers of measurement spheres numbered in ascending order for each layer from left to right (-X to +X sphere center location). Thus, layer 1 has measurement spheres 1 to 7, layer 2 has 8 to 14 and so on. In the figure, only the first and the last measurement sphere of a layer are labeled, individual stresses are calculated for each measurement sphere and average stresses are calculated for each of the layers.

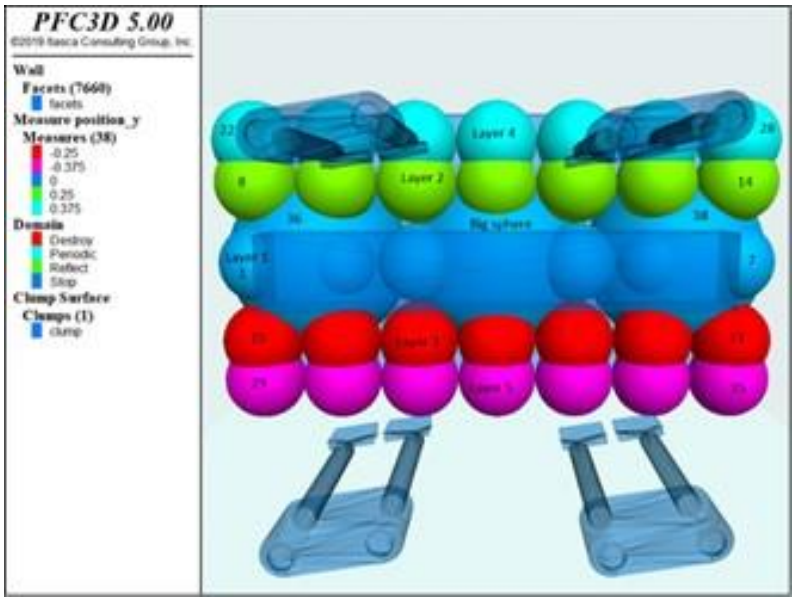

Figure 30 Measurement spheres

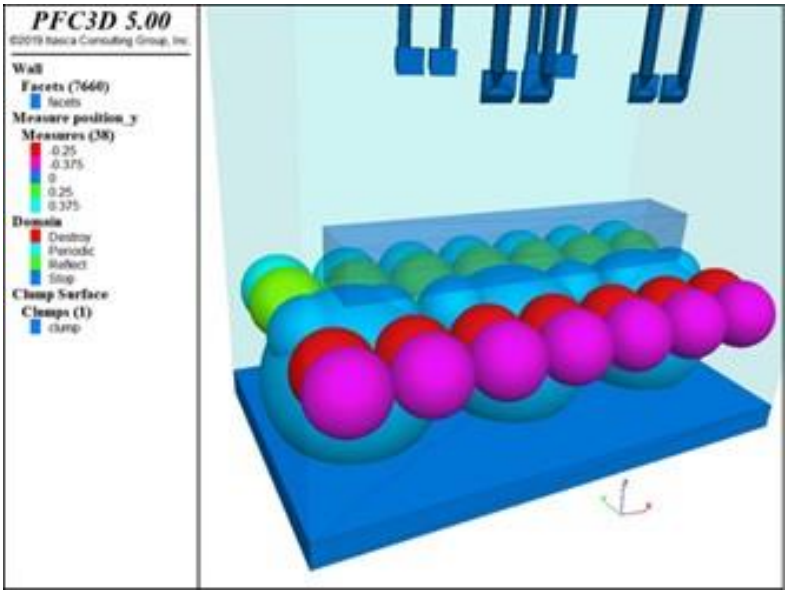

Figure 31 Measurement spheres seen from another view angle

Drowning Sleeper

The settled sleeper state is loaded and an additional **1400** ballast particles (Crib ballast) are generated around the periphery of the sleeper such that there is a 1.5 in gap between sleeper top layer and ballast top surface. Gradation of this ballast is identical to the previously specified gradation. This generation of ballast around sleeper corresponds to the actual track laying process where additional ballast is dumped after a track has been laid. This generated ballast is then allowed to settle until the velocity of all individual particles is close to zero. The latest model state is finally saved in the end.

If a newly introduced particle overlaps any existing particles, then normal forces, which may disturb the existing system, maybe generated at subsequent cycles (depending on the contact model being used). A similar caution applies if walls are added to the system. Second, if a newly compacted assembly is required, the compaction procedure should be done in a way that minimizes disturbance to the existing particles. Thus, based on this the sleeper position is mildly changed in the z-direction (sink down by 5 mm) even though it attains a state of equilibrium in the previous data file (5.2.2) because of the addition of new clumps which add disturbance to the system.

Load Cycle on Sleepers

This data file replicates traffic loading cycles on the settled sleeper to obtain the realistic compaction state of ballast below the sleeper. If compaction of ballast below the sleeper is already known, then it can instead be modeled in the first data file and this file can be omitted from the model. The output of this file is saved as the final state of the model before tamping and is loaded while simulating different tamping parameters. Therefore, data files 1 to 4 are only required to be solved once at the start of the study.

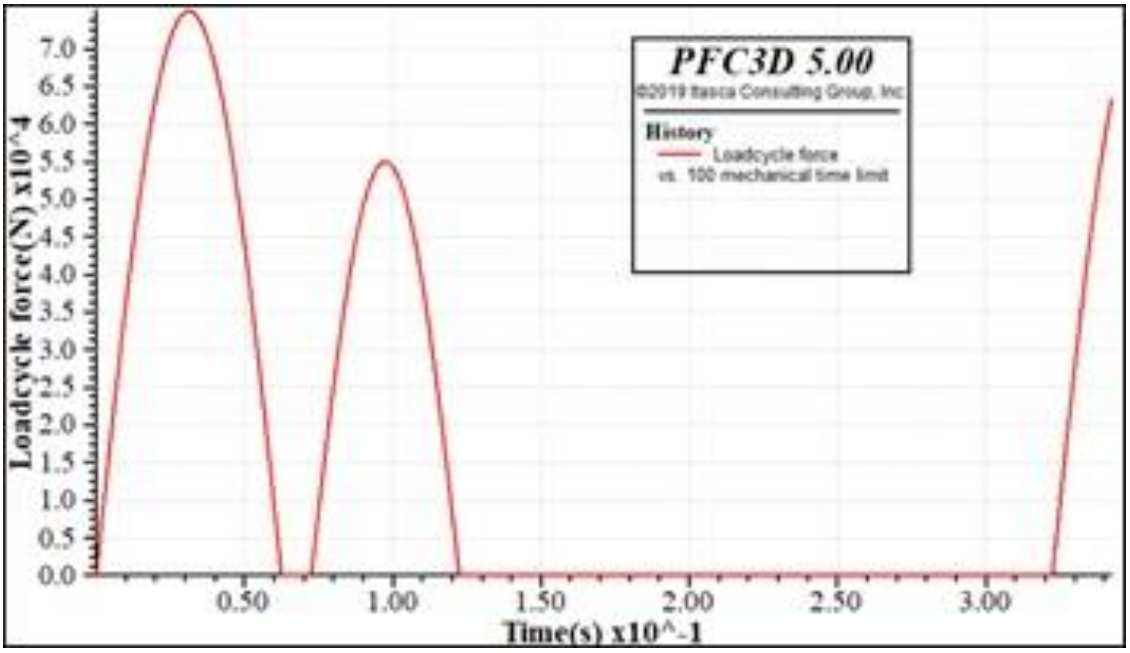

Figure 32 Load cycle applied on the sleeper

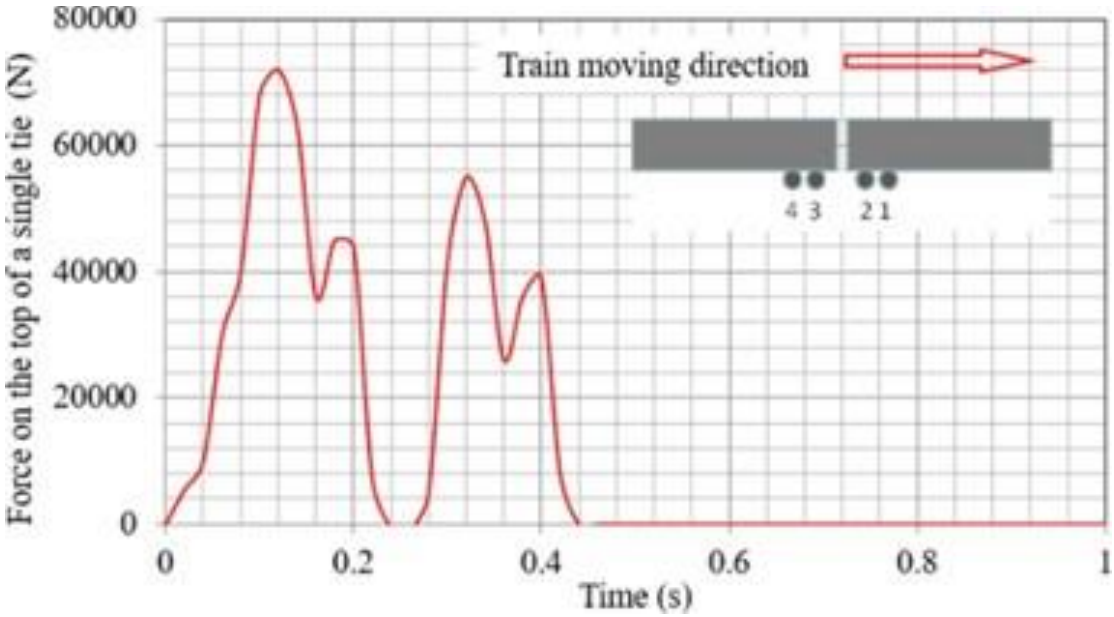

Figure 33 Load cycle reference (Tutumluer et al. 2009)

Load cycle applied on the sleeper is shown in Figure 32. The load cycle, shown in Figure 5.14, is similar to the one found in Tutumluer et al. (2009). The load cycle used is applied on the sleeper such that force on the sleeper is in the downward direction and thus the two cycles shown are actually applied reversed in the negative direction, but are shown this way for better understanding. The load cycle applied by us is a simplified version of Tutumluer et al. (2009) with a bigger amplitude peak of $7.5 * 10^4$ N and a smaller one of $5.5 * 10^4$ N with a frequency of 8 Hz and 10 Hz. It is shown in Federal Railroad Administration (2018) that the peaks, frequency and shape of the loading

cycle waveform change based on the train speed. Due to this load cycle, the sleeper further sinks down by 1.2 in (0.03048 m). Four tines are then imported in the simulation and properly positioned before the beginning of the tamping process.

Tamping Cycle

Tamping is the last data file. The simulation model after the end of the loading cycle and before the beginning of the tamping cycle is represented in Figure 34. It loads the last saved ballast state from the previous (4th) data file, lifts the sleeper up, and performs tamping operation according to the values of the parameters defined in the script within the file. All final output variables are recorded at the start and at the end of the tamping cycle. Only this file needs to be run repeatedly for parametric studies by changing tine motion parameters.

Tungsten carbide material is used for tines with properties: Young's Modulus = $6 * 10^{11}$ Pa, Poisson's ratio = 0.31(https://en.wikipedia.org/wiki/Tungsten_carbide). Tine properties are specified and the contact model is redefined to include tine parameters. Sleeper is lifted by 1.38 in (0.035 m) before the start of the tine insertion motion. Sleeper position after tamping is the same as the sleeper position before the load cycle (before sleeper sink due to traffic) meaning it is the same as at the end of 3rd data file. Tines are inserted till 3.74 in (0.095 m) below the sleeper bottom face. All the tines are provided the same constant velocity of 10 m/s while in air. The constant velocity of tines in ballast is decided by the Taguchi table shown in Figure 40. Measurement spheres location is modified such that spheres are always directly below the sleeper bottom face and output variables are recorded before tamping (before sleeper lift) and after tamping (after sleeper drop on completion of the tamping cycle). This file can run both linear and elliptical tamping cycle. For elliptical tamping, squeeze and release motions of linear tamping gets replaced by elliptical tine motion. The entire tamping process is shown in Figure 34.

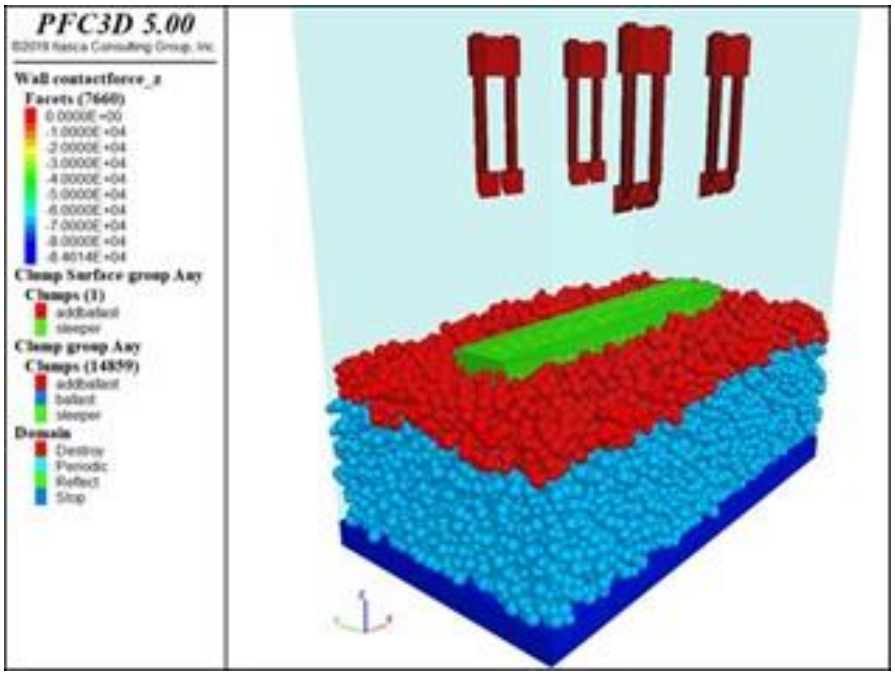

Figure 34 Simulation Model before tamping

Input Parameters

Input variables for the tamping model can be classified into three categories-

- Parameters for configuration of model physics,
- Parameters defining ballast gradation and behavior, and
- Process variables of tamping

Parameters related to the model physics and ballast, even though act as an input to the

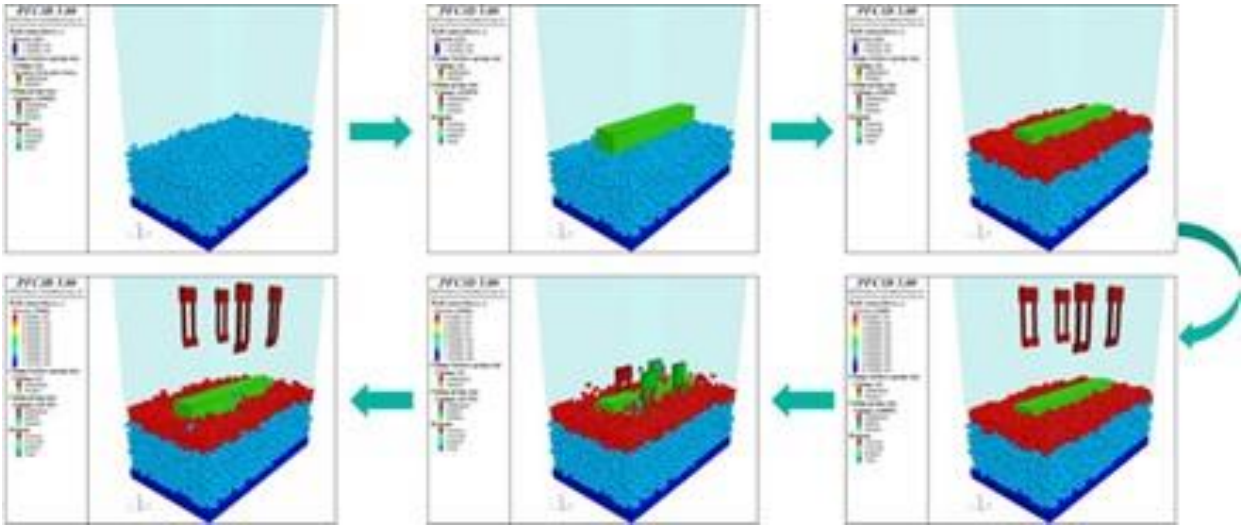

Figure 35 Entire tamping cycle

model are held constant throughout the project and are not the focus of the study. These parameters have already been discussed in previous chapters in detail. Input parameters and variables corresponding to the simulation of tamping in the model include the following:

1) Sleeper Lift: It is the vertical height by which the sleeper is lifted from its originally settled position before the start of the tamping cycle.

2) Shape of Tamping Tines The overall geometric shape and features of the tines affect the tamping results. These tines can be created in a CAD software and imported as .stl file. Figure 36 shows the CAD model of a pair of tamping tine.

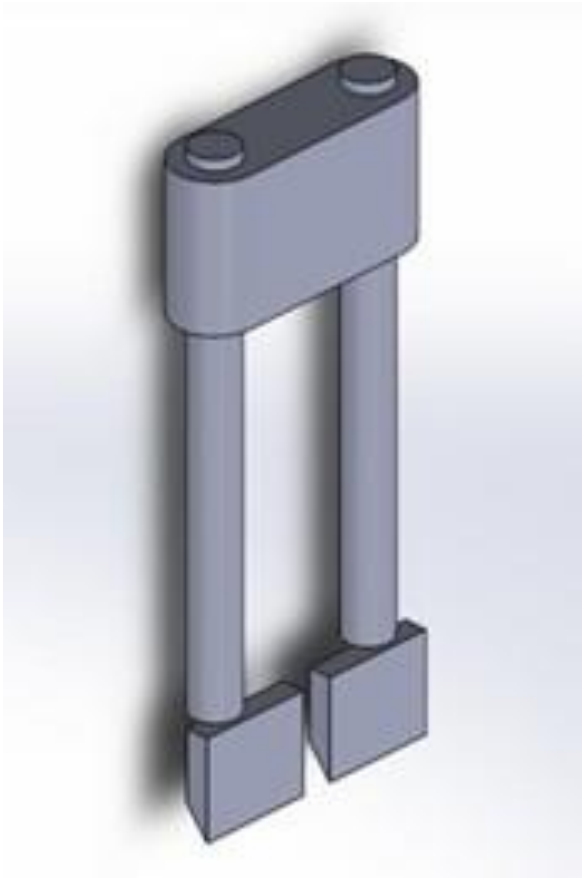

Figure 36 CAD model of tamping tine

3) Motion of Tamping Tines: One linear tamping cycle consists of lifting the sleeper up and four tine motion steps insertion, squeezing with hold, release and withdrawal and then dropping the sleeper on the ballast. This tamping cycle is shown in Figure 37. The squeezing and release of ballast below the sleeper have been modeled as parallel traversing of the opposite pair of tines towards and away from each other. It can alternatively be modeled as a clockwise and anti-clockwise rotation of the opposite pairs about a remote axis of rotation.

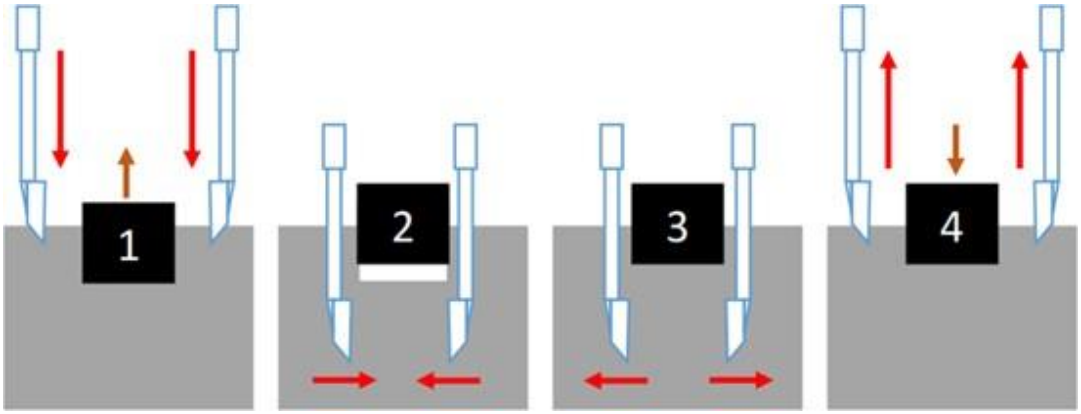

Figure 37 Steps of tine motion during one linear tamping cycle

4) Characteristic Trajectory of Tine Vibration There are usually 8 pairs of tines acting per sleeper during tamping, 4 pairs around the either rail. As specified in Chapter 2, each pair is vibrating continuously along its vertical axis throughout the operation. The motion of a pair during vibration can have several different possibilities and the nature of this trajectory greatly influences the results achieved by the equipment. Different widely used characteristic trajectories of tine vibration are shown in Figure 38.

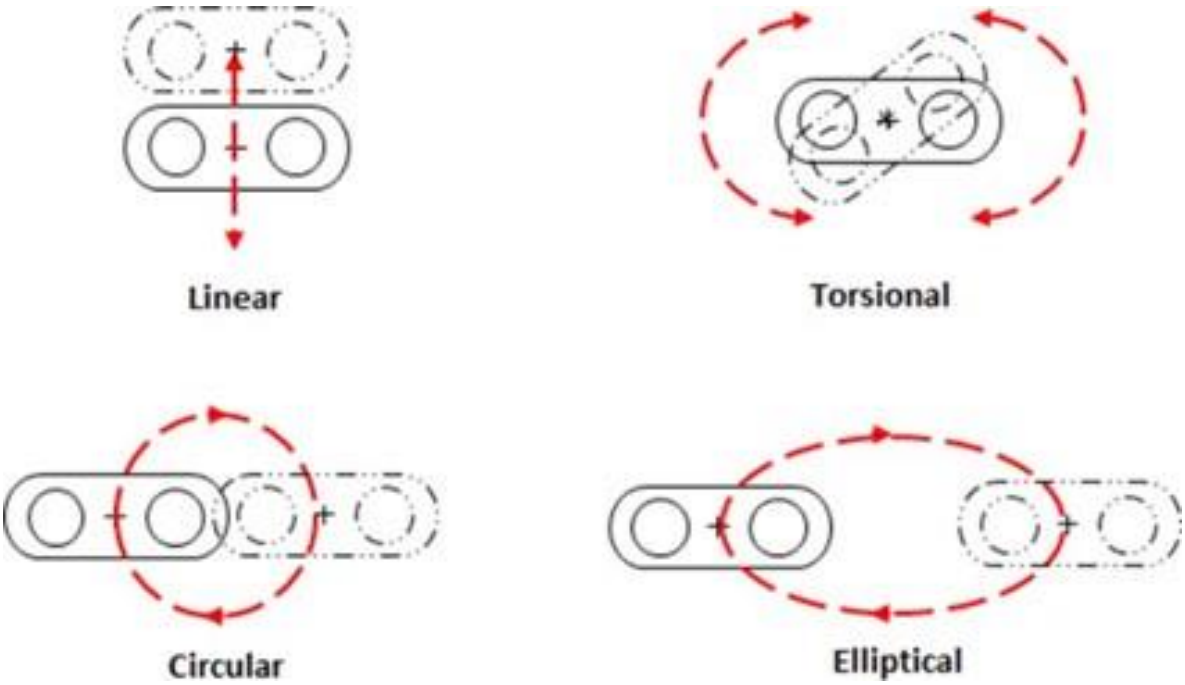

Figure 38 Widely used characteristic vibratory motions of tamping tines (Jain 2017).

5) Tine Vibration Amplitude: The amplitude of the vibration of the tines needs to be specified as: a length measurement for linearly vibrating tines, an angle measurement for torsional vibration, and a mathematical function for vibrations with a closed-loop trajectory.

6) Tine Vibration Frequency: The tine vibration frequency is associated with the liquefaction of ballast while tamping and is a critical parameter for controlling the ballast compaction below the sleepers.

7) Tine Insertion Velocity: Constant downward velocity is applied to the tines till they reach the desired depth.

8) Depth of Insertion: This is the vertical depth below the sleeper till which the tines enter.

9) Squeezing Velocity: Ideally, the squeeze force is used to define the squeeze required. But since squeeze pressure/force is difficult to model in the *PFC*, a constant squeeze velocity has been used in this research. The force generated by squeeze velocity that is provided to the tines should be proportional to the practically used values of squeezing pressure. A squeeze limit is defined as the minimum distance between the opposing pairs of tines at which the squeezing action will be halted to prevent squeeze pressure from being exceeded.

10) Squeeze Hold Time This happens for short duration in between step 2 and 3 of Figure 5.18. This is done to momentarily stop the disturbance of the ballast caused due to the squeezing phase.

11) Release Velocity Tines are retracted after the squeezing phase by providing this constant velocity. Squeeze velocity is equal to the release velocity in this research.

12) Withdrawal Velocity This is the constant velocity at which the tines are withdrawn from the ballast vertically. Tine insertion velocity is equal to the tine withdrawal velocity in this research. This is the last step of the tamping cycle after which the sleeper is dropped on the ballast.

Output Parameters

A measurement sphere is a user-defined spherical volume in the simulation environment which monitors selected mesoscopic properties for all particles lying within or intersecting with the measurement sphere. It doesn't influence the physics of the system. The output parameters that can be calculated by measurement spheres are: Porosity, Coordination Number, Stress, and Strain rate.

The output parameters that are monitored in this research include the following:

1) Ballast Compaction *PFC* measurement spheres calculate porosity values where porosity is defined as the ratio of total void volume within the measurement region to the measurement region volume. Ballast compaction is expressed as a solid fraction, i.e., the percentage of the total volume occupied by a solid mass of ballast particles. This is calculated as $1 - Porosity$. Higher compaction results in higher vertical track stability.

2) Ballast Coordination Number Ballast coordination number C_n is also calculated as a measure of the stability of a particular arrangement of ballast particles. It is defined as the average number of active contacts per body (where a body can be ball/clump), i.e., the average number of contacts a particle has with its immediate neighboring bodies. Higher C_n results in high overall track stability.

3) Ballast Particle Stress Individual stress components and net stress value of ballast particles are indicative of crushing forces exerted by the tamping tines on the ballast particles due to a particular squeezing pressure value and also help understand the state of the ballast aggregate before tamping and after tamping. Stress is a property of the continuum and the stress measurement of discrete particles is represented by averaging the individual calculations for all particles present within the measurement sphere as given in Christoffersen, et al. (1981).

4) Contact Forces on Tines Contact forces acting on tamping tines during their motion inside the ballast are recorded for studying the relative power requirements of tamping based on tine design and ballast gradations. Individual vector components and the net resultant force is recorded for all pairs of tines at every time-step. These graphical plots can be saved as a series of sequential model states at every time-step in the form of a video clip.

5) Graphical Load Distribution The distribution of external loading and excitation from the sleeper and the tines across the volume of the ballast is plotted at every time-step, but no numerical data is recorded. This distribution is shown by representing contact force components at all contact points within the model with vectors scaled in thickness proportional to their magnitude and aligned parallel to the orientation of the force. It determines the mechanical behavior of ballast and rate of track settlement.

6) Simulation Time The time taken to solve each data file individually and their cumulative time are important factors as well to determine the model efficiency. This determines the computational efficiency of the model. It is affected by various factors like particle complexity, histories recorded, number of bodies, etc. The simulation time usually helps to compare various graphs as this time remains common for most of them and is plotted on X-axis. A schematic of the information flow structure of the simulation model is shown in Figure 39.

Parametric Studies

Three different values have been considered for each of the linear tamping parameters whose effect on the ballast behavior needs to be observed. Insertion velocity and withdrawal velocity are kept equal and squeeze and release velocity of tines are kept equal. Thus, since, we have 4 major parameters - tine motion amplitude, tine motion frequency, insertion velocity and squeeze velocity, using a full factorial design would lead to running the simulation model for $3^4 = 81$ times. This is not advisable and feasible given that even one simulation takes so long to solve. Thus, a Taguchi method of Design of Experiment is used where we only need to perform nine experiments as shown in Figure 40. This table was created using JMP 14 software JMP (1989)The velocity has the units of m/s, the frequency unit is Hz while the amplitude is defined in mm (/ degrees).

This Taguchi set of 9 runs is done on simple clumps composed of 2 spheres. The best combination of value for the given parameters is found out and then these parameter values can be used to study tamping using real-shaped (3D scanned) clumps or ballast represented by convex blocks. The real shaped clumps aren't solved using Taguchi method and discussed here since they take a lot of time to solve, almost a week.

From this set of experiments, the best set of values for tine motion parameters for linear tamping is found out. Then, these parameters are used to study elliptical tamping where squeeze and release motion is replaced by elliptical tine motion. Finally, the results of linear and elliptical tamping are compared and analyzed.

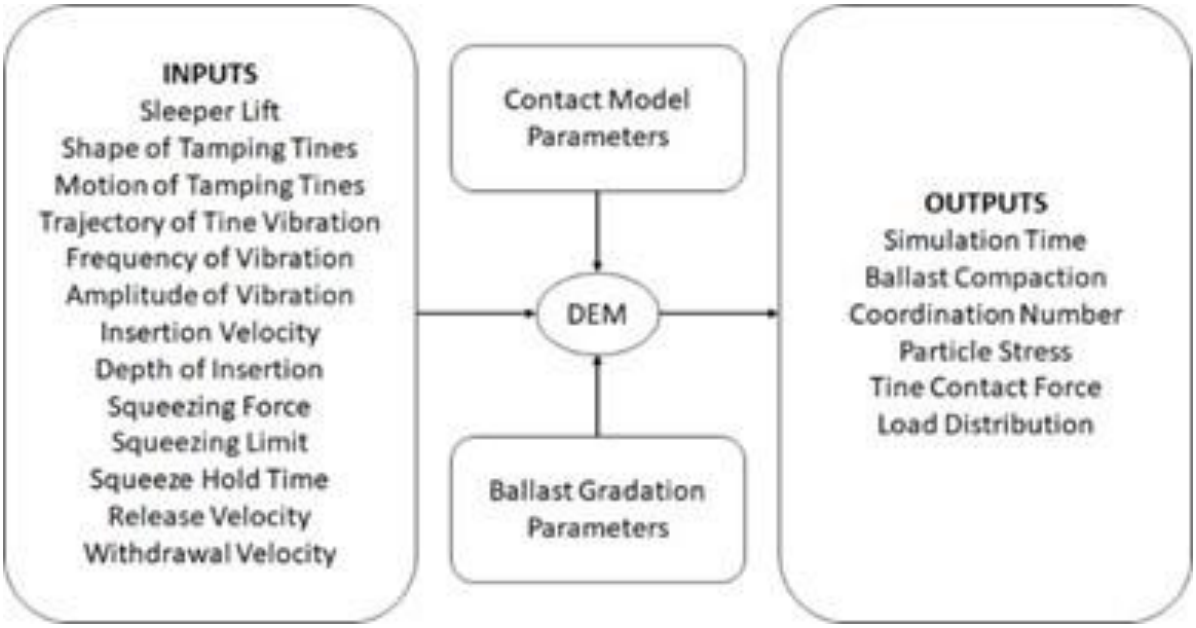

Figure 39 Schematic of the information flow structure of the tamping simulation model

	Tine motion amplitude	Tine motion frequency	Insertion velocity	Squeeze velocity	Pattern
1	4	28	0.75	0.5	----
2	4	35	1	0.75	-000
3	4	42	1.5	0.35	-+++
4	3	28	1	0.35	0-0+
5	3	35	1.5	0.5	00+-
6	3	42	0.75	0.75	0+-0
7	5	28	1.5	0.75	+-+0
8	5	35	0.75	0.35	+0-+
9	5	42	1	0.5	++0-

Figure 40 Taguchi Table

RESULTS AND DISCUSSION

Ballast velocity, contact force, unbalanced force; loadpath; sleeper position, velocity, contact force; porosity, coordination number and stress-XX, YY, ZZ in all layers, small and big measurement spheres; tine position, velocity and contact force, etc. are the graphs which were monitored while running the simulation. However, every graph has not been presented in the document and only the unique relevant ones have been highlighted and explained.

Coordination number results are given more importance in evaluating the performance of a given tamping set of parameters because of the reason discussed in Chapter 3 (Agnolin and Roux 2007). Linear tamping was performed using 9 different sets of combinations as shown in Figure 40. The average of compaction, coordination number, stress- xx, yy, zz values were recorded in the seven small spheres directly below the sleeper (layer 1) and also in three big measurement spheres.

Table 4 shows the results in terms of output parameter values before tamping.

Table 4 Output parameter values before linear tamping on 2-sphere clumps

Sr. No.	Compaction before	Coordination No. before	Stress XX before (lbf/in^2)	Stress YY before (lbf/in^2)	Stress ZZ before (lbf/in^2)
Small spheres	53.71628	3.249467	-0.1769008	-0.2151359	-0.3589339
Big spheres	49.83414	3.958316	-0.3366152	-0.3332443	-0.5801185

Linear Tamping

The values of the parameters used for each of the nine simulations that were run are mentioned in Figure 5.21. **Table 5** shows output parameter values after tamping and a percentage change in the parameter values after tamping using small measurement spheres. Similarly,

Table 6reports output parameters by using big measurement spheres. For percentage change calculations, the entire value (7 digits after the decimal point) shown by *PFC* (Itasca Consulting Group, Inc., 2019). is used.

In **Table 5**, cell colored with green background indicates that particular simulation had the highest value while the yellow background indicates the second highest value for that parameter. Now, as can be seen from **Table 5** and

Table 6, it is difficult to judge the simulation performance based on the stress values. Stress is a quantity that would differ because of the random orientation of the ballast and thus one cannot judge the tamping efficiency based on this parameter. Thus, we use compaction and coordination number to find out which simulation trial yields a better tamping performance. It is seen that both the compaction and the coordination number are better for simulation 8 when measured using big measurement spheres. Also, it gives the second possible best (higher) values even when measured using small spheres. It was earlier discussed that big measurement spheres yield many accurate results since they cover a bigger area and so most of the physics is recorded. Thus, simulation 8 of 5.21 gives the best linear tamping results using 2-sphere clumps (clump made up of 2 spheres as shown in Figure 29. This claim is also supported by Lichtberger (2011) who says that the optimum tine vibrating frequency is 35 Hz with an amplitude of 5 mm. Liquefaction of ballast occurs if tine vibrating frequency is beyond 35 Hz resulting in poor compaction and poor tamping performance. Also at higher frequencies, much higher tine squeezing speed is required to ensure compaction impulse but is difficult due to ballast resistance.

Table 5 Output parameter values after linear tamping on 2-sphere clumps: Small measurement spheres

	1	2	3	4	5	6	7	8	9
Comp-action after	51.501	51.503	50.648	52.853	51.591	50.350	51.233	51.609	51.371
Comp-ac-tion % change	-4.125	-4.121	-5.713	-1.607	-3.956	-6.268	-4.623	-3.923	-4.365
Coordi-nation No. after	4.004	3.911	3.943	3.788	3.84	4.138	3.869	4.04	4.005
Coordi-nation No.% change	23.216	20.36	21.355	16.583	18.161	27.359	19.073	24.315	23.259
Stress XX after (lbf/in^2)	-0.195	-0.211	-0.165	-0.236	-0.223	-0.204	-0.228	-0.214	-0.17
Stress XX % change	10.053	19.226	-6.452	33.29	25.8	15.502	29.073	20.82	-3.67
Stress YY after (lbf/in^2)	-0.175	-0.244	-0.235	-0.206	-0.238	-0.204	-0.208	-0.199	-0.191
Stress YY % change	-18.873	13.315	9.048	-4.328	10.793	-5.348	-3.212	-7.572	-11.313
Stress ZZ after (lbf/in^2)	-0.249	-0.338	-0.293	-0.335	-0.342	-0.275	-0.275	-0.329	-0.255
Stress ZZ % change	-30.757	-5.9	-18.339	-6.68	-4.812	-23.29	-23.316	-8.338	-29.055

Table 6 Output parameter values after linear tamping on 2-sphere clumps: Big measurement spheres

	1	2	3	4	5	6	7	8	9
Comp-action after	53.243	52.736	53.104	53.135	53.013	52.377	52.84	53.409	52.942
Comp-ac-tion % change	6.841	5.823	6.561	6.623	6.379	5.102	6.033	7.174	6.237
Coordi-nation No. after	4.417	4.331	4.376	4.369	4.352	4.418	4.229	4.446	4.437
Coordi-nation No.% change	11.587	9.425	10.541	10.383	9.945	11.615	6.838	12.332	12.085
Stress XX after (lbf/in^2)	-0.366	-0.367	-0.364	0.371	-0.376	-0.366	-0.343	-0.383	-0.345
Stress XX % change	8.799	9.152	8.196	10.35	11.559	8.816	1.864	13.706	2.577
Stress YY after (lbf/in^2)	-0.385	-0.38	-0.393	-0.389	-0.411	-0.384	-0.391	-0.399	-0.38
Stress YY % change	15.639	14.072	17.802	16.782	23.193	15.302	17.408	19.706	13.956
Stress ZZ after (lbf/in^2)	-0.582	-0.591	-0.591	-0.607	-0.605	-0.572	-0.597	-0.607	-0.575
Stress ZZ % change	0.378	1.852	1.96	4.622	4.259	-1.372	3.031	4.62	-0.929

With careful observation, it is also visible that the highest compaction values using small measurement spheres happen in simulation 4, 8, 5 as seen from **Table 5**. Squeeze velocity and tine frequency are lesser in these 3 simulations compared to other simulations. Simulation 4 has tine frequency set as 28 Hz. Such smaller frequencies are not good for overall tamping efficiency since, at such frequency, the resistance offered by the ballast to tines would be more resulting in more input power requirement. From

Table 6, simulation 8, 1, 4 record the highest compaction values. So, it can be concluded that for better compaction, squeeze velocity and tine frequency should be less. This also makes sense since, lesser squeeze and release velocity (squeeze = release velocity in this simulation) will allow the particles to compact well and rearrange themselves in a better way.

Some of the important parameters that were recorded throughout the simulation using *history* command are presented below. The values of the parameters in the graphs use English Imperial units and are mentioned on the axes of the graphs. These are only presented for simulation 8 but the nature and the trend of the graphs were similar even while running the other eight simulations. The five data files that were used in the code as represented by subsections of Section 5.2 were run sequentially in the following way: 5.2.1 to 5.2.4 were run in that order, the result was saved as the initial state and then 5.2.5 was run nine times by changing values as mentioned in Figure 40. The mechanical simulated time (different from the time the *PFC3D* software takes to solve - approximately 20 hours) to solve these files are mentioned in the **Table 7**. Time for each kind of tine motion is indicated in the table. The time taken by *PFC3D* software to solve Simulation 8 is (total 32 hr 54 min 12 s):

1. Ballast Settlement - 51 min 47 s
2. Sleeper Settlement - 4 hr 13 min 54 s
3. Drowning Sleeper - 4 hr 55 min 02 s
4. Load cycle on Sleeper - 2 hr 33 min 28 s
5. Tamping Cycle - 20 hr 20 min 01 s

Table 7 Simulated Time for file runs

	Individual time (s)	Cumulative time (s)
Ballast Settlement	0.95	0.95
Sleeper Settlement	0.8	1.75
Drowning Sleeper	0.73	2.48
Load cycle on Sleeper	0.34	2.82
Tamping Cycle (Insert motion in Air)	0.09	2.91
Tamping cycle (Insert motion in Ballast)	0.38	3.29
Tamping Cycle (Squeeze)	0.55	3.84
Tamping cycle (Release)	0.46	4.3
Tamping Cycle (Withdraw motion in Ballast)	0.37	4.67
Tamping Cycle (Withdraw motion in Air)	0.05	4.72
Tamping Cycle (Sleeper released from Hold)	0.08	4.8

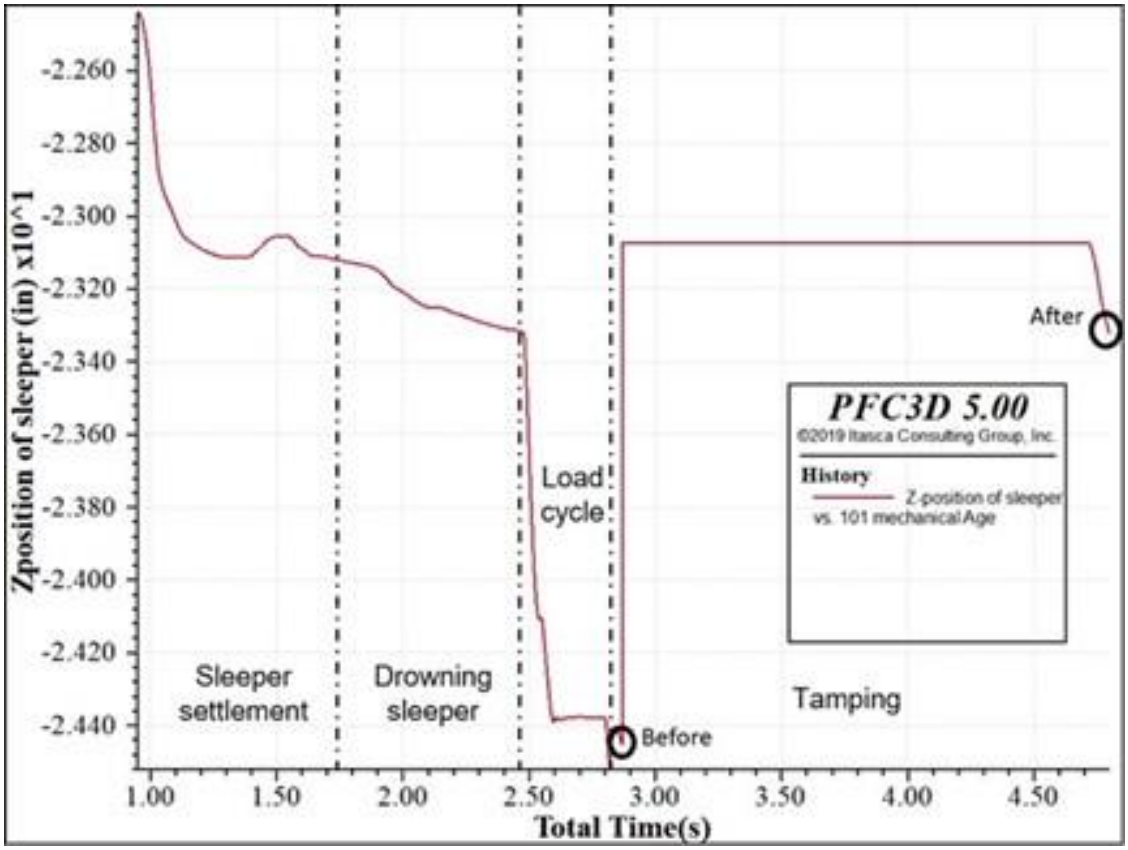

Figure 41 Sleeper z-direction position

The z-position of the sleeper during the entire tamping cycle is shown in Figure 41 The sleeper almost comes in an equilibrium condition around time 1.75 s which marks the end of the 2nd data file. Then due to the addition of a new ballast, a disturbance is created in the *PFC3D* model and the sleeper goes further down into the ballast (0.19685 in = 0.005 m). Due to load cycle sleeper dips by 1.2 inch (3.048 cm sink). The sleeper is then lifted by 1.38 in (0.035 m) to perform the tamping operation. The before and after position hollow circles marked on the graph indicate the position at which the compaction, coordination number, etc. and other parameters are recorded and these are shown in **Table 4**, **Table 5** and

Table 6

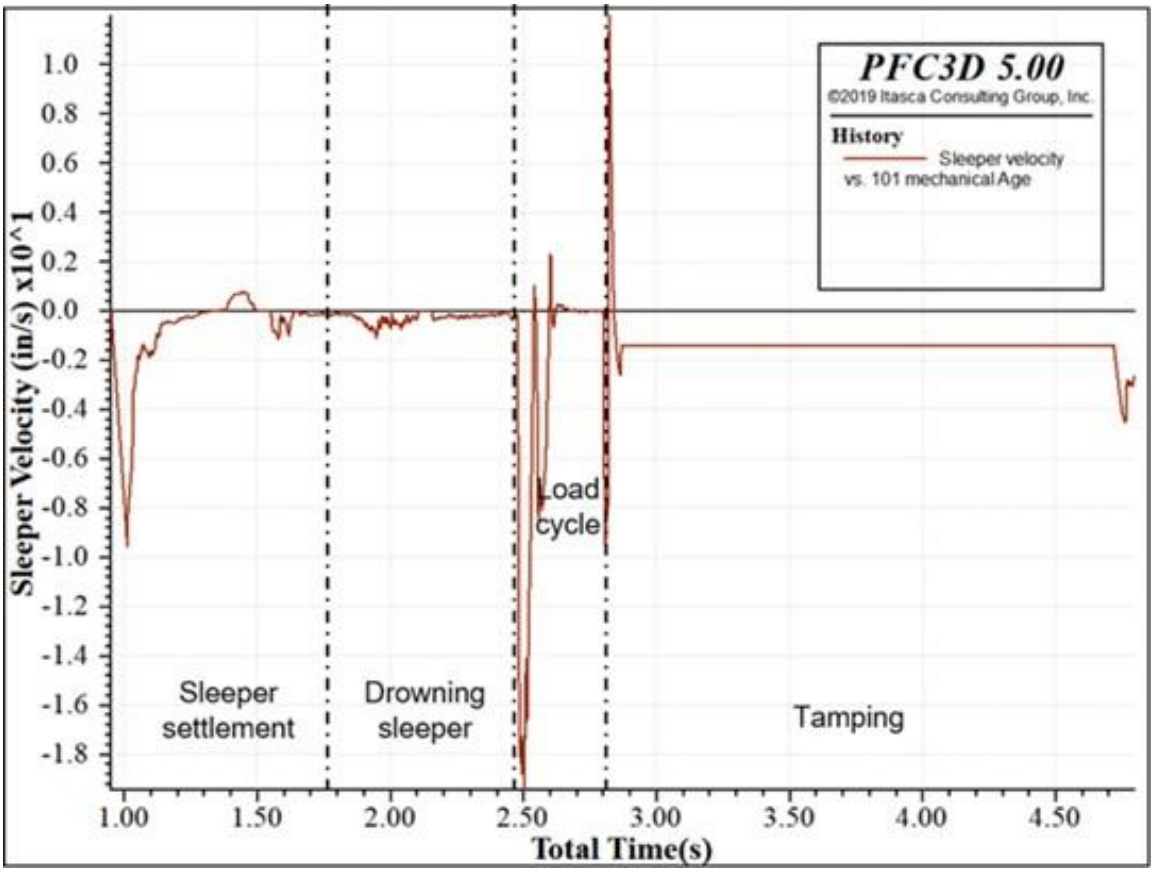

Figure 42 Sleeper Velocity

Sleeper velocity is as shown in Figure 42. The early part shows a decline in sleeper velocity as it is naturally allowed to settle under the influence of gravity. As soon as the sleeper hits the ballast, due to the forces exerted by the ballast on the sleeper, the downward negative velocity of the sleeper reduces and it fluctuates close to zero as sleeper slowly attains equilibrium. During the load cycle, the sleeper velocity increases rapidly due to the high amount of force applied by the load cycle. Finally, during the tamping operation since sleeper is lifted up and kept at that point sleeper velocity is fixed at a particular value. However, with that negative velocity sleeper isn't allowed to go downward by providing a forcing condition in the PFC3D software on its position.

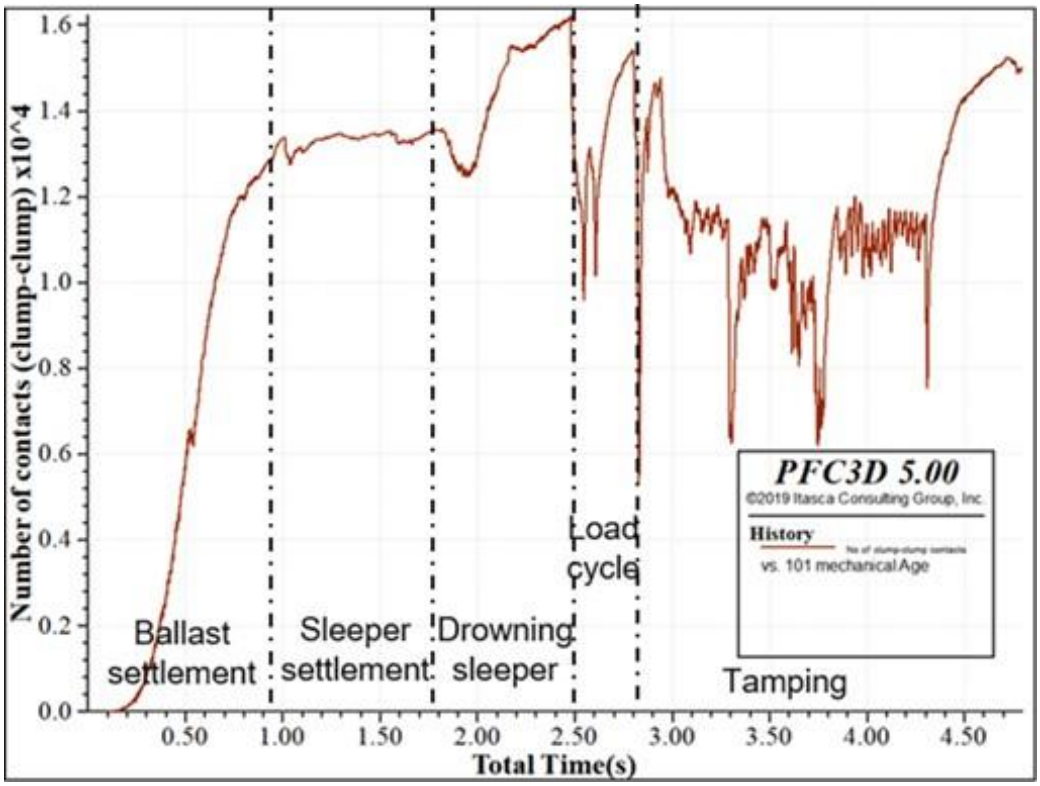

Figure 43 Number of contacts for clump-clump interactions

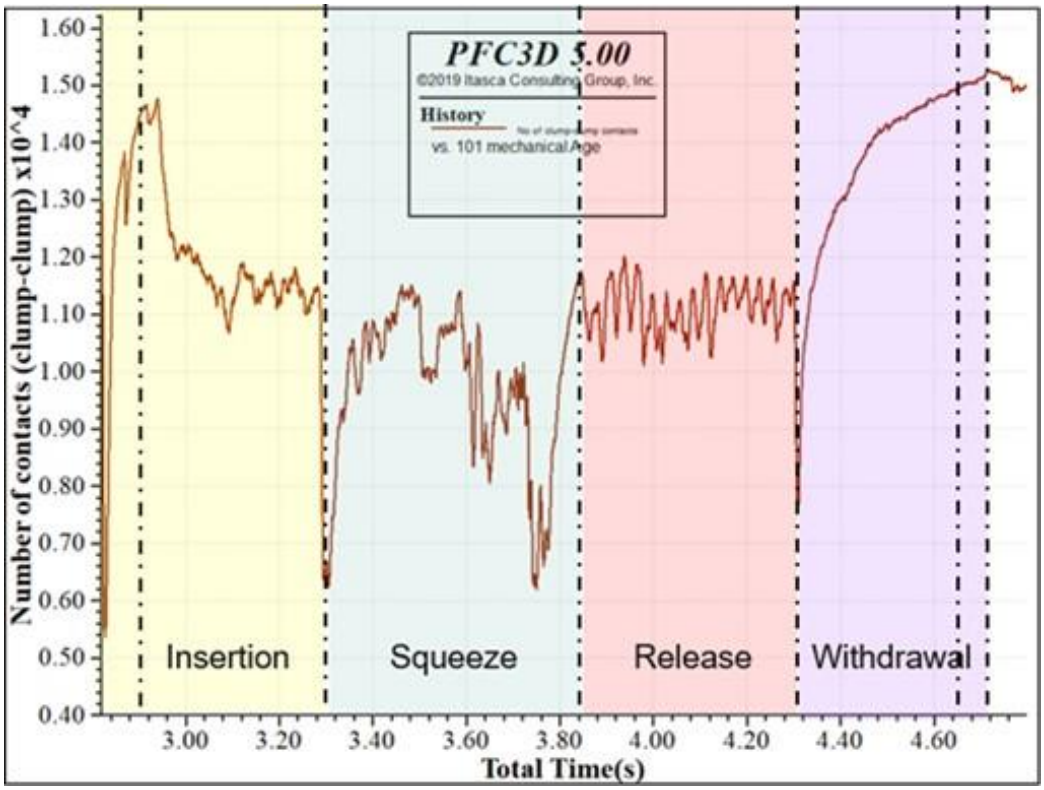

Figure 44 Number of contacts for clump-clump interactions during Tamping

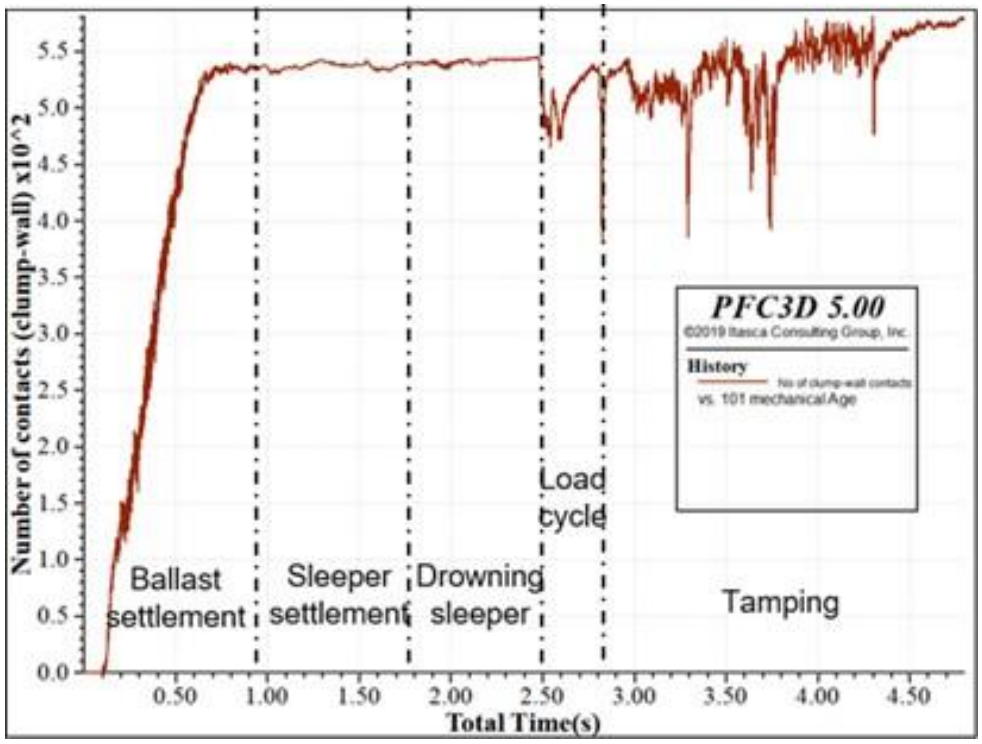

Figure 45 Number of contacts for clump-wall interactions

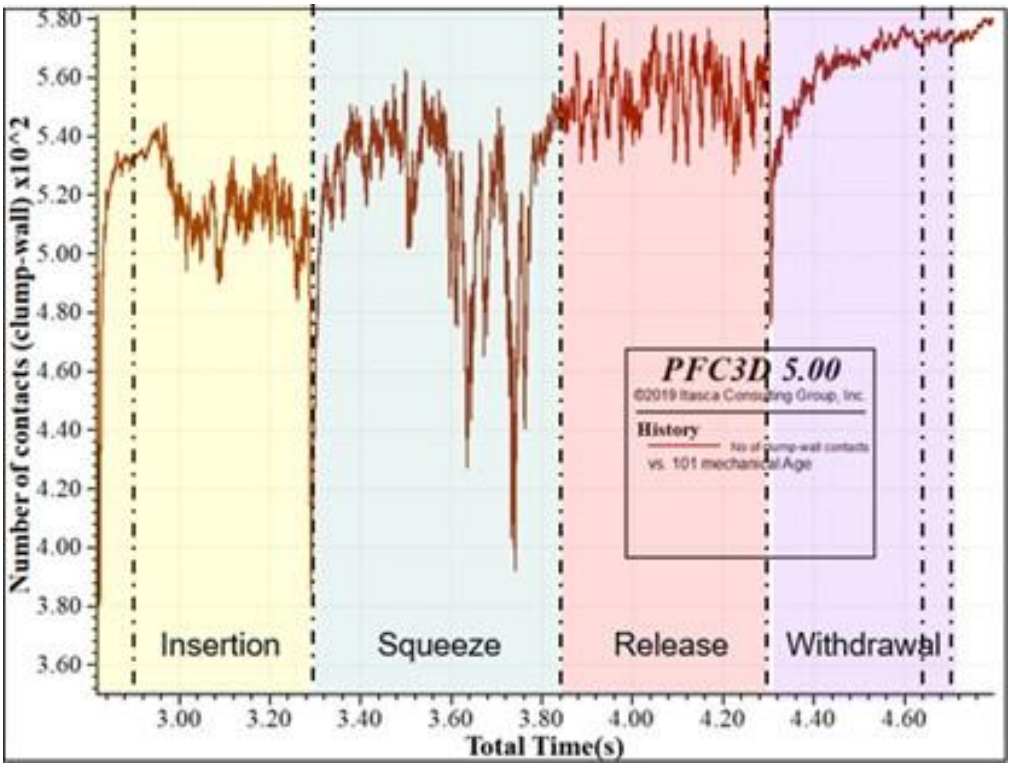

Figure 46 Number of contacts for clump-wall interactions during Tamping

Figure 43 shows the transition in the number of clump-clump contacts throughout the simulation model and Figure 44shows the transition in the number of clump-clump contacts during the

tamping cycle (zoomed-in view). In Figure 43, the number of contacts is 0 almost till 0.1 s. Since at first the ballast is generated using clump generate command, clumps don't overlap with each other and after they start settling, contacts start forming between different clumps and the number of clump-clump contacts increase. Due to the addition of crib ballast in data file Drowning sleeper, there is an increase in clump-clump contacts. During the Load cycle, the number of clump-clump contacts decreases as the downward force on the sleeper exerts pressure on the ballast particles causing them to move away from each other. The same thing happens during insertion (in ballast) and squeeze motion where the number of contacts decreases heavily due to the heavy force applied to the ballast particles and then increases again after reorganizing themselves. At the end of the squeezing phase, the number of contacts in Figure 6.4 become minimum, since many of the ballast particles get liquidized and some even fly off a little but after the 'squeeze-hold' phase, all that extra momentum of the particles starts coming to rest, thereby increasing the contacts gradually again. During the withdrawal phase, the contacts increase since the clumps which were earlier in contact with tines (but maybe not with other clumps), can now only be in contact with other clumps. Number of contacts and Coordination number increase to maximum in the Withdrawal stage of the tamping cycle (considering all the tamping stages).

Figure 45 shows a similar transition but for clump-wall contacts and Figure 6.6 shows clump- wall contacts during the tamping cycle (zoomed-in view), where wall from PFC3D software refers to the boxholder at the bottom and the tamping tines. Clumps, when generated in the first file of Ballast generation, are not in contact with boxholder and thus, clump-wall contacts start forming around 0.1s when these clumps start falling under the action of gravity and come in contact with boxholder. The addition of crib ballast makes no difference to Figure 45 since clump-wall contacts are not affected by new ballast addition which would happen at the top surface of the ballast layer, not in contact with boxholder. A similar concept as explained in the paragraph above explains the contacts trend for loading and tamping phase in case of clump-wall contacts as well.

To better visualize these graphs, they have been colored as per the processes discussed in **Table 7**. These graphs correspond to the total number of contacts formed between clump- clump and clump-wall in a given ballast aggregate at each particular timestep. For 7400 clumps generated in the given simulation, max clump-clump contacts are around 16000 which means at an average given clump is in contact with 2 other clumps. However, this thinking is not true since there would be many clumps at the edge of the domains which would make very few contacts with clump or wall and there would be clumps near the center of the domain and below the sleeper that would have many contacts. Thus, the average number of contacts a clump makes with another body (clump and wall) can be better understood by seeing the coordination number graph. Thus to summarize, it can be said, in Figure 43, the number of clump-clump contacts decreases which happens because the tamping process essentially rearranges the ballast particles from its totally stressed state (caused due to train traffic) by causing ballast particles to move away from each other. Also, the number of clump-wall contacts doesn't get affected much because the tamping tines are in contact with these clumps during the tamping process. The number of contacts at the end of the Loading cycle is the least followed by Insertion and squeezing stage of tamping.

Coordination number is 6-9 practically. It follows a similar trend in the case of both small and big measurement spheres as can be seen from
Figure 47 and Figure 48. As mentioned in 6.4, Insertion and Withdrawal stages are split into two parts highlighted by dotted lines. The tamping phase (Insertion to Withdrawal) of the graph is highlighted using colors. The small measurement sphere in

Figure 47 is measurement sphere 4 which is a small measurement

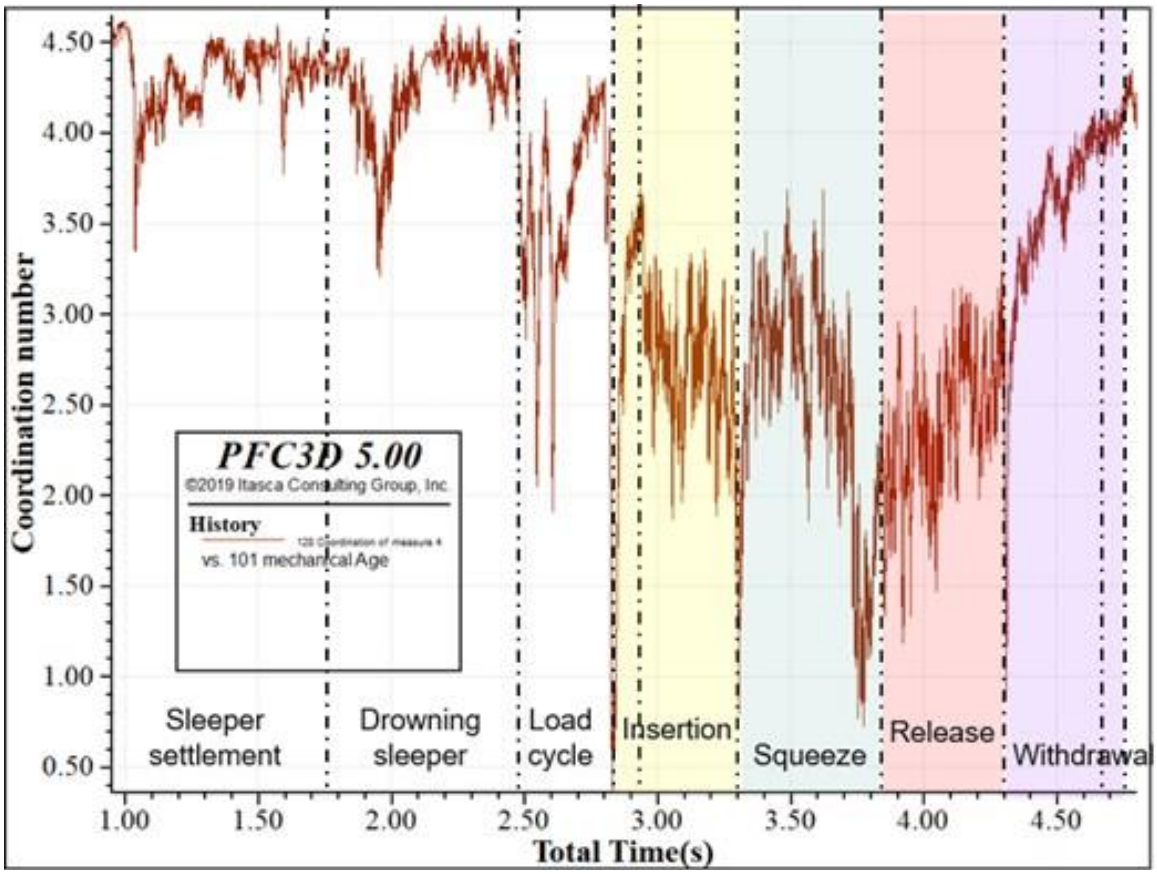

Figure 47 Coordination number measured in small measurement sphere

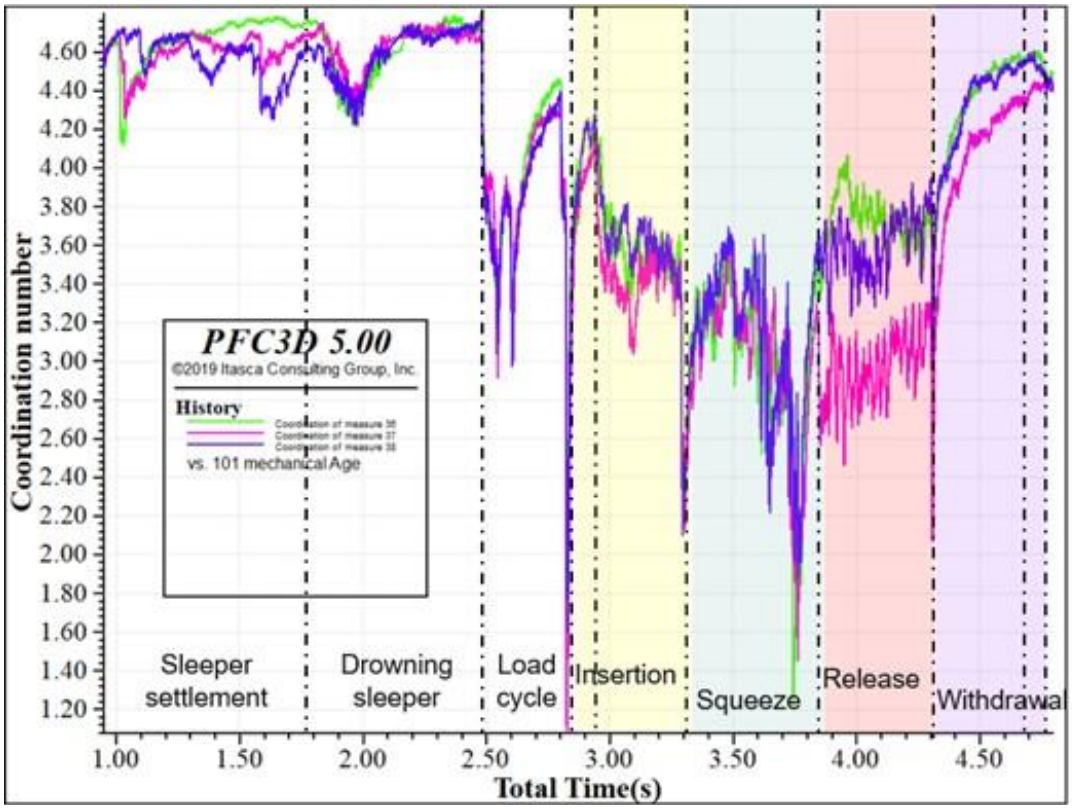

Figure 48 Coordination number measured in big measurement spheres

sphere located at the center of the domain and directly below the sleeper. It is easy to make an observation that the coordination number graph is quite similar to the number of contacts graph discussed before. Coordination number reaches the lowest value at the end of the traffic loading cycle. This is because the sleeper sinks by a maximum amount during this stage and the sleeper sink amount = effective displacement of particles away from each other resulting in a lesser number of contacts among themselves and thus lower coordination number. As squeezing results in compaction, coordination increases for a while till the squeezing becomes extreme and the ballast liquefies and ballast particles move away. Coordination number has very less value when times are very close to the sleeper in the y-direction (region of max squeezing, time=3.7 to 3.84s) and also at the end of the insertion cycle for similar reasons. Big measurement spheres report a slightly higher value of coordination number because the total number of particles in consideration is higher. It is very interesting to note that in the Release stage of the tamping process, the number of contacts almost remains constant, however, the coordination number increases (especially in small measurement sphere).

Ballast compaction is 62%-67% practically, meaning porosity is 33-38%. Porosity is constant during the sleeper settlement phase and decreases a bit as additional ballast is added in sleeper settlement. Porosity increases as the load cycle is started as sleeper due to applied traffic load displaces ballast particles and porosity decreases a little as particles rearrange themselves towards the end of the loading cycle. Porosity decreases in the insertion phase but rapidly rises in squeezing as particles start moving with tine squeezing. As discussed before, the squeezing phase liquefies the ballast and thus compaction does not happen and so porosity increases. Porosity is the least in the extreme measurement spheres and highest in the region where tines come in contact with measurement spheres as can be seen from Figure 49and Figure 50. This may be an error in using

the measurement spheres as tines take up space and displace some clump particles out of the measurement sphere.

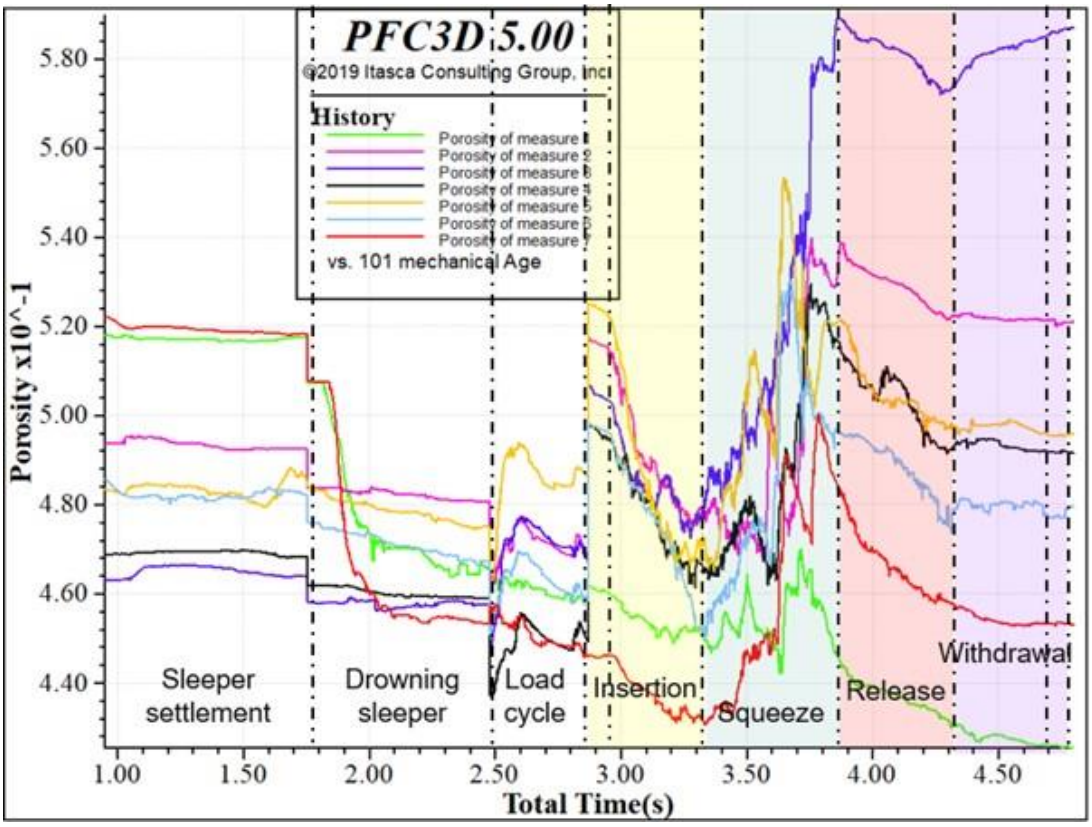

Figure 49 Porosity in 7 small spheres of layer 1

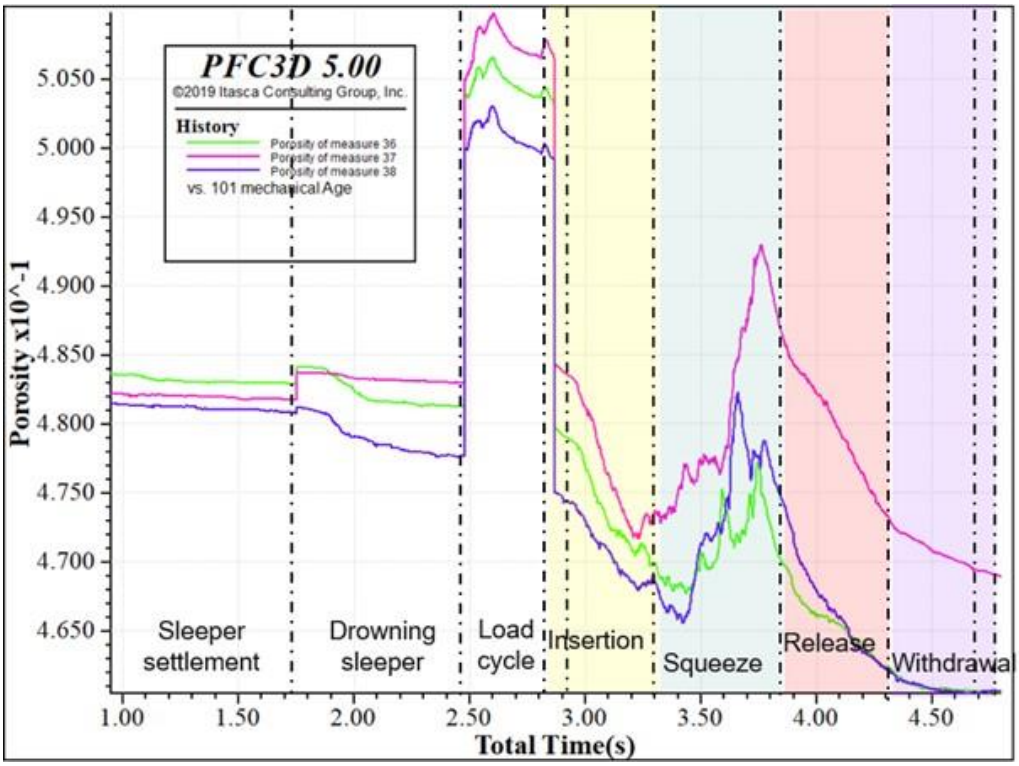

Figure 50 Porosity in 3 big measurement spheres

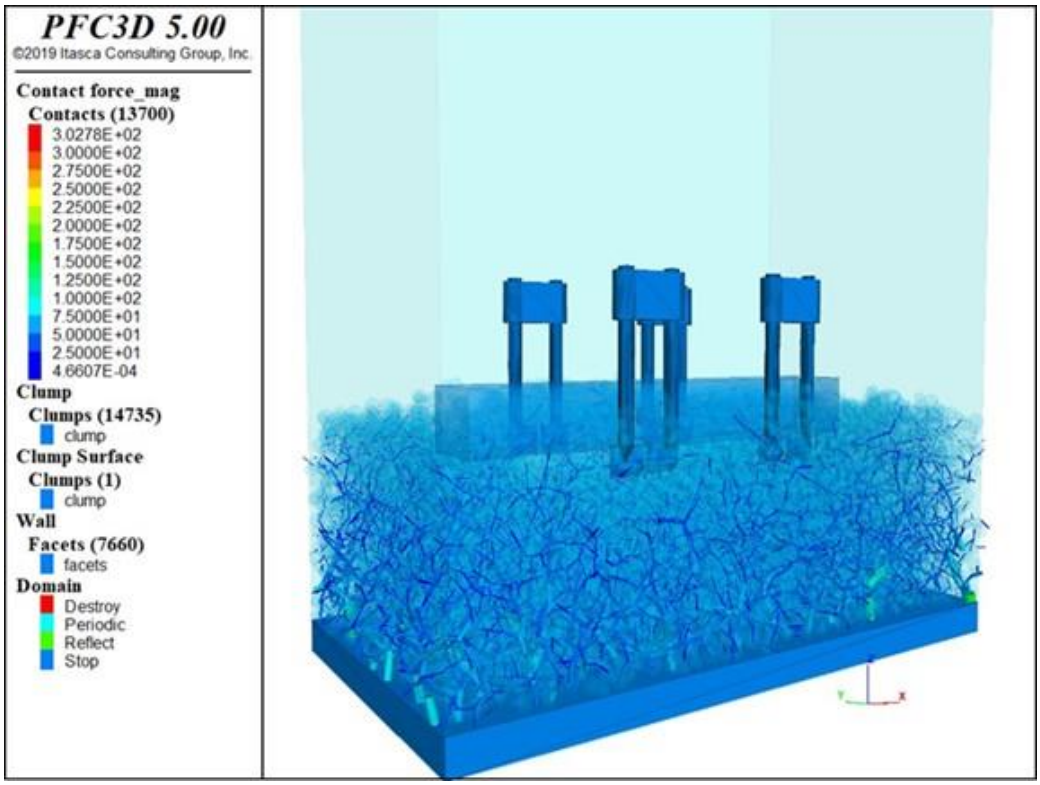

Figure 51 Loadpath during Linear Tamping

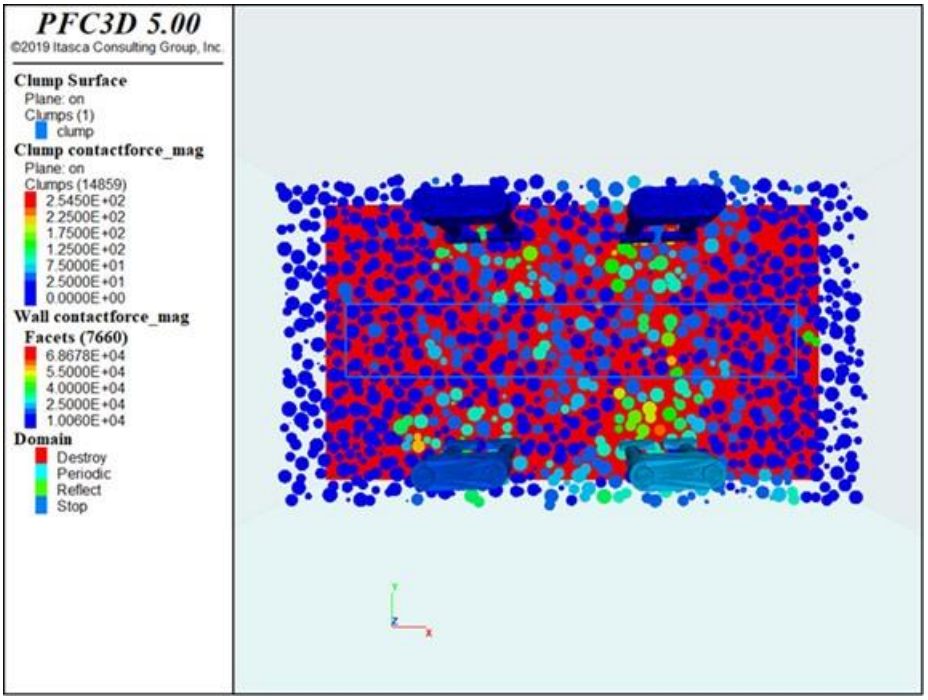

Figure 52 Contact forces generated during Linear Tamping: Top view

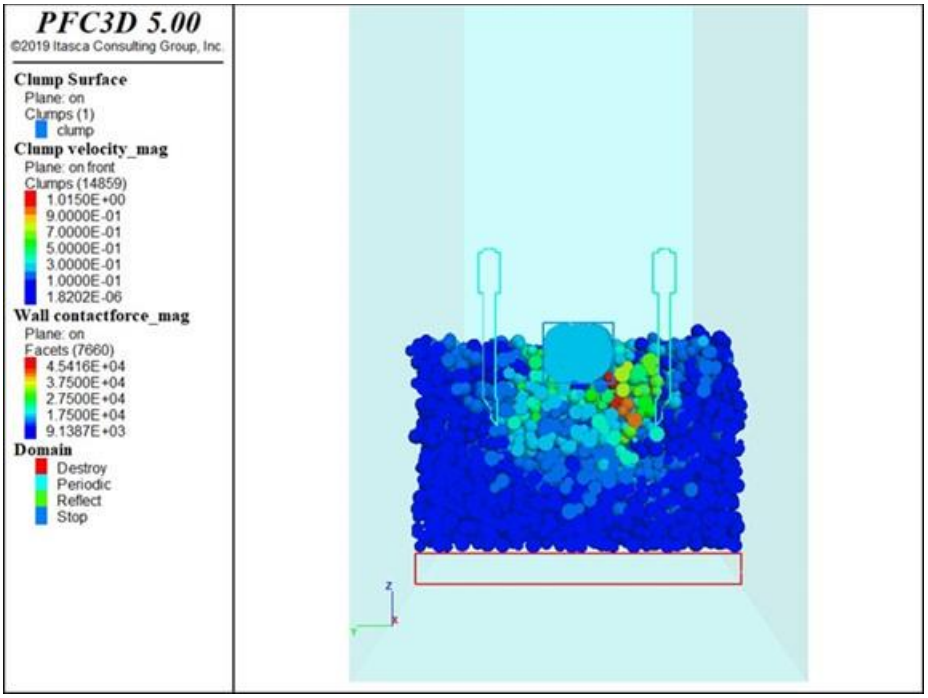

Figure 53 Clump velocity during Squeeze motion: Cross-section view

Figure 6.11 shows the load distribution during the insertion phase of linear tamping. For Figure 52 to 6.14, a cross-section plane was taken to view the clumps. This helps us to view the exact state of the ballast at an inside location (not the topmost or the visible layer). Figure 52 shows the contact force on the clumps and the walls from a top angle view. Figure 53 shows the clump velocities and

tine contact forces during the squeeze motion.During the squeeze motion, central clumps have higher velocities due to the force applied by the tines and during release, the extreme clumps have higher velocities.

Elliptical Tamping

Elliptical tamping is done by using the same parameters as obtained from simulation 8. However, the squeeze and the release stage of tamping are replaced by the elliptical motion of tines. The values of compaction and coordination number before tamping are the same for both linear and elliptical tamping. There is no squeeze hold while performing elliptical tamping. All the graphs generated using elliptical tamping are very similar to linear tamping graphs. Better compaction is provided using elliptical tamping as shown by Table 6.5. Linear tamping is better in all other aspects, so linear tamping is better than elliptical tamping.

Table 8 Elliptical tamping v/s Linear tamping

		Compaction after	Compaction % change	Coordination No. after	Coordination % change
Linear tamping Simulation 8	Small	51.609	-3.923	4.04	24.315
	Big	53.409	7.174	4.447	12.332
Elliptical tamping	Small	52.698	-1.895	3.726	14.659
	Big	53.172	6.7	4.304	8.735

Results Calibration and Repeatability

The information presented in this section has been discussed before in the earlier sections but to validate the obtained results, this section has been put forward. Granular systems like railway ballast are random, disordered and chaotic. Results obtained from a simulation or experiment may be different each time and thus the perfect behavior cannot be assured but only estimated. For example, it has been shown that two identical rail tracks with identical ballast gradations and subsoil do not settle at the same rate when subjected to identical loading conditions. Thus, direct verification of simulation results is difficult. Also, output variables like coordination number, ballast compaction, inter-particle contact forces, distribution of contacts, etc. are impractical and very difficult to monitor directly in physical experiments. This makes it difficult to compare simulation results with experimental results. The results obtained can be trusted if the contact parameters are properly calibrated for which various methods are available. The most used one is to compare simulation results with experimental results (based on the overall collision time between two bodies and their coefficient of restitution).

The simulations in PFC3D software were run twice to ensure repeatability. The simulations were run in “deterministic” mode to ensure repeatability as explained in Section 3.1. More information about “deterministic” mode and its features can be found in [19]. The results obtained were almost identical which gives enough assurance that the simulation model and boundary conditions are set properly and the results obtained aren’t strange to be discarded. The given results were in agreement with the experimental or empirical data provided in Lichtberger (2011). Also, the results obtained here were compared with results obtained by other researchers as specified in Chapter 2. It was observed that the order of magnitude of the obtained results was in agreement with the

results obtained by other researchers. Also, we believe that by modeling ballast as clumps, we would obtain less repeatable results as compared to spherical ballast due to the random orientation and arbitrary shape of these clump particles resulting in different contact forces each time a contact is created, resulting in different movements and position of the particle in each new simulation run.

CONCLUSIONS

Since all ballast-related track behavior can be captured using DEM techniques, the model developed in this research can be extended for undertaking general studies related to railway ties (sleepers) and ballasts, such as:

1. Different track maintenance methods like Dynamic Track Stabilization (DTS), Stone blowing, etc. can also be simulated and compared with each other [48].
2. Improvements in track stability can be analyzed by comparing the performance of different sleeper designs and materials [49].
3. Geometrical features of tamping tines can be further developed to improve their efficacy by reducing particle breakage, maximizing particle mobilization, increasing service life, and lowering power requirements.
4. Different ballast gradations can be compared to study their effect on track stability, including the effects of fouling and contamination of ballast. Differences in response of fouled or contaminated ballast to tamping can also be explored.
5. Influence of factors like traffic speed, axle loads, and loading frequency on track settlement rates can be investigated using DEM as well.
6. Development of engineered ballast gradations and instrumented ballast particles for data acquisition has been an area of recent interest. DEM techniques are invaluable in the research and design of such advanced ballast systems.

Following are the important points that were discovered with the help of this research:

1. Spheres have less number of contacts with sleepers than irregular particles, thereby reducing lateral track stability.
2. Due to lack of interlocking, spherical aggregates disassemble at a higher rate and therefore increase defects in track geometry.
3. Spheres have highly concentrated load paths whereas irregular particles have diffused load paths.
4. Spherical particles will yield at lower load values due to poor load distribution and higher particle stresses.
5. Spherical particles will result in the overestimation of track geometry defects in identical conditions as lack of interlocking causes spheres to disassemble at a higher rate.
6. Spherical particles offer lower resistance to penetration by tines and thus lead to under-estimation of power required to tamp the ballast.
7. Best results for linear tamping are given by simulation with values - Amplitude = 5 deg, Frequency = 35 Hz, Insertion velocity = 0.75 m/s, Squeeze velocity = 0.35 m/s.
8. Linear tamping results are in validation with Lichtberger (2011). At higher frequencies, liquefaction of ballast occurs resulting in poor compaction and faster deterioration of ballast.
9. At higher frequencies, much higher squeezing speed is required to ensure compaction impulse but it is difficult due to the resistance offered by the ballast.
10. Squeeze and release velocity should be lesser to allow particles to compact and rearrange themselves better. Tine frequency should also be less (but good enough to overcome ballast resistance and thus not require extra input power).
11. Location and size of measurement spheres in *PFC3D* play a critical role in estimating output variables. Big measurement spheres give a better accurate value of compaction, coordination number, number of contacts because the total number of particles in consideration is higher. But small spheres may help in noticing details in a smaller region.

12. Tamping process essentially rearranges the ballast particles from its totally stressed state (caused due to train traffic) by causing ballast particles to move away from each other resulting in lower contacts and lower coordination number during tamping.
13. Number of contacts and coordination number are very closely related but are not the same or directly proportional.
14. Coordination number increases in small measurement sphere during the Release stage of the Tamping process, even though the number of contacts almost remains constant.
15. Porosity is the least in the extreme measurement spheres and highest in the region where tines come in contact with measurement spheres (this may be an error in measurement technique as walls take up space in the measurement region thereby reducing the number of clump particles in consideration).
16. Number of contacts at the end of the Loading cycle is the least followed by Insertion and squeezing stage of tamping.
17. Number of contacts and Coordination number increase to a maximum in the Withdrawal stage of the tamping cycle (considering all the tamping stages).
18. Linear tamping is better than elliptical tamping.

Future Work

Model parameters pertaining to physics and contact behavior of the bodies require experiment-based calibration for ensuring the validity of the simulation results. Contact parameters like frictional behavior, contact stiffness, contact damping, and contact force laws are calibrated using a series of standardized physical tests and experiments discussed in Chapter 4. This ensures the accuracy of mesoscopic ballast properties and gross ballast behavior in the model.

Second category of the parameter that requires calibration affects the accuracy of the mechanical behavior of the bodies and determines the computational costs of the model. This category includes geometrical parameters of the model like particle shape, and particle shape detail and their calibration is discussed in Chapter 4 and 5. After due calibration of the afore- mentioned model parameters as discussed, a parametric study of the tamping process could be performed, and recommendations could be made to improve current industry practices.

Simulation is computationally intensive. Computational time is dependent on the number of bodies, the complexity of particle shape, number of active contacts, etc. The current computational time for the model with 3D scanned ballast sample takes weeks to solve. The current model relies totally on the measurement spheres location for judging tamping performance. A better method to record stress, compaction values should be found out to better evaluate the tamping performance results. Some of the important issues that can be targeted in the near future include:

First, modeling of actual ballast shape using rigid block in PFC 6.0 or clumps with many spheres
The accuracy of the current model can be increased by modeling complex arbitrarily shaped ballast particles using clumps or rigid blocks (PFC 6.0) with proper ballast properties calibration.

Second, Optimum lifting value. The amount by which the sleeper should be lifted before tamping is a debatable parameter and parametric studies need to be performed for finding the optimum value of lift before the tamping operation is performed.

Third, extension of model to include particle breakage. Particle breakage and crushing should be considered in the simulation model to represent the ballast more accurately.

Fourth, sleeper modification. Sleeper's design and material can be modified and the resulting track stability can be evaluated and compared with the current sleeper design.

Fifth, tamping tines modification. Geometrical features of tines can be made better to reduce particle breakage, maximize particle mobilization, increase service life and lower power requirements.

Sixth, comparison of different ballast gradations. Effects like fouling and contamination of ballast on the tamping process can be studied along with the different size distribution (gradation) in a given sample of ballast aggregate.

Seventh, inclusion of post tamping operations like dynamic track stabilization (DTS). After tamping, the ballast is allowed to settle by passing trains at a very low speed for some period of time. Instead, DTS operation can be done. DTS holds the track in position and applies a horizontal vibration and vertical load to simulate the passage of trains. This process can be simulated as well in the future.

REFERENCE

[1]. Grossniklaus, R. Advances in Tamping Technology. AusRAIL 2016. MATISA Materiel Industriel SA. Adelaide, Nov. 2016.

[2]. Lichtberger, B. Track Compendium: Track System, Substructure, Maintenance, Economics.Second. Hamburg: DVV Media Group GmbH | Eurailpress, 2011.

[3]. Kerchof, B. Research and Tests at Norfolk Southern. Virginia Tech Railway Technologies Laboratory Annual Review- Personal Communication. Nov. 2016.

[4]. Audley, M., Andrews, J. The Effects Of Tamping On Railway Track Geometry Degradation. Proceedings of the Institution of Mechanical Engineers, Part F: Journal of Rail and Rapid Transit 227.4 pp. 376–391, 2013.

[5]. Koc, W., Wilk, A., Chrostowski, P., Grulkowski, S. Tests on Lateral Resistance in Rail- Way Tracks During the Operation of a Tamping Machine. Proceedings of the Institution of Mechanical Engineers, Part F: Journal of Rail and Rapid Transit 225.3 pp. 325–340., 2011.

[6]. Soleimanmeigouni, I., Ahmadi, A., Arasteh Khouy, I., Letot, C. Evaluation of the Effect of Tamping on the Track Geometry Condition: A Case Study. Proceedings of the Institution of Mechanical Engineers, Part F: Journal of Rail and Rapid Transit 232.2, pp. 408–420. 2018.

[7]. Esveld, C., Jourdain, A., Kaess, G., Shenton, M. Historic Data on Track Geometry in Relation To Maintenance. Rail Engineering International, Edition 2, p16, 1988,

[8]. Suiker, A. S. J. The Mechanical Behaviour of Ballasted Railroad Tracks, 2002.

[9]. Knapton, S. Heatwave Could Buckle Train Tracks and Melt Roads, Travelers Warned. June 2015. url: https://www.telegraph.co.uk/news/weather/11707973/Travel- chaos-forecast- as- 35C- heatwave- could- buckle- train- tracks- and- melt roads.html, visited on Apr. 26, 2019.

[10]. Plasser & Theurer Ballast Tamper, Chester Railway Station. 2010. url: https : / / commons.wikimedia.org/wiki/File:Plasser_%5C%26_Theurer_ballast_tamper,_Chester_ Railway_Station_-_DSC05883.JPG, visited on Feb. 21, 2019.

[11]. Deresiewicz, H. Mechanics Of Granular Matter. Advances in applied mechanics. Vol. 5. Elsevier, pp. 233–306. 1958.

[12]. Jain, A. Discrete Element Modeling of Railway Ballast for Studying Railroad Tamping Operation. MA thesis. Blacksburg: Virginia polytechnic Institute and State University, 2017.

[13]. Tutumluer, E., Huang, H., Hashash, Y., Ghaboussi, J. Aggregate Shape Effects on Ballast Tamping and Railroad Track Lateral Stability". AREMA Annual Conference, Loisville, KY, pp. 17–20, Sept. 2006.

[14]. Cundall, P. A. A Computer Model for Simulating Progressive Large-Scale Movement in Blocky Rock Systems. Proceedings of the Symposium of the International Society of Rock Mechanics (Nancy, France, 1971). Vol. 1, Paper No. II-8. 1971.

[15]. Cundall, P. A., Strack, O. D. A Discrete Numerical Model For Granular Assemblies. Geotechnique 29.1 pp. 47–65,1979.

[16]. Cundall, P. A. Formulation of a Three-Dimensional Distinct Element Model — Part I. A Scheme to Detect and Represent Contacts in A System Composed of Many Polyhedral Blocks. International Journal of Rock Mechanics and Mining Sciences & Geomechanics Abstracts 25.3 pp. 107–116. issn: 0148-9062, 1988, doi: https://doi.org/10.1016/0148-9062(88)92293-0. url: http://www.sciencedirect.com/science/article/pii/0148906288922930.

[17]. Hart, R., Cundall, P. A., Lemos, J. Formulation of a three-dimensional distinct element model—Part II. Mechanical calculations for motion and interaction of a system composed

of many polyhedral blocks". 25.3 pp. 117–125. issn: 0148-9062, 1988, doi: https://doi.org/10.1016/0148-9062(88)92294-2.
[18]. Cundall, P. A., Hart, R. D. "Numerical modelling of discontinua". Engineering computations 9.2 pp. 101–113, 1992.
[19]. Itasca Consulting Group. PFC-Particle Flow Code. 5.0. Minneapolis, 2015.
[20]. Tutumluer, E., Qian, Y., Hashash, Y., Ghaboussi, J., Davis, D. D. "Field validated discrete element model for railroad ballast". Proc., Annual Conference of the American Railway Engineering and Maintenance-of-Way Association, pp. 18–21, 2011,
[21]. Tutumluer, E., Huang, H., Hashash, Y., Ghaboussi, J. "Discrete element modeling of railroad ballast settlement". AREMA Annual Conference. 2007.
[22]. Lu, M. "Discrete element modelling of railway ballast". PhD thesis. University of Nottingham, 2008.
[23]. Irazábal González, J. "Numerical modeling of railway ballast using the discrete element method". MA thesis. Universitat Politècnica de Catalunya, 2015.
[24]. Cholet, C., Oviedo, X., Combe, G., Gautier, P., Sab, K., Moreau, J. J., Forêt, G., Josse, F., Cleon, L. "Study of the mechanical behavior of the ballast using discrete approach". World Congress on Railway Research: Markets, Products, Technology. 2001.
[25]. Stahl, M., Konietzky, H. "Discrete element simulation of ballast and gravel under special consideration of grain-shape, grain-size and relative density". Granular Matter 13.4 pp. 417–428, 2011,
[26]. Hossain, Z., Indraratna, B., Darve, F., Thakur, P. "DEM analysis of angular ballast breakage under cyclic loading". Geomechanics and Geoengineering: An International Journal 2.3, pp. 175–181. 2007.
[27]. Saussine, G., Cholet, C., Gautier, P., Dubois, F., Bohatier, C., Moreau, J.-J. "Modelling ballast behaviour under dynamic loading. Part 1: A 2D polygonal discrete element method approach". Computer methods in applied mechanics and engineering 195.19-22 pp. 2841–2859. issn: 0045-7825, 2006, doi: https : / / doi . org / 10 . 1016 / j . cma.2005.07.006. url: http://www.sciencedirect.com/science/article/pii/ S0045782505002823.
[28]. Indraratna, B., Ngo, N. T., Rujikiatkamjorn, C., Vinod, J. "Behavior of fresh and fouled railway ballast subjected to direct shear testing: discrete element simulation". International Journal of Geomechanics 14.1, pp. 34–44., 2012.
[29]. Lu, M., McDowell, G. "Discrete element modelling of railway ballast under monotonicand cyclic triaxial loading". Géotechnique 60.6, p. 459, 2010.
[30]. Lu, M., McDowell, G. R. "Discrete element modelling of railway ballast under triaxial conditions". Geomechanics and Geoengineering: An International Journal 3.4, pp. 257–270, 2008.
[31]. Lim, W., McDowell, G. "Discrete element modelling of railway ballast". Granular Matter 7.1 pp. 19–29, 2005.
[32]. McDowell, G. R., Lim, W. L., Collop, A. C., Armitage, R., Thom, N. H. "Laboratory simulation of train loading and tamping on ballast". Proceedings of the institution of civil engineers-transport. Vol. 158. 2. Thomas Telford Ltd. pp. 89–95. 2005.
[33]. Indraratna, B., Thakur, P. K., Vinod, J. S. "Experimental and numerical study of railway ballast behavior under cyclic loading". International Journal of Geomechanics 10.4 pp. 136–144, 2009.
[34]. Lobo-Guerrero, S., Vallejo, L. E. "Discrete element method analysis of railtrack ballast degradation during cyclic loading". Granular Matter 8.3-4, p. 195, 2006.

[35]. Tutumluer, E., Huang, H., Hashash, Y., Ghaboussi, J. “AREMA gradations affecting ballast performance using discrete element modeling (DEM) approach”. Proceedings of the AREMA 2009 Annual Conference, Chicago, Illinois, September. pp. 20–23, 2009.
[36]. Boler, H., Qian, Y., Tutumluer, E. “Influence of Size and Shape Properties of Railroad Ballast on Aggregate Packing: Statistical Analysis”. Transportation Research Record 2448.1 pp. 94–104, 2014.
[37]. Lu, M., McDowell, G. R. “The importance of modelling ballast particle shape in the discrete element method”. Granular Matter 9.1 p. 69. issn: 1434-7636, 2006, doi: 10.1007/s10035-006-0021-3. url: https://doi.org/10.1007/s10035-006-0021-3.
[38]. Zhou, T. Y., Hu, B., Wang, X. J., Yan, B. “Discrete Element Method Analysis of Mechanical Properties of Railway Ballast during Tamping Process under Different Amplitude”. Fluid Dynamic and Mechanical Electrical Control Engineering. Vol. 233. Applied Mechanics and Materials. Trans Tech Publications Ltd, pp. 224–227, Dec. 2012, doi: 10.4028/www.scientific.net/AMM.233.224.
[39]. Zhou, T. Y., Hu, B., Wang, X. J., Yan, B. “Discrete Element Method Analysis of Mechanical Properties of Railway Ballast during Tamping Process under Different Vibration Frequency”. Digital Manufacturing Automation III. Vol. 190. Applied Mechanics and Materials. Trans Tech Publications Ltd, pp. 369–372, Sept. 2012. doi:10.4028/www.scientific.net/AMM.190-191.369.
[40]. Zhou, T., Hu, B., Sun, J., Yan, B. “Discrete Element Method Study on the Evolution of Contact Force inside Railway Ballast under Tamping Operation”. 4th International Conference on Computer, Mechatronics, Control and Electronic Engineering. Atlantis Press. 2015.
[41]. Saussine, G., Azéma, E., Perales, R., Radjai, F. “Compaction of railway ballast during tamping process: a parametric study”. AIP Conference Proceedings. Vol. 1145. 1. AIP. pp. 469–472, 2009.
[42]. Saussine, G., Azéma, E., Gautier, P., Peyroux, R., Radjai, F. “Numerical modeling of the tamping operation by Discrete Element Approach”. World Congress Rail Research. pp. 1–9, 2008.
[43]. Perales, R., Saussine, G., Milesi, N., Radjai, F. “Numerical investigation of the tamping process”. 9th World Congress on Railway Research. 2011.
[44]. Perales, R., Saussine, G., Radjai, F. “Optimization of the Tamping Process to Reduce Track Settlement”. 7th Euromech Solid Mechanics Conference. 2009.
[45]. Wang, X., Chi, Y., Li, F., Wang, Q., Gao, L., Cao, Y., Peng, Y. “Study on Discrete Element Modeling Simulation of the Railway Ballast Tamping”. International Journal of Digital Content Technology and its Applications 6.
[46]. Thakur, P., Vinod, J. S., Indraratna, B. “Effect of particle breakage on cyclic densification of ballast: A DEM approach”. IOP Conference Series: Materials Science and Engineering. Vol. 10. 1. IOP Publishing. 2010, p. 012229.23, p. 660, 2012,
[47]. Huang, H., Tutumluer, E., Hashash, Y. M., Ghaboussi, J. “Discrete element model- ing of aggregate behavior in fouled railroad ballast”. 2009 GeoHunan International Conference-Recent Advancement in Soil Behavior, In Situ Test Methods, Pile Foundations, and Tunneling, pp. 33–41, 2009.
[48]. Ferellec, J.-F., Perales, R., Nhu, V.-H., Wone, M., Saussine, G. “Analysis of com- paction of railway ballast by different maintenance methods using DEM”. EPJ Web of Conferences. Vol. 140. EDP Sciences. p. 15032, 2017.

[49]. Laryea, S., Baghsorkhi, M. S., Ferellec, J., McDowell, G., Chen, C. "Comparison of performance of concrete and steel sleepers using experimental and discrete element methods". Transportation Geotechnics 1.4 pp. 225–240, 2014).
[50]. Stevens, A., Hrenya, C. "Comparison of soft-sphere models to measurements of collision properties during normal impacts". Powder Technology 154.2 (2005), pp. 99–109. issn: 0032-5910. doi: https:// doi. org/ 10 . 1016 / j. powtec. 04. 033, 2005. url: http://www.sciencedirect.com/science/article/pii/S0032591005001658.
[51]. Pöschel, T., Schwager, T. Computational granular dynamics: models and algorithms. Springer Science & Business Media, 2005.
[52]. Navarro, H. A., de Souza Braun, M. P. "Determination of the normal spring stiffness coefficient in the linear spring–dashpot contact model of discrete element method". Powder technology 246, pp. 707–722, 2013.
[53]. Shäfer, J., Dippel, S., Wolf, D. "Force schemes in simulations of granular materials". Journal de physique I 6.1, pp. 5–20, 1996.
[54]. Itasca Consulting Group, Inc., PFC3D. Version 5.00 Release 040. Minneapolis, MN, 1994-2019.
[55]. Agnolin, I., Roux, J.-N. "Internal states of model isotropic granular packings. III. Elastic properties". Physical Review E 76.6, p. 061304, 2007.
[56]. Roux, J.-N. Geometric Origin Of Mechanical Properties Of Granular Materials. Physical Review E 61.6, p. 6802, 2000.
[57]. Cheng, Y., Nakata, Y., Bolton, M. Discrete Element Simulation Of Crushable Soil. Geotechnique 53.7, pp. 633–641, 2003.
[58]. Potyondy, D. O., Cundall, P. "A bonded-particle model for rock". International journalof rock mechanics and mining sciences 41.8, pp. 1329–1364, 2004.
[59]. Potyondy, D. O. The Bonded-Particle Model As A Tool For Rock Mechanics Research And Application: Current Trends And Future Directions. Geosystem Engineering 18.1, pp. 1–28. 2015.
[60]. Starfield, A. M., Cundall, P. Towards A Methodology For Rock Mechanics Modelling. International Journal of Rock Mechanics and Mining Sciences & Geomechanics Abstracts. Vol. 25. 3. Elsevier, pp. 99–106, 1988.
[61]. Blow, J., Binstock, A. J. How To Find The Inertia Tensor (Or Other Mass Properties) Of A 3D Solid Body Represented By A Triangle Mesh. 2004. url: http://number-none.com/blow/inertia/index.html, visited on July 13, 2019.
[62]. Mindlin, R. D. "Elastic spheres in contact under varying oblique forces". J. Applied Mech. 20, pp. 327–344, 1953.
[63]. Goldsmith, W., Frasier, J. Impact: The Theory And Physical Behavior Of Colliding Solids. American Society of Mechanical Engineers Digital Collection, 1961.
[64]. Taghavi, R. Automatic Clump Generation Based On Mid-Surface". Proceedings, 2nd International FLAC/DEM Symposium, Melbourne, pp. 791–797, 2011.
[65]. Abbaspour-Fard, M. H. Discrete Element Modelling Of The Dynamic Behavior Of Nonspherical Particulate Materials. PhD thesis. Newcastle University, 2000.
[66]. Azéma, E., Radjai, F., Saussine, G. Quasistatic Rheology, Force Transmission and Fabric Properties of a Packing of Irregular Polyhedral Particles. Mechanics of Materials 41.6, pp. 729–741, 2009.
[67]. Matuttis, H.-G., Chen, J. Understanding The Discrete Element Method: Simulation of Nonspherical Particles For Granular And Multi-Body Systems. John Wiley & Sons, 2014.

[68]. Ricci, L., Nguyen, V.-H., Sab, K., Duhamel, D., Schmitt, L. Dynamic Behavior of Ballasted Railway Tracks: A Discrete/Continuous Approach. Computers & Structures 83.28-30, pp. 2282–2292, 2005.
[69]. Weaire, D., Aste, T. The Pursuit of Perfect Packing. CRC Press, 2008.
[70]. Schultz, R. A. Brittle Strength of Basaltic Rock Masses with Applications to Venus. Journal of Geophysical Research: Planets 98.E6, pp. 10883–10895, 1993.
[71]. Track Ballast. url: https://en.wikipedia.org/wiki/Track_ballast, visited on June 12, 2019.
[72]. AREMA Manual for Railway Engineering Volume 1: Track. 2010.
[73]. Rock Types and Specific Gravities. url: http://www.edumine.com/xtoolkit/tables/sgtables.htm, visited on July 27, 2019.
[74]. Foundations - Modulus of Elasticity. url: http://community.dur.ac.uk/~des0www4/cal/dams/geol/mod.htm, visited on July 17, 2019.
[75]. Avallone, E. A., Baumeister, T., Sadegh, A. Marks' Standard Handbook for Mechanical Engineers (Standard Handbook for Mechanical Engineers. eleventh. McGraw-Hill Professional, 2006.
[76]. Bergman, Richard; Cai, Zhiyong; Carll, Charlie G.; Clausen, Carol A.; Dietenberger, Mark A.; Falk, Robert H.; Frihart, Charles R.; Glass, Samuel V.; Hunt, Christopher G.; Ibach, Rebecca E.; Kretschmann, David E.; Rammer, Douglas R.; Ross, Robert J.; Star Year: 2010. Wood Handbook: Wood as an Engineering Material. USDA Forest Service, Forest Products Laboratory, General Technical Report FPL-GTR-190, 2010: 509 p. 1 v. 190, 2010.
[77]. Federal Railroad Administration, Discrete Element Modeling of Railroad Ballast Behavior. Tech. rep. DOT/FRA/ORD-18/20. U.S. Department of Transportation, Federal Railroad Administration, url: https://www.fra.dot.gov/eLib/details/L19570%5C#p1%5C_z5%5C_gD, July 2018.
[78]. Tungsten Carbide. url:https://en.wikipedia.org/wiki/Tungsten_carbide, visited on July 21, 2019).
[79]. Christoffersen, J., Mehrabadi, M. M., Nemat-Nasser, S. A Micromechanical Description of Granular Material Behavior. Journal of applied mechanics 48.2, pp. 339–344, 1981.
[80]. JMP®. Version 14. SAS Institute Inc., Cary, NC. 1989-2019.

APPENDIX A

The graphs shown below show the variation of porosity with time in different measurement spheres layers. Each layer has seven (small) measurement spheres numbered from left to right in the positive x-direction. The position of the layers is shown in Figure 30. Layer 1 (which is directly below the sleeper) porosity trend as represented in Figure A.1. Figures A.1, A.2, A.3 show that the leftmost and the rightmost measurement spheres in a layer have the least porosity and thus maximum compaction. The second and the second last sphere have higher porosity than the first and the last sphere but lesser than the 4th sphere (central sphere in the layer). An important thing to notice here is about the third and the third last measurement spheres which come in contact with tamping tines. The porosity in these spheres is much higher and can be explained by saying that tines displace many of the ballast particles in these measurement spheres during their insertion, squeeze and release motions, i.e., liquefy the ballast and thus porosity in these layers increase. The tines while squeezing only reach inside the region of measurement sphere layer 1 by a certain amount and thus the Figure A.1 doesn't show similar high porosity peaks for third and third last measurement spheres. As shown in Table 7, tines are inserted into ballast from 2.91 to 3.29 s, the ballast is squeezed from time 3.29 s to 3.84 s and then released from 3.84 s to 4.3 s. So accordingly, the porosity in the third and third last measurement spheres which come in contact with tines, show an increase in porosity till 3.7 s approximately and then a decline is seen in porosity since both the tines (in +Y and -Y direction) would keep on squeezing and go out of layer 2 and layer 3 regions and enter layer 1 region. The release motion starts from 3.84 s, so tines would now come out of layer 1 and enter layer 2 (+Y tines) and layer 3 (-Y tines) region. This happens around 4 s and thus one can again see a rise in the porosity curve from 4 s to 4.3 s (end of release phase) since the tines would displace the volume of clumps equal to the tines volume. At the end of the release phase, tines are withdrawn vertically upwards and thus displaced ballast starts settling down resulting in a better compaction, i.e.. decreased porosity. Figure 50 shows a similar porosity curve which shows that porosity increases in the squeezing phase from 3.29 to 3.84 s and then decreases. Tines are inserted at a location which is majorly covered by the leftmost and the rightmost big measurement spheres, i.e., measurement sphere number 36 and 38. Thus, at the end of tamping, they both have almost the same amount of porosity. Porosity graphs are as shown below:

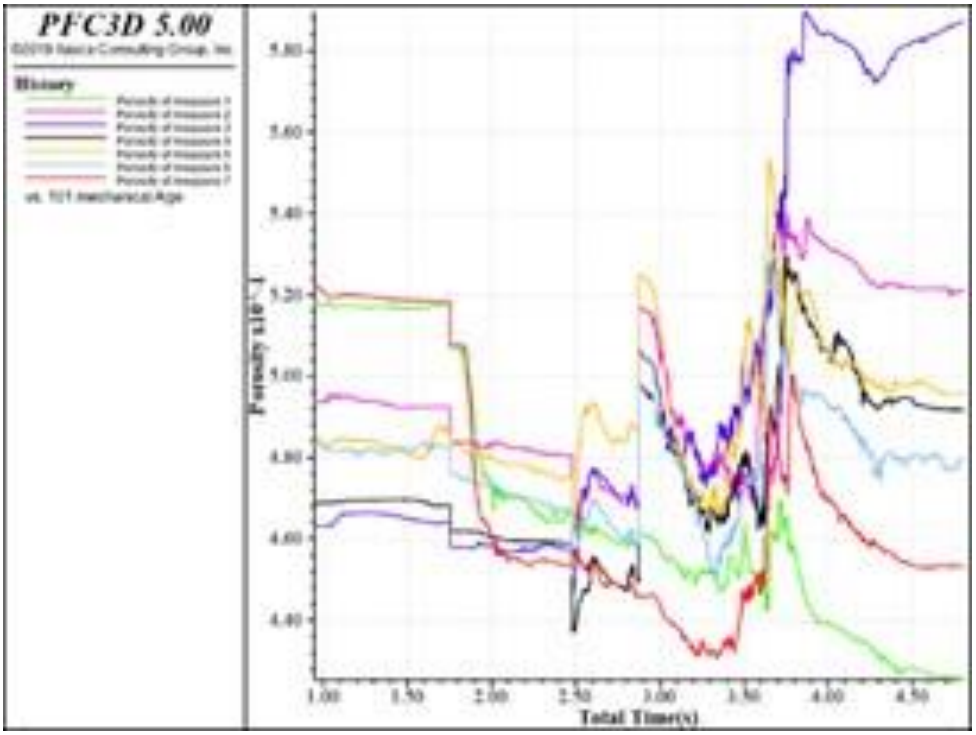

Figure A.1

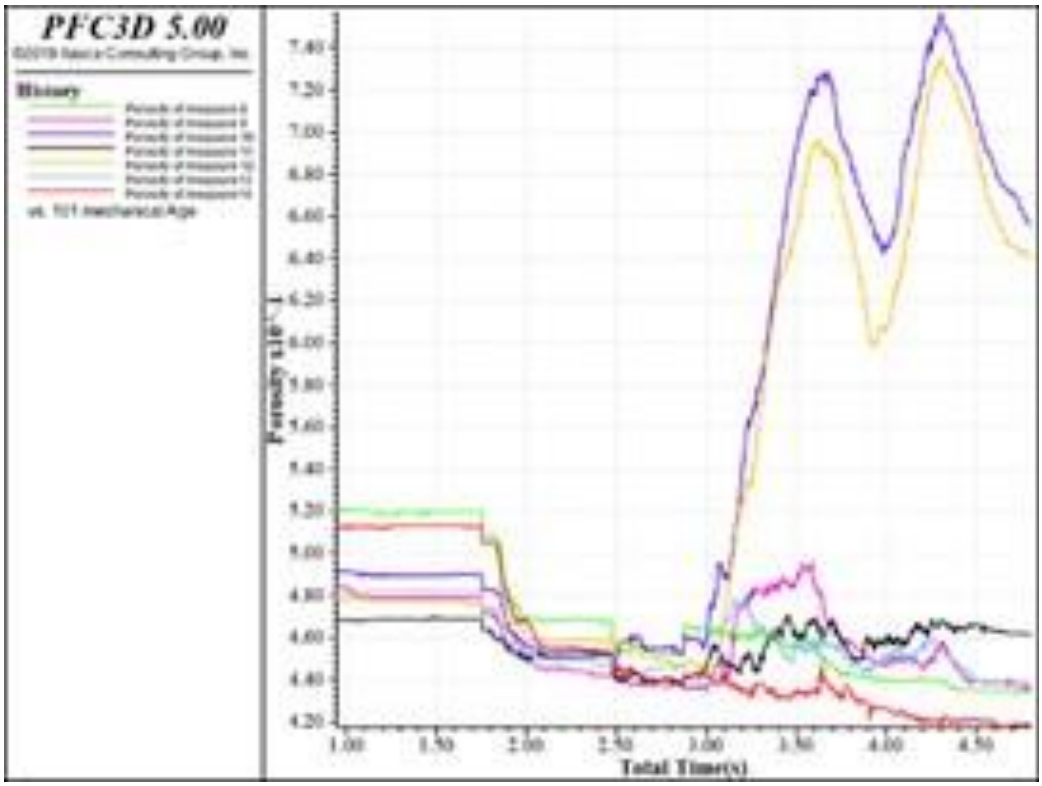

Figure A.2

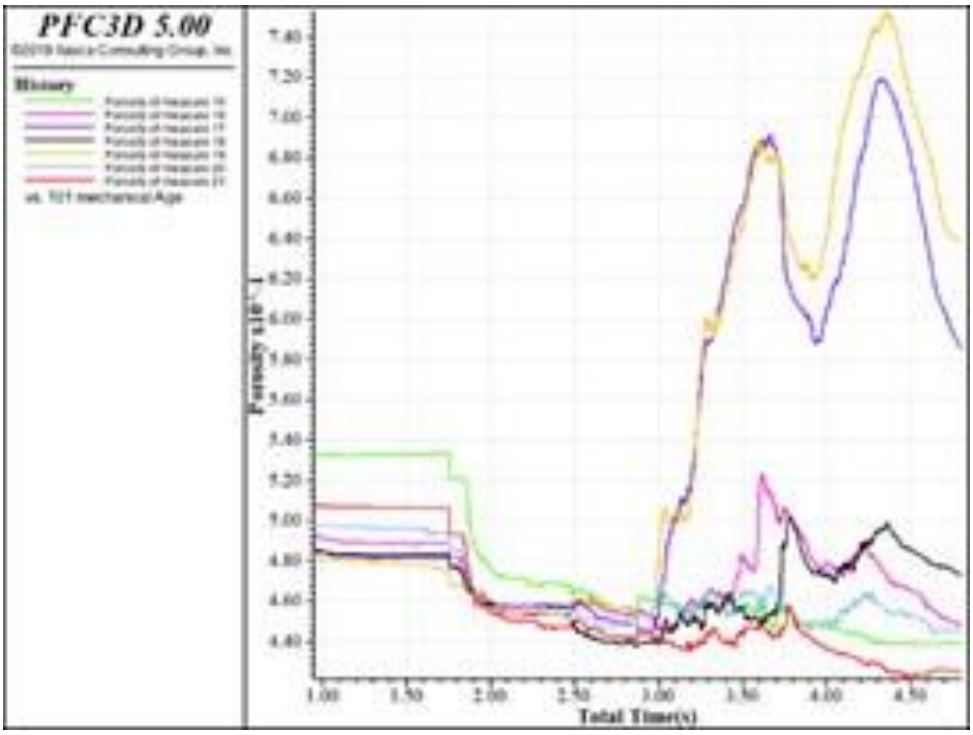
PFC3D 5.00
History
vs. 101 mechanical Age
Porosity
Total Time(s)

Figure A.3

ACKNOWLEDGEMENTS

The authors wish to thank and acknowledge the US Department of Transportation, University Transportation Center Program (RailTEAM UTC) for funding support for this research.

ABOUT THE AUTHORS

Mehdi Ahmadian

Dr. Mehdi Ahmadian is a Dan Pletta Professor of Mechanical Engineering at Virginia Tech, where he also holds the position of Director of Center for Vehicle Systems and Safety (CVeSS), and the Railway Technologies Laboratory (RLT). Dr. Ahmadian has authored more than 130 archival journal publications and more than 250 conference publications, including a number of keynote lectures. He has served as Editor or Editor-in-Chief for four journals on Vehicle System Dynamics, Vibration and Control, Shock and Vibration and Automobile Engineering. Dr. Ahmadian is Fellow of American Society of Mechanical Engineers of the American Institute for Aeronautics and Astronautics (AIAA). He has received many distinguished scholar awards.

Nilesh Dama

Mr. Nilesh Dama was a graduate research assistant for his Masters' degree in the Department of Mechanical Engineering at Virginia Polytechnic Institute and State University